Studies on some aspects of Gravitational Waves and Black Holes in Massive Gravity

Thesis submitted to

Cochin University of Science and Technology

in partial fulfillment of the requirements for the award of the degree

of

DOCTOR OF PHILOSOPHY

Prasia P.

Theory Division

Department of Physics

Cochin University of Science and Technology

Kochi - 682022

APRIL 2017

Studies on some aspects of Gravitational Waves and Black Holes in Massive Gravity

Ph. D thesis in the field of Extended Theories of Gravity

Author:

Prasia P.

Part-time Research Scholar

Department of Physics

Cochin University of Science and Technology

Kochi - 22

prasiapankunni@gmail.com

Research Supervisor:

Prof. Kuriakose V. C. (Rtd.)

Department of Physics

Cochin University of Science and Technology

Kochi - 22

vck@cusat.ac.in

CERTIFICATE

Certified that the work presented in this thesis is a bonafide research work done by Ms. Prasia P. under our guidance in the Department of Physics, Cochin University of Science and Technology, Kochi-682022, Kerala and has not been included in any other thesis submitted previously for the award of any degree. All the relevant corrections and modifications suggested by the audience during the pre-submission seminar and recommended by the Doctoral Committee have been incorporated in this thesis.

Prof. V. C. Kuriakose

(Supervising Guide)

Kochi-22

April, 2017

Prof. Ramesh Babu T.

(Joint Guide)

iii

DECLARATION

I hereby declare that the work presented in this thesis is based on the original research work done by me under the guidance of Prof. V. C. Kuriakose, Professor (Rtd.) and Prof.Ramesh Babu T., Department of Physics, Cochin University of Science and Technology, Kochi- 682022, Kerala and has not been included in any other thesis submitted previously for the award of any degree.

Kochi-22

April, 2017   Prasia P.

ACKNOWLEDGEMENTS

First of all, I would like to thank my supervising guide Prof. V. C. Kuriakose. He has been generous, but at the same time he timely intervenes on the progress of the research work. Especially during my part-time research, he has been very considerate, has given me enough time and encouragement. The best thing about him is the freedom he gives to researchers under his guidance to choose a topic of their own interest and never go against it unless it violates the ethics or the physics. I have been lucky enough to have him as a teacher from my post graduation onwards. His effort in running the lab, IUCAA Resource Centre (IRC), hard work and knowledge in theoretical physics has been a constant encouragement for me. He gave me opportunity to join in the skywatch program for school and college students conducted by IRC every year which was an entirely different experience. His patience and shrewdness in addressing problems in physics is exemplary. I hope and wish that I have learned something from him.

I also extend my gratitude to my Joint Guide Prof. Ramesh Babu T., for his support.

I would like to express my gratitude towards the head of the department of Physics, Prof. M. Junaid Bushiri and former heads for their support. I thank all the faculty members of Department of Physics, CUSAT who are also my teachers during my post graduation for their support and encouragement. I also extend my gratitude towards the students and non-teaching staff of the department. I would like to acknowledge UGC, New Delhi for providing Junior Research Fellowship (JRF).

My lab-mates Lini Devassy (lini chechy), Nima chechy and Bhavya chechi have been of great help, support and company to me during my research. I express my heartfelt thanks to them. I thank Jerin Mohan for his great help. I also express my thanks to Saneesh Sebastian, Jishnu Suresh, Nijo Varghese, Prashob C B, Tharanath R, Paxy George, Athira Sashidharan, Krishna, Dinto, Thaskeena and all my fellow researchers in the department of Physics.

I thank Dr. Vivek M. (post doctoral fellow, University of Utah) for being my friend and for the great support and encouragement that he has been giving. Thanksgiving would be incomplete without mentioning my best buddies Gayathri C. R. and Bini B Nair (Assistant Professor, St.Thomas College, Ranni). I express my heartfelt thanks to them for their constant encouragement, understanding and support. I would like to thank my friend Saleena M (Researcher, School of Management Studies) for her companionship. I thank all my friends who have been there for me. I would like to thank all my roommates in the hostel and friends there who have supported me.

xviii

I take this opportunity to thank the Principal, Govt. College Chittur, Palakkad, where I teach. I also thank the Head of the Department, Sri. M.V. Vijayakrishnan and all my colleagues there for being very co-operative. The jovial atmosphere created by Sri.C. D. Ramabadran and Sri. Dhandapani K. R. and their company gave much of a relaxation to me during my research days. I also would like to acknowledge my project students (M.Sc. and B.Sc.) for the interaction and enthusiasm they have showered on me. I thank all my students in Govt. College Chittur for having been encouraging. I also would like to thank all teaching and non-teaching staff of Govt. College Chittur, Palakkad.

And lastly, but not the least, I express my love and gratitude to my father (Dr. V Pankunni), mother (K C Yesoda Devi), grandmother (Meenakshi A) and sisters (Dr. Praseetha P and Natasha P).

CONTENTS

The General Theory of Relativity (GTR) put forward by Albert Einstein has led us to have a new outlook of the Universe. It paved the way for a dynamical approach that is liable to scientific modeling and physical measurements, for the first time in the history of Physics. For any theory of gravity to be valid, it should explain the current astronomical observations. GTR succeeded in many of the experimental tests. However recent astronomical observations as well as some theoretical motivations demand that GTR has to be modified. Primarily, GTR is non-renormalizable and it cannot serve as a fundamental theory if we attempt to give a complete quantum description of gravity and space-time. The observation of an accelerated universe shows that GTR is inadequate for describing universe at the extreme regimes. The presence of big bang singularity, flatness, horizon and monopole problems could not be explained using the standard cosmological models based on GTR. The explanations for matter dominated and radiation dominated universe, dark energy and dark matter could not be successfully explained using GTR. A plethora of cosmological models were proposed to explain the cosmological, astrophysical discrepancies and conceptual problems. However, they are plagued by

the so called coincidence problem and cosmological constant problem.

It is expected that adding higher order curvature invariants to the Einstein-Hilbert action could solve the problems. Consequently, it would be worth addressing the problems by modifying GTR. This approach can avoid the dark components in cosmology and will also provide a deeper understanding of the relevant issues and gravitation. The class of theories called 'Extended Theories of Gravity' (ETG) or 'Modified Theories of Gravity' came with such a motive. Amongst all modified gravity theories, the $f(R)$ theory of gravity is one simple theory that can sufficiently describe the properties of higher-order gravitational effects, by extending the gravitational Lagrangian as an arbitrary function of the Ricci scalar. The theory is devoid of instabilities and can explain the late time acceleration of the Universe in a unified way. The question whether the graviton can acquire a mass has been seeding interest among theorists for decades, on the other hand. This approach is addressed in the class called 'Massive Gravity' theories and is considered to be a viable model to explain the late time acceleration of the universe.

Modified theories of gravity will be valid only if they are tested. The best testing ground for massive gravity or any modified theory of gravity would be around a black hole. The best way to find out the presence of a black hole is to search for its "Quasi Normal Modes" (QNMs). Theoretically, the QNMs can be studied by perturbing the black hole and knowing its response towards such a perturbation. The analogy of black hole mechanics with the classical thermodynamics

is also emerging as a new area of interest and shows interesting results like phase transition. The thermodynamics of black holes show different behavior for different theories of gravity. Study of thermodynamics of black holes may help in constructing a quantum theory of gravity. And finally, searching for the gravitational waves (GWs) itself will lead to drawing conclusions regarding the validity of a modified theory. The current configuration of GW detectors are designed for the polarizations coming from GTR alone. Hence, studies have to be done for detecting the modes from theories of massive gravity also.

The subject of this thesis work is to study the different aspects of massive gravity theories. In this work the important aspects such as QNMs and thermodynamics of black holes and GWs in massive gravity theories are explored in detail for new results. The thesis is organized into six chapters:

Chapter 1 : In this chapter, a general theoretical introduction to GTR, what are its peculiarities, what does it predict, what are the short comings and how they can be overcome are discussed. The black hole solutions proposed by such theories and also the importance of the study of thermodynamics of such theories are discussed in this chapter. An introduction to the emanation of Gravitational Waves (GWs) based on GTR and the possibility of detecting GWs based on ETG are given in brief.

Chapter 2 : Chapter 2 deals with the black hole solution of $(3+1)$ dimensional dRGT massive gravity and its QNMs. The space-time around such a black hole is perturbed using a massless scalar

and the QNMs are calculated from the resulting master equation using Improved Asymptotic Iteration Method (Improved AIM). The QNMs thus got are compared with the GTR case. Studies on the thermodynamics of such a black hole are also presented in this chapter. The P-V criticality of the resulting black hole is checked for phase transition behavior. The behavior of holographic entanglement entropy is also studied for the aforesaid black holes.

Chapter 3 : In Chapter 3, the QNMs are calculated for a $(2+1)$ dimensional BTZ black hole in massive gravity. The black hole space-time is subjected to a massless scalar perturbation and the resulting master equation is used for calculating QNMs using Improved AIM. The resulting QNMs are checked for phase transition. The dependency of QNMs and phase transition on the graviton mass is also checked. The property of phase transition is checked for de Sitter (dS) as well as Anti de Sitter (AdS) space-times and also the dependency of transition behavior on the charge of the black hole and on the cosmological constant are studied. The thermodynamic behavior of these black holes are then studied and is used to explore phase transition behavior and the results are compared from QNM studies.

Chapter 4 : The production and detection of massive GWs from $f(R)$ theory of gravity are studied in Chapter 4. The field equation for a specific form of $f(R)$ is obtained and is linearized to get GW solutions. The spherical antenna detection of the massive component of the above GW solutions is then studied.

The energy sensitivity is also calculated. The detectability of massive mode is checked for a Truncated Icosahedral Gravitational wave Antenna (TIGA). In this work, a Modified TIGA is proposed for detecting the monopole modes and their energy sensitivity are also calculated.

Chapter 5 : In this chapter the possibility of the detection of massive GW emanated from $f(R)$ theory of gravity is studied for LIGO (Laser Interferometric Gravitational wave Observatory). The beam pattern functions are calculated for detecting a massive mode. This is done for Gamma Ray Burst (GRB) sources chosen at random. The detection possibility of a massive GW from a GRB source in LIGO is studied using Bayesian analysis.

Chapter 6 A summary of the new results are presented in this chapter and also the possible application and future plan of studies are presented.

INTRODUCTION

1.1 General Theory of Relativity

General Theory of Relativity (GTR) is one of the most distinguished accomplishments of 20th-century physics. GTR proposed by Albert Einstein in 1915 gives a comprehensive and coherent description of space-time, gravity and matter at the macroscopic level. In GTR the space-time is considered to be dynamic in nature and is determined from the distribution of matter and energy. The formulation of GTR involved three major steps[1, 2]:

1. Formulating equivalence principle in 1907

2. Introducing the metric tensor as the important mathematical concept for a general relativistic theory of gravitation in 1912

3. The formulation of generally covariant field equations of gravitation in 1915 that resulted in the final form of GTR

Einstein in his theory proposed that gravity could not be considered as a 'Force' in the conventional sense but as a manifestation of the curvature of space-time caused by the presence of matter. The equivalence principle restricts the curved space-time to pseudo-Riemannian[3, 4]. In the formulation of GTR, the Riemann curvature tensor denoted as $R^{\mu}_{vk\alpha}$ which measures the curvature of the space-time is given by[5],

$$(1.1) \qquad R^{\mu}_{v\kappa\alpha} = \partial_{\kappa}\Gamma^{\mu}_{v\alpha} - \partial_{\alpha}\Gamma^{\mu}_{v\kappa\alpha} + \Gamma^{\mu}_{\lambda\kappa}\Gamma^{\lambda}_{v\alpha} - \Gamma^{\mu}_{\lambda\alpha}\Gamma^{\alpha}_{v\kappa},$$

where the Christoffel symbol Γ is obtained from the metric tensor $g_{\mu v}$ and is given by,

$$\Gamma^{\sigma}_{\mu v} = \frac{1}{2}g^{\sigma\rho}\left(\partial_{\mu}g_{v\rho} + \partial_{v}g_{\rho\mu} - \partial_{\rho}g_{\mu v}\right).$$

The curvature tensor vanishes for flat space-time. By differentiating the components of the Riemann tensor one can prove the Bianchi identity,

$$\nabla_{\sigma}R^{\mu}_{v\kappa\alpha} + \nabla_{\kappa}R^{\mu}_{v\alpha\sigma} + \nabla_{\alpha}R^{\mu}_{v\sigma\kappa} = 0,$$

where the gradient symbol denotes the covariant derivative. Contracting the Bianchi identities twice and using the antisymmetry of the Riemann tensor one obtains the following relation,

$$\nabla_{v}\left(R_{\mu v} - \frac{1}{2}g_{\mu v}R\right) = 0.$$

Then Einstein proposed his field equation as[6],

$$(1.2) \qquad R_{\mu v} - \frac{1}{2}g_{\mu v}R = \kappa T_{\mu v},$$

where the metric tensor $g_{\mu v}$ contains the information of the space-time geometry, $\kappa = 8\pi G/c^4$, G is the gravitational constant, $T_{\mu v}$ is the

stress-energy tensor and R is the Ricci scalar obtained by contracting the Ricci tensor as, $R = g^{\mu\nu}R_{\mu\nu}$. $R_{\mu\nu}$ is the Ricci tensor formed by the contraction of Riemann curvature tensor as,

$$R_{\mu\nu} = R^{\alpha}_{\mu\alpha\nu}$$
$$= \frac{\partial\Gamma^{\alpha}_{\mu\nu}}{\partial x^{\alpha}} - \frac{\partial\Gamma^{\alpha}_{\mu\alpha}}{\partial x^{\nu}} + \Gamma^{\alpha}_{\mu\nu}\Gamma^{\beta}_{\alpha\beta} - \Gamma^{\alpha}_{\mu\beta}\Gamma^{\beta}_{\nu\alpha}.$$

The field equation given by (1.2) can also be arrived at by varying the gravitational action given by the Einstein-Hilbert action,

$$(1.3) \qquad\qquad S = \frac{1}{2\kappa}\int\sqrt{-g}R\,d^4x.$$

GTR survived many experimental tests. Einstein could explain the precession of the orbit of the planet Mercury using his GTR. Newton's theory could not explain the observed value of the precision. But GTR could perfectly account for the observed discrepancy[7]. Another prediction made by Einstein based on his GTR is the bending of light rays in strong gravitational field. In 1919, Arthur Eddington observed the effect of gravitational lensing[8, 9]. He observed the apparent shift in the position of stars, due to the light deflection by the gravitational field of the Sun, as predicted by GTR. The existence of black hole is another prediction of GTR. The first study along this line was made by Karl Schwarzschild[10]. Black holes are singularities in space-time that are formed when a star dies. They are points of singularity of infinite mass and density from which nothing, even light, can escape. Cygnus X-1, discovered by Charles Thomas Bolton, Louise Webster and Paul Murdin in 1972[11] is considered to be a strong candidate for a black hole. Later more candidates were found.

Another important experimental test of GTR is the existence of 'Gravitational Waves (GWs)'. Gravitational waves are 'ripples' in the fabric of space-time caused by matter. GWs are obtained as solutions of linearized field equation of GTR. It shows that massive accelerating objects such as neutron stars or black holes that orbit each other would disrupt the space-time in such a manner that waves of distorted space-time will be radiated from the source. Furthermore, these ripples travel at the speed of light through the universe, carrying with them the information about their origins, as well as valuable information on the nature of gravity itself. Even though the mathematical calculations predicted its existence in 1916, it took a very long time, 100 years, to get the experimental evidence. An indirect evidence was got in 1974 when Hulse and Taylor discovered a binary pulsar[12]. It was observed that as the binary system approaches towards the merger, its period decreases. According to GTR it must be due to the emission of GWs. Calculations of the so called 'Hulse-Taylor' pulsar showed that the rate of decrease in its period matches with the prediction made by GTR . Very recently, in 2016, the path-breaking discovery of gravitational waves from black hole collision was observed at LIGO (Laser Interferometric Gravitational wave Observatory). The discovery also substantiated the existence of black holes in the universe.

Soon after the publication of GTR, scientists started questioning the theory. In 1919, Weyl[13] and in 1923, Eddington[14] added higher order invariants to the Einstein-Hilbert action. Such attempts

were made out of scientific curiosity in order to understand the then proposed theory. At the same time, scientists thought it to be not-so-appealing to complicate the Einstein-Hilbert action without any proper theoretical or experimental motivation and for that reason, attempts towards this direction for modifying GTR slowed down. However, there came astrophysical and cosmological as well as theoretical motivations for modifying GTR. In 1960s, while attempting to unify GTR with quantum mechanics, it is found that GTR is not re-normalizable. GTR is a classical theory and fails to serve as a fundamental theory since a full quantum description of space-time and gravity is not available now. In 1962, Utiyama and De-Witt showed that re-normalization at one loop level demands adding higher-order curvature terms to the Einstein-Hilbert action[15]. Later, Stelle showed that higher-order actions are re-normalizable, but not unitary[16]. More recent results show that, when quantum corrections or string theory are taken into account, the effective low-energy gravitational action admits higher order curvature invariants[17–19]. And recently the observations of an accelerated expanding universe prove that GTR is inadequate for describing the universe at extreme regimes. The presence of big bang singularity, flatness, horizon and monopole problems could not be explained using the standard cosmological models based on GTR. Also, the explanations for matter dominated and radiation dominated universe, dark energy and dark matter could not be successfully explained using GTR. A plethora of cosmological models were proposed to explain the cosmological and astrophysical discrepancies. However, they are plagued by the so called coincidence

problem and cosmological constant problem[20, 21].

With these theoretical as well as astrophysical and cosmological motivations at hand, modifying GTR is necessitated that would avoid the dark components in cosmology and would also provide a deeper understanding of the relevant issues in gravitation.

1.2 Extended Theories of Gravity

Several attempts are made to modify GTR which together forms the so called 'Extended Theories of Gravity'. From a phenomenological point of view any relativistic theory of gravity should satisfy certain minimal requirements[22]. It has to explain the astrophysical observations such as the orbits of planets, self-gravitating structures etc., it has to reproduce Newtonian dynamics in the weak field limit, it has to pass the experimentally well founded classical solar system tests and also should reproduce the galactic dynamics. It must address the problem of large scale structure such as clustering of galaxies and also the cosmological dynamics, ie., it should reproduce in a consistent way the cosmological parameters as the expansion rate, the Hubble constant, the density parameter and so on. From a theoretical point of view, there are certain fundamental properties that any modification of gravity may satisfy. Any theory of gravity should be well motivated from fundamental physics. This fundamental theory would solve some fundamental problems in physics, such as late-time acceleration, the incompatibility between quantum mechanics and GTR, the existence of dark matter etc. The theory should have a well-posed initial value formulation meaning that a wide class of freely specifiable initial

data must exist, such that there is a uniquely determined solution to the modified field equations that depends continuously on this data. Also, any such theories should leave space for a strong field inconsistency. ie., the theory must lead to observable deviations from GTR in the strong-field regime. Accordingly, many classes of theories are proposed to meet these requirements.

1.2.1 f(R) theory of gravity

Amongst all modified theories of gravity, the $f(R)$ theory of gravity is the one simple theory that can sufficiently describe the properties of higher-order gravitational effects, by extending the gravitational Lagrangian as an arbitrary function of the Ricci scalar. In such theories a function of the Ricci scalar $f(R)$ is employed instead of R in the Einstein-Hilbert action[23, 24]. The general action for an $f(R)$ theory of gravity is given by,

$$(1.4) \qquad S = \frac{1}{2\kappa} \int \sqrt{-g} f(R) d^4 x.$$

To arrive at the field equation, the above action must be varied and the action can be varied in two ways[25]. One way is to vary it with respect to metric alone treating the metric as the only variable present. Second method is to treat both, the metric and connection, as variables and vary the action with respect to both in order to arrive at the field equation. The former is called the 'metric formalism' and the latter is called the 'Palatini formalism'. Accordingly there are primarily two types of $f(R)$ gravity, the metric $f(R)$ gravity and the Palatini $f(R)$ gravity. Incorporating these two $f(R)$ theories, there is a generalized theory called 'Metric-affine $f(R)$ gravity'. This comes out

if one uses the Palatini variation, but abandons the assumption that the matter action is independent of the connection. Under suitable assumptions, this theory would reduce either to metric or Palatini formalism. $f(R)$ theory of gravity can be treated as an easy-to-handle deviation from GTR that can be used to understand the principles and limitations of modified gravity. $f(R)$ theory of gravity makes a good toy model for two reasons[25]: a) they are sufficiently general to encapsulate some of the basic characteristics of higher-order gravity, but at the same time they are simple enough to be easy to handle and b) they are unique among higher-order gravity theories, in the sense that they seem to be the only ones which can avoid the long known and fatal Ostrogradski instability[26].

Other modifications of GTR includes the 'Brans-Dicke' theory[27], the 'Modified Quadratic Gravity' where higher order curvature terms are included in the action in addition to $f(R)$ term[28], the 'Variable G Theories' which are modifications of GTR where Newton's gravitational constant is promoted to a space-time function[29, 30], but the theory is found to break the equivalence principle. The theory of 'non-commutative geometry'[31, 32] is a gravitational theory that generalizes the continuum Riemannian manifold of Einstein's theory with the product of it with a tiny, discrete, finite non-commutative space, composed of only two points.

1.2.2 Massive gravity

An important class of modification of GTR that gain interest is the 'massive graviton' theories where the gravitational interaction is

propagated by a massive gauge boson called graviton with a mass, $m \neq 0$. From the perspective of the modern particle physics, GTR can be thought of as the unique theory of a massless spin-2 particle called graviton[33–35]. If the assumption behind the uniqueness theorem is broken, it can lead to alternative theories of gravity. Theories concerning the breaking of Lorentz invariance and spin have been explored in depth and representing gravity as a manifestation of a higher order spin, thereby maintaining the Lorentz invariance and spin has also been explored largely in the literature[36]. Yet another possibility that has been recently explored is the so called 'Massive Gravity' (MG) theory[37, 38]. In this model gravity is considered to be propagated by a massive spin-2 field. The theory gets complicated especially when the massive spin-2 field interacts with matter. In that case, the theory goes completely non-linear and consequently non-renormalizable. A non-self interacting massive graviton model was first suggested by Fierz and Pauli[39] which is now called the 'linear massive gravity'. However this model suffers from a pathology thereby ruling out the theory on the basis of solar system tests. Later, Vainshtein[40] proposed that the linear massive gravity model can be recovered to GTR through 'Vainshtein Mechanism' at small scales by including non-linear terms in the hypothetical massive gravity theory. But the Vainshtein mechanism is later found to suffer from the so called 'Boulware-Deser' (BD) ghost[41]. Recently it is shown by de Rham, Gabadadze and Tolly in their series of papers[42–44] that the BD ghost can be avoided for a sub-class of massive potentials. This is called dRGT massive gravity which includes dynamical and

9

fixed metrics. This holds true for its bi-gravity extension also[45]. The general action for a dRGT massive gravity is given by,

$$(1.5) \qquad S_{MG} = \frac{M_{Pl}^2}{2} \int d^4x \sqrt{-g} \left(R + \frac{m^2}{2} \sum_{n=0}^{\infty} \alpha_n \mathscr{L}_n[\mathscr{K}[g,f]] \right),$$

where,

$$(1.6) \qquad \mathscr{U} = -\frac{M_{Pl}^2}{4} \sqrt{-g} \sum_{n=0}^{\infty} \alpha_n \mathscr{L}_n[\mathscr{K}[g,f]],$$

is the overall potential of massive gravity, $\mathscr{K}$ corresponds to the extrinsic curvature and $\mathscr{L}[\mathscr{K}[g,f]]$ is the massive Lagrangian for dynamical variables $g_{\mu\nu}$ and $f_{\mu\nu}$. Along with these developments, other theories of massive gravity has been sprouting on the way. One is the 'New Massive Gravity' where a diffeomorphism and parity invariant theory in three dimensions is given[46]. In its original formalism, the action is given by,

$$(1.7) \qquad S_{NMG} = \frac{1}{\kappa^2} \int d^3x \sqrt{-g} \left[\sigma R + \frac{1}{m^2} \left(R_{\mu\nu} R^{\mu\nu} - \frac{3}{8} R^2 \right) \right],$$

where $\kappa = \frac{1}{M^3}$ defines the three dimensional Planck mass, $\sigma = \pm 1$ and m is the mass of the graviton. There are also formulations of 'Lorentz Violating Massive Theory'[47] of gravity and 'Non-local Massive Gravity'[48]. The Non-local massive gravity is formulated without any reference metric.

1.3 Black Holes

All the proposed theories discussed in the previous section will be valid and acceptable only if the theories are tested and proved. The best testing ground for any modified theory of gravity will be to search for black hole solutions. Before discussing the black hole solutions in ETG, the black hole solutions in GTR will be looked into first.

1.3.1 Black holes in general theory of relativity

Black Holes were conceptualized by Reverend Michell[49] in 1783 while searching for means to measure the mass of stars by evaluating the reduction in the speed of light due to the gravitational pull of the star. Michell reasoned that the maximal effect measurable would be limited by the escape velocity from the star, which is the speed of light. Any star more massive than this maximal limit would not permit light to escape from its surface (no constraint regarding the speed of light were proposed at that time) and were named 'Dark Stars'. Such stars would be dark since an outside observer would not be able to see it but its gravitational influence on nearby luminous objects could be observed and the relation between mass and radius of such stars would be $R = \sqrt{\frac{2GM}{c^2}}$. This method failed since light moved through space at constant speed regardless of the local strength of gravity. French mathematician Pierre-Simon Laplace also proposed the same idea a few years later in 1796.

The 'Dark Stars' are now called black holes and it took nearly two centuries after Michell to unleash the paradoxes present with regard to the concept of black holes. The physical concept of a black hole is the same as Michell and Laplace contemplated. A black hole is a massive object having an escape velocity that of light, that will absorb anything falling in and will emit nothing and hence would appear dark. The earliest and the simplest known example of a black hole with no spin and electric charge is the static spherically symmetric

11

Schwarzschild solution given by[50],

$$(1.8) \qquad ds^2 = -c^2\left(1 - \frac{r_h}{r}\right)dt^2 + \frac{1}{\left(1 - \frac{r_h}{r}\right)}dr^2 + r^2 d\Omega^2,$$

where $r_h = \frac{2GM}{c^2}$ is the horizon radius beyond which no information would be passed and indicate apparent singularities at $r = 0$ and at $r = r_h$ and $d\Omega^2 = d\theta^2 + \sin^2\theta d\phi^2$ is the standard line element on a two-sphere. This is called the Schwarzschild metric.

The Schwarzschild geometry was discovered by Karl Schwarzschild in the late 1915, at the same time as Einstein was approaching towards his final draft of GTR and then independently by Johannes Droste in 1916. The idea that Schwarzschild geometry describes a collapsed object called black hole was not realized when it was proposed. It was only in the 1950s that kind of realization came. The black holes are formed out of the gravitational collapse of a star. For most stars the gravitational collapse ends in a high density remnant called white dwarf. White dwarf's existence has been known even before 1915. However the physical mechanism by which the internal pressure of such a dense object was balanced, was a mystery. In 1926 Fowler realized that white dwarfs are held by electron degeneracy pressure. Due to the Pauli exclusion principle, the electrons take up a high characteristic Fermi energy and the energy levels are widely spaced in a white dwarf.

In 1931, S. Chandrasekhar[51, 52] realized that as the mass of the white dwarf increases it becomes denser and the gravitational field will get stronger. He proposed a critical mass of $1.4M_\odot$ called Chan-

drasekhar limit beyond which gravity would overwhelm the degeneracy pressure and then no stable solution would be possible and the gravitational collapse would continue. After the discovery of neutron it was realized that at some stage during the collapse it is possible to form neutron out of electron-proton interaction and would lead to a 'neutron star' in which pressure is supported by the neutron degeneracy pressure. There exists a maximum mass limit above which no stable neutron star configuration is possible and stars having mass above this maximum would collapse to form black holes. This maximum mass limit given by $3M_\odot$ is called the Oppenheimer-Volkoff limit.

Schwarzschild black hole is the simplest black hole with only mass and no spin or electric charge. A static spherically symmetric metric with mass(M) and electric charge(Q) was given independently by Hans Reissner[53] (1916), Hermann Weyl[54] (1917), and Gunnar Nordstrom[55] (1918) and is called Reissner-Nordstrom geometry,

$$(1.9) \qquad ds^2 = -c^2 \Delta dt^2 + \Delta^{-1} dr^2 + r^2 d\Omega^2,$$

where Δ is the horizon function given by,

$$(1.10) \qquad \Delta \equiv 1 - \frac{2GM}{c^2 r} + \frac{Q^2}{r^2}.$$

The black hole solution coming out of this geometry is called as Reissner-Nordstrom black hole. Even though this was proposed earlier, the meaning of this geometry was only lately clarified in 1960 by Graves and Brill[56]. Unlike Schwarzschild geometry, Reissner-

Nordstrom space-time has two horizons:

$$(1.11) \qquad r_{\pm} = M \pm \sqrt{M^2 - Q^2}.$$

The geometry of a spinning and uncharged black hole was found out unexpectedly by Roy Kerr[57] in 1963. Later this work was extended to include the charge by Newmann[58] in 1965. He proposed a rotating black hole with electric charge. This was later called as Kerr-Newmann geometry and is given by,

(1.12)
$$ds^2 = -\frac{R^2 \Delta}{\rho^2} \left(dt - a\sin^2\theta d\phi \right)^2 + \frac{\rho^2}{R^2 \Delta} dr^2 + \rho^2 d\theta^2 + \frac{R^4 \sin^2\theta}{\rho^2} \left(d\phi - \frac{a}{R^2} dt \right)^2,$$

where R and ρ are given by,

$$(1.13) \qquad R \equiv \sqrt{r^2 + a^2}, \; \rho \equiv \sqrt{r^2 + a^2 \cos^2\theta},$$

Δ is the horizon function given by,

$$(1.14) \qquad \Delta \equiv 1 - \frac{2GMr}{c^2 R^2} + \frac{Q^2}{R^2},$$

and a is the spin parameter.

Since black hole solutions are one important aspect of GTR, any modifications of GTR are expected to afford black hole solutions that would lead to black hole solutions in GTR in the weak field limit.

1.3.2 Black holes in massive gravity

A plethora of works have been done on black hole solutions in massive gravity. It has also been observed that massive gravity admits more number of spherically symmetric solutions than in GTR that may or may not be physically feasible ones. Generally the massive gravity

theory is described by the Lagrangian density of the form[59],

$$(1.15) \qquad \mathcal{L} = \frac{\sqrt{-g}}{2\kappa^2} \left(R + m^2 \mathcal{U}(g, \phi^a) \right),$$

where ϕ^a is the scalar field with,

$$(1.16) \qquad \mathcal{U} = \mathcal{U}_2 + \alpha_3 \mathcal{U}_3 + \alpha_4 \mathcal{U}_4,$$

$$(1.17) \qquad \mathcal{U}_2 = [\mathcal{K}]^2 - [\mathcal{K}^2],$$

$$(1.18) \qquad \mathcal{U}_3 = [\mathcal{K}]^3 - 3[\mathcal{K}][\mathcal{K}^2] + 2[\mathcal{K}^3],$$

$$(1.19) \qquad \mathcal{U}_4 = [\mathcal{K}]^4 - 6[\mathcal{K}]^2[\mathcal{K}^2] + 8[\mathcal{K}^3][\mathcal{K}] + 3[\mathcal{K}^2]^2 - 6[\mathcal{K}^4],$$

$$(1.20) \qquad \mathcal{K}^\mu_\nu = \delta^\mu_\nu - \sqrt{g^{\mu\alpha} f_{ab} \partial_\alpha \phi^a \partial_\nu \phi^b},$$

$[\mathcal{K}] = Tr(\mathcal{K}) = \mathcal{K}^\mu_\mu$ and f_{ab} is the fiducial metric (reference metric). The four scalar field ϕ^a are the Stückelberg scalars, introduced to restore the general covariance of the theory. $\mathcal{U}$ can be recognized as symmetric polynomials of $\mathcal{K}$. It is constructed in such a way that the theory admits the Minkowski background, $g_{\mu\nu} = \eta_{\mu\nu}$, $\phi^a = x^\mu \delta^a_\mu$.

Even though there are more number of solutions in this theory when compared to GTR, in order to check whether the theory leads to GTR when the mass of the graviton tends to zero, it would be helpful to consider the solutions that are common in both. For this purpose, considering the black hole solution in de Sitter space-time, the equation of motion in empty space is obtained as[60],

$$(1.21) \qquad G_{\mu\nu} + m^2 X_{\mu\nu} = 0,$$

15

where $G_{\mu\nu}$ is the Einstein tensor and,

(1.22)

$$
X_{\mu\nu} = -\frac{1}{2}[\mathcal{K} g_{\mu\nu} - \mathcal{K}_{\mu\nu} + \alpha(\mathcal{K}_{\mu\nu}^2 - \mathcal{K} \mathcal{K}_{\mu\nu} +
$$
$$
\frac{1}{2} g_{\mu\nu}([\mathcal{K}]^2 - [\mathcal{K}^2])) + 6\beta(\mathcal{K}_{\mu\nu}^3 - \mathcal{K} \mathcal{K}_{\mu\nu}^2 +
$$
$$
\frac{1}{2} \mathcal{K}_{\mu\nu}([\mathcal{K}]^2 - [\mathcal{K}^2]) - \frac{1}{6} g_{\mu\nu}([\mathcal{K}]^3 - 3[\mathcal{K}][\mathcal{K}^2] + 2[\mathcal{K}^3]))].
$$

The constraint on the metric can be obtained from Bianchi identity as,

(1.23)
$$
m^2 \nabla^\mu X_{\mu\nu} = 0.
$$

By employing additional constraints on the parameters α and β, the solutions can be obtained. An exact de Sitter solution will be obtained if we take,

(1.24)
$$
m^2 X_{\mu\nu} = \lambda g_{\mu\nu},
$$

where λ is a constant. The solution of (1.21) satisfying the condition given by (1.23) can be obtained as,

(1.25)
$$
ds^2 = -\kappa^2 dt^2 + \left(\frac{\alpha}{\alpha+1} dr \pm \kappa \sqrt{\frac{2}{3\alpha}} \frac{\alpha}{\alpha+1} mrdt \right)^2 + \frac{\alpha^2}{(\alpha+1)^2} r^2 d\Omega^2,
$$

where κ is an integration constant and α is positive and arbitrary.

Similarly Reissner-Nordstrom solution on de Sitter space-time in ghost free massive gravity coupled to Maxwell's theory of electromagnetism can be obtained under the restriction that $\beta = -\alpha^2/6$ as[59],

(1.26) $ds^2 = -dt^2 + \left(\tilde{\alpha} dr \pm \sqrt{\frac{r_g}{2r} + \frac{2\tilde{\alpha}^2}{3\alpha} m^2 r^2 - \frac{\tilde{Q}^2}{\tilde{\alpha}^4 r^2}} \, dt \right)^2 + \tilde{\alpha}^2 r^2 d\Omega^2,$

where $\tilde{\alpha} \equiv \frac{\alpha}{\alpha+1}$, r_g is an integration constant and the electromagnetic field, $E = \frac{\tilde{Q}}{r^2}$ and $B = 0$. Upon re-scaling the above metric as,

(1.27)
$$r \to \frac{r}{\tilde{\alpha}},$$

(1.28)
$$dt \to dt + f'(r)dr,$$

with,

$$f'(r) \equiv \frac{-g_{01}}{g_{00}} = \pm \frac{\sqrt{\frac{r_g}{r} + \frac{2}{3\alpha}m^2r^2 + \frac{\tilde{Q}^2}{\tilde{\alpha}^2r^2}}}{1 - \frac{r_g}{r} - \frac{2}{3\alpha}m^2r^2 + \frac{\tilde{Q}^2}{\tilde{\alpha}^2r^2}},$$

leads to the form,

(1.29)
$$ds^2 = -\left(1 - \frac{r_g}{r} - \frac{2}{3\alpha}m^2r^2 + \frac{\tilde{Q}^2}{\tilde{\alpha}^2r^2}\right)dt^2 + \frac{dr^2}{1 - \frac{r_g}{r} - \frac{2}{3\alpha}m^2r^2 + \frac{\tilde{Q}^2}{\tilde{\alpha}^2r^2}} + r^2d\Omega^2,$$

which is the familiar form of the metric for a Reissner-Nordstrom (AdS) black hole in GTR. Now using the choice of parameter $\beta = -\frac{\alpha^2}{8}$, we get the metric given by,

(1.30)
$$\begin{aligned}
ds^2 = &-\frac{(\alpha+2)^3\alpha^2}{(\alpha+2)^5 + \alpha^5\delta}\left(1 - \frac{r_g(\alpha+2)}{r\alpha}\right)dt^2 \\
&\pm \frac{2\alpha(\alpha+2)}{(\alpha+2)^5 + \alpha^5\delta}\sqrt{\frac{r_g^2(\alpha+2)^6}{r^2} + \frac{r_g\alpha^6\delta}{r}}\,dtdr \\
&+ \frac{\alpha^2}{(\alpha+2)^2}\left(1 + \frac{r_g(\alpha+2)^6}{\alpha r((\alpha+2)^5 + \alpha^5\delta)}\right)dr^2 + \frac{\alpha^2r^2}{(\alpha+2)^2}d\Omega^2.
\end{aligned}$$

The transformation of coordinates given by,

(1.31)
$$r \to \frac{\alpha+2}{\alpha r}$$

(1.32) $dt \to \zeta(dt + f'(r)dr)$ with $\zeta^2 \equiv \frac{(\alpha+2)^2}{\alpha^2} + \frac{\alpha^3}{(\alpha+2)^3}\delta,$

leads to the metric,

(1.33)
$$ds^2 = -(1 - \frac{r_g}{r})dt^2 + \frac{dr^2}{1 - \frac{r_g}{r}} + r^2d\Omega^2,$$

17

which is Schwarzschild-like. In $f(R)$ theory of gravity also there are black hole solutions, some of which are the familiar ones in GTR. Black hole solution coming out of the Lagrangian $R + aR^2$ where, a is a constant parameter, is studied in the work of B. Whitt[61]. It was found that Schwarzschild solution is the only static spherically symmetric solution and such black holes have no hair. Also solutions for which $R = (-2a)^{-1}$, have no counterparts in the conformally related theory (GTR). Modified gravity model with Lagrangian $R + aR^2 - 2\Lambda$, where Λ is the cosmological constant, is studied in detail in the work of Cognola et al[62]. In their work they have discussed of a class of constant curvature ($R = R_0$) solutions,

$$(1.34) \qquad\qquad R_0 \;\; = \;\; 4\Lambda$$

$$(1.35) \qquad\qquad R_0^2 \;\; = \;\; 3\mu_1,$$

where μ_1 is a constant parameter. Such classes contain $4-$dimensional black hole solutions in the presence of a non vanishing cosmological constant, like the Schwarzschild-(Anti) de Sitter solutions and all the topological solutions associated with a negative Λ_{eff}, where $\Lambda_{eff} = \frac{R_0}{4}$. For metric $f(R)$ theories without constant curvature Jebsen-Birkhoff theorem does not hold and therefore other black hole solutions exist in a general metric $f(R)$ gravity. The existence of Kerr black holes have been discussed in the work of Dimitrios Psaltis et al.[63].

1.4 Black Holes and Quasi Normal Modes

The existence of black holes is an outcome of Einstein's General Theory of Relativity (GTR). The question then is how to realize their existence and one natural way to identify them is to try to perturb and know their responses to the perturbation (scalar, electromagnetic, Fermi or gravitational). Regge and Wheeler started way back in 1950s studying perturbations of black hole space-time[64] and later, serious studies were initiated by Zerilli and then by Kip S. Thorne and his collaborators[65]. While studying the black hole perturbations, Zerilli aimed at searching for the stability issues of black holes under small perturbations.

1.4.1 Linear perturbations of black holes

Black hole perturbation is analyzed by first considering the unperturbed metric which for a Schwarzschild black hole is,

$$
\begin{aligned}
ds^2 &= g^{\circ}_{\mu\nu}dx^{\mu}dx^{\nu} \\
&\equiv -\left(1-\frac{2M}{r}\right)dt^2 + \left(1-\frac{2M}{r}\right)^{-1}dr^2 + r^2 d\Omega^2.
\end{aligned}
$$
(1.36)

Here the values of G and c are taken to be unity and $g^{\circ}_{\mu\nu}$ represents the metric in background static space-time. Now, upon this static space-time, if a small perturbation, $h_{\mu\nu}$ is introduced, the metric will become,

$$
g_{\mu\nu} = g^{\circ}_{\mu\nu} + h_{\mu\nu}.
$$
(1.37)

Since the background is static and taken to be vacuum the Einstein tensor for vacuum can be written as,

$$
R^{\circ}_{\mu\nu} = 0.
$$
(1.38)

where $R^{\circ}_{\mu\nu}$ is the Ricci tensor for the static background. With the above condition the field equation for the perturbed space-time will be obtained as,

$$\delta R_{\mu\nu} = 0. \tag{1.39}$$

Using the tensor spherical harmonics with axial and polar terms, the perturbations are be of two types:

1. Odd-parity perturbations

2. Even-parity perturbations

and accordingly there are two solutions to the metric $h_{\mu\nu}$. For odd-parity perturbations, the Einstein equation along with *Regge-Wheeler* gauge leads to the equations given by[64],

$$0 = \frac{\partial^2 Q}{\partial t^2} - \frac{\partial^2 Q}{\partial r_*^2} + \left(1 - \frac{2M}{r}\right)\left[\frac{l(l+1)}{r^2} - \frac{6M}{r^3}\right]Q, \tag{1.40}$$

$$\frac{\partial h_0}{\partial t} = \frac{\partial}{\partial r_*}(r_* Q), \tag{1.41}$$

where,

$$Q = \frac{h_1}{r}\left(1 - \frac{2M}{r}\right), \tag{1.42}$$

and,

$$r_* \equiv r + 2M \ln\left(\frac{r}{2M} - 1\right), \tag{1.43}$$

is the tortoise coordinate, and h_0, h_1 are unknown functions that can be suitably chosen.(1.40) is called Regge-Wheeler equation and can be considered to be a wave equation in a scattering potential barrier with potential $V(r)$ given as,

$$V(r) = \left(1 - \frac{2M}{r}\right)\left[\frac{l(l+1)}{r^2} - \frac{6M}{r^3}\right]. \tag{1.44}$$

20

Even-parity perturbation leads to the *Zerilli Equation*[65],

$$(1.45) \qquad \frac{\partial^2 Z}{\partial t^2} - \frac{\partial^2 Z}{\partial r_*^2} + \tilde{V}Z = 0,$$

where Z is the Zerilli function given by,

$$(1.46) \qquad Z \equiv \frac{4re^{-4\lambda}k_2 + l(l+1)rk_1}{l(l+1) - 2 + 6M/r},$$

where $e^{-\lambda} = 1 - \frac{2M}{r}$ and k_1, k_2 are functions just like h_0 and h_1 in the odd-parity case, that can be chosen. The Zerilli equation can be considered to be a wave equation with a scattering potential barrier,

$$(1.47) \qquad \tilde{V} = \left(1 - \frac{2M}{r}\right)\left[\frac{2q(q+1)r^3 + 6q^2Mr^2 + 18qM^2r + 18M^3}{r^3(qr + 3M)^2}\right],$$

where $q \equiv (l-1)(l+2)/2$. It is possible to transform the axial solution in to polar solution by suitable differential operators.

Linear perturbation of black hole resulted in the wave equations (1.40) and (1.45) and it was Vishveshwara[66] who first noticed the existence of quasinormal modes (QNMs) under linear perturbation of black holes.

1.4.2 Quasi normal modes

Vishveshwara had proposed the existence of QNMs by studying the scattering of GWs by Schwarzschild black holes. Later, the scattering of scalar, electromagnetic and Fermi fields by different black hole space-times have been studied by many[67–70] and references cited therein. In the frame work of GTR, QNMs arise as perturbations of black hole space-times. QNMs are the solutions to perturbation equations and they are distinguished from normal modes because they decay at certain rates having complex frequencies. The remarkable

property of the black hole QNMs (also called ring down of black holes) is that their frequencies are determined only by the mass, angular momentum and charge (if any) of black holes. The QNMs are independent of the perturbations that produce it. Black holes can be detected by observing the QNMs through GWs. When a star collapses to form a black hole or when two black holes collide or a black hole and a star collide, gravitational waves (GWs) are emitted. As a result, a black hole with higher mass that absorbs the emitted GWs is formed[71]. Hence the emitted GWs decay quickly. The decay of oscillations are characterized by complex frequencies which are called as $QNMs$. Since QNMs are not stationary modes and they exponentially decrease, the black hole space-time will radiate energy away to infinity through gravitational waves. Thus, QNMs indicate the '*Characteristic Sound*' of a black hole.

The propagation of waves in black hole space-times can in general be represented as,

$$\frac{\partial^2 \Psi}{\partial r^2} - \frac{\partial^2 \Psi}{\partial t^2} - V\Psi = 0, \tag{1.48}$$

where V is the r-dependent potential. The horizon of black hole space-time is taken to be at $-\infty$. Employing a variable separation given by,

$$\Psi(t,r) = e^{-i\omega t}\phi(r), \tag{1.49}$$

where ω is the Quasi Normal (QN) frequency, leads to the radial part of wave equation,

$$\frac{\partial^2 \phi}{\partial r^2} + \left(\omega^2 - V\right)\phi = 0. \tag{1.50}$$

The boundary conditions of QNMs are that the solutions should be purely outgoing at infinity ($r = +\infty$) and ingoing at the horizon ($r = -\infty$), meaning entering in to the black hole, ie.,

$$(1.51) \qquad\qquad \phi \quad \sim \quad e^{-i\omega r}, \ r \to -\infty$$

$$(1.52) \qquad\qquad \phi \quad \sim \quad e^{i\omega r}, \ r \to +\infty.$$

Vishveshwara proved that the QN frequency for a Schwarzschild space-time possesses negative imaginary part. This means, on the one hand the QNMs are decreasing exponentially in time and on the other the black hole space-time is loosing its energy in the form of gravitational waves.

Analytical solutions have been obtained for different black hole space-times using WKB method by S. Iyer and C. M. Will[72–74]. As the space-time gets complicated, it is difficult to obtain analytical solutions. Therefore several attempts have been made to calculate QNMs numerically. After these pioneering works, perturbation calculations have been done by many to get QNM oscillations. A semi-analytic method has then been explored[75] that has its own limitations of accuracy. Later, the Continued Fraction Method (CFM) was proposed by Leaver[76]. This method is a hybrid of analytic and numerical and can calculate QNM frequencies by making use of analytic infinite series representation of solution. The WKB approximation is very commonly employed and a powerful one too. However all these methods have their own limitations. In recent years a new approach has been introduced to study black hole QNMs called Asymptotic Iteration Method (AIM) which is previously used to solve eigenvalue

problems[77, 78]. This method has been shown to be efficient and accurate for calculating QNMs of black holes[79].

1.5 Thermodynamics of Black Holes

Interests in the black hole thermodynamics initially sprouted when it was found that black holes in classical GTR obey laws that are analogous to the laws of thermodynamics. This was initiated by Hawking[80] who proposed that the area of the black hole event horizon never decreases. This is analogous to the second law of thermodynamics with area of event horizon playing the role of entropy in thermodynamics where it is stated that the entropy never decreases. This analogy, together with the fact that information is irretrievably lost after the horizon led Bekenstein[81] to propose that the black hole entropy is proportional to the area of event horizon. However, there came inconsistencies when the idea that a black hole absorbs everything that falling into it but emit nothing violates second law of thermodynamics. This is solved when quantum effects are taken in to consideration where a black hole would create and emit particles as if it were a hot body with a temperature of $\frac{\kappa}{2\pi}$, called 'Hawking Temperature'[82, 83]. Then, Hawking[84] proposed that black holes actually radiate and called it as 'Hawking radiation' This is analogous to the zeroth law of thermodynamics where the quantity κ, called as surface gravity on the horizon, is a constant for a black hole. An analogous first law in black hole mechanics is also proposed. This first law relates the change in the parameters Mass (M), Horizon area (A) and the angular momentum (J) for a rotating black hole when

perturbed. The relation is given as,

$$(1.53) \qquad \delta M = \frac{\kappa}{8\pi} A + \Omega \delta J,$$

where Ω is the angular velocity of the rotating black hole. With all these factors the black hole can be considered to be a thermodynamic object with :

1. Entropy proportional to the area of event horizon: $S = \frac{A}{4}$,

2. Temperature proportional to the surface gravity: $T = \frac{\kappa}{2\pi}$,

3. Internal energy proportional to the mass: $H = M$,

and the laws of Black hole mechanics can be stated as[85, 86] :

Zeroth law : Surface gravity is constant over the event horizon.

First law : Differences in mass between nearby solutions are equal to differences in area times the surface gravity plus additional work-type terms.

Second law : The area of the event horizon never decreases in any physical process provided the energy of matter is positive and space-time is regular[80, 81].

Third law : No procedure can reduce the surface gravity to zero by a finite number of steps.

An immediate consequence of these studies is that they bring together quantum theory, gravity and thermodynamics and one can hope for a quantum theory of gravity. Black hole thermodynamics in different space-times based on GTR has been explored widely in the literature starting from Hawking[87].

In thermal systems, Van der Waals equation modifies the equation of state for an ideal gas to one that approximates the behavior of real

fluids and is given by,

$$(1.54) \qquad \left(P + \frac{a}{v^2}\right)(v - b) = T,$$

where P is the pressure, v is the specific volume and a and b are constants. In such fluids, the critical point occur at $T = T_c$ where P would have an inflection point at $P = P_c$ and $v = v_c$ and obey the universal relation $\frac{P_c v_c}{kT_c} = \frac{3}{8} = 0.375$ for any fluid. A liquid/gas phase transition takes place at temperatures $T < T_c$ and obeys *Maxwell's equal area law* which states that the two phases co-exist when the areas above and below a line of constant pressure drawn through a $P - V$ curve are equal.

An interesting observation noted while studying charged black holes was that they behave as Van der Waals fluid. Thus the thermodynamic studies of black holes led to a novel perspective 'Phase Transition' in black holes.

1.6 Holographic Entanglement Entropy of Black Holes

The study of thermodynamics led people into the study the most important factor in thermodynamics, called entropy. The black hole entropy was first calculated by Bekenstein[81, 83, 88] and is called 'Bekenstein-Hawking' entropy. Unlike the usual thermal entropy that is proportional to the volume, the important feature of Bekenstein-Hawking entropy is that it is proportional to the area of the horizon. The question why black holes have entropy then became one of the mysteries in modern physics[89]. One such move to address

the question is made by the concept of entanglement entropy (EE). Entanglement is one of the most non-classical feature of quantum mechanics and is microscopic in nature. It was first recognized by 't Hooft[90] that EE could also play a pivotal role in understanding the microscopic origin of the black hole entropy and for solving the information puzzle in black hole physics. A quantum state in a black hole geometry is divided by the horizon into two disconnected parts, and an external observer has to trace over the part of the state in the black hole interior[91]. One interesting point to note about the entanglement entropy is that, like Bekenstein-Hawking entropy, EE also scales like the area of the bounding surface and the entanglement entropy behaves in a similar fashion as the thermal entropy. The holographic entanglement entropy which relates the holographic understanding of entanglement entropy in the AdS/CFT correspondence is given by[92],

$$(1.55) \qquad\qquad S_{ent} = \frac{\gamma}{4G_N^{(d+2)}},$$

where γ is the d dimensional minimal surface whose boundary is given by $(d-1)$ dimensional manifold $\partial\gamma = \partial A$, where A is the area of the surface. Entanglement entropy, also called as von Neumann entropy is UV divergent with the leading divergence being given by the area of the entangling surface. However, a finite part of EE contains non-trivial information about the quantum state and most of the analysis of EE considers this finite region[93]. Studies on the holographic entanglement entropy and the associated phase transition are done in the literature[94] and references cited therein. The

27

behavior of entanglement entropy near first and second order phase transition is dealt in the aforesaid work. It was found that corresponding to the Hawking Page first order phase transition showed a jump in the entanglement entropy which is due to the increase in number of degrees of freedom to a phase where the entropy rises with the temperature. The temperature from entanglement and Hawking temperature are found to be matching with each other for almost all black hole space-times[95]. Thus, the study of entanglement entropy may help in constructing a quantum theory of gravity and therefore is relevant in the realm of massive gravity.

1.7 Gravitational Waves

For GTR, to be compatible with special theory of relativity, the notion of gravity must be causal meaning that any change to a gravitating source must be communicated to distant observers with a speed not faster than that of light, c. This immediately leads to the idea that there should exist the so called Gravitational radiation or 'Gravitational Waves'(GWs). The GW equation is obtained by linearizing Einstein's field equations[96] assuming that the space-time metric $g_{\mu\nu}$ deviates only slightly from the flat space-time metric $\eta_{\mu\nu}$,

$$(1.56) \qquad g_{\mu\nu} = \eta_{\mu\nu} + h_{\mu\nu}, \quad \| h_{\mu\nu} \| \ll 1,$$

where $\eta_{\mu\nu}$ is given to be diag$(-1,1,1,1)$. The condition $\| h_{\mu\nu} \| \ll 1$ means that the field is weak. In this process only the terms that are linear in $h_{\mu\nu}$ would be considered and higher orders of $h_{\mu\nu}$ would be neglected. The Christoffel symbol is then given by,

$$(1.57) \qquad \Gamma^{\mu}_{\nu\alpha} = \frac{1}{2}\left(\partial_{\alpha}h^{\mu}_{\nu} + \partial_{\nu}h^{\mu}_{\alpha} - \partial^{\mu}h_{\nu\alpha}\right).$$

The Riemann curvature tensor can be obtained from the Christoffel symbols as,

$$\begin{aligned}
R^{\mu}_{\ \nu\alpha\beta} &= \partial\Gamma^{\mu}_{\nu\beta} - \partial_{\beta}\Gamma^{\mu}_{\nu\alpha} \\
&= \frac{1}{2}\left(\partial_{\alpha}\partial_{\nu}h^{\mu}_{\ \beta} + \partial_{\beta}\partial^{\mu}h_{\nu\alpha} - \partial_{\alpha}\partial^{\mu}h_{\nu\beta} - \partial_{\beta}\partial_{\nu}h^{\mu}_{\ \alpha}\right).
\end{aligned}$$

(1.58)

From (1.58), the Ricci tensor can be constructed as,

$$\begin{aligned}
R_{\mu\nu} &= R^{\alpha}_{\ \mu\alpha\nu} \\
&= \frac{1}{2}\left(\partial_{\alpha}\partial_{\nu}h^{\alpha}_{\ \mu} + \partial^{\alpha}\partial_{\mu}h_{\nu\alpha} - \Box h_{\mu\nu} - \partial_{\mu}\partial_{\nu}h\right),
\end{aligned}$$

(1.59)

where $\Box = \partial_{\alpha}\partial^{\alpha} = \nabla^2 - \partial_t^2$ is the wave operator and the Ricci scalar can be obtained as,

$$\begin{aligned}
R &= R^{\mu}_{\ \mu} \\
&= \partial_{\alpha}\partial^{\mu}h^{\alpha}_{\ \mu} - \Box h.
\end{aligned}$$

(1.60)

Now, the Einstein tensor can be written as,

$$\begin{aligned}
G_{\mu\nu} &= R_{\mu\nu} - \frac{1}{2}\eta_{\mu\nu}R \\
&= \frac{1}{2}(\partial_{\alpha}\partial_{\nu}h^{\alpha}_{\ \mu} + \partial^{\alpha}\partial_{\mu}h_{\nu\alpha} - \Box h_{\mu\nu} - \\
&\quad \partial_{\mu}\partial_{\nu}h - \eta_{\mu\nu}\partial_{\alpha}\partial^{\beta}h^{\alpha}_{\ \beta} + \eta_{\mu\nu}\Box h).
\end{aligned}$$

(1.61)

The rather messy equation above can be simplified by using the trace reversed perturbation $\bar{h}_{\mu\nu} = h_{\mu\nu} - \frac{1}{2}\eta_{\mu\nu}h$ instead of $h_{\mu\nu}$[97]. Then the Einstein tensor would become,

$$G_{\mu\nu} = \frac{1}{2}\left(\partial_{\alpha}\partial_{\nu}\bar{h}^{\alpha}_{\ \mu} + \partial^{\alpha}\partial_{\mu}\bar{h}_{\nu\alpha} - \Box\bar{h}_{\mu\nu} - \eta_{\mu\nu}\partial_{\alpha}\partial^{\beta}\bar{h}^{\alpha}_{\ \beta}\right).$$

(1.62)

This equation can be further simplified by employing the coordinate transformation given by,

$$x'^a = x^a + \xi^a,$$

(1.63)

where $\xi(x^b)$ is an arbitrary infinitesimal vector field and the Lorentz gauge condition,

$$(1.64) \qquad \partial^\mu h_{\mu\nu} = 0.$$

Einstein tensor would then become,

$$(1.65) \qquad G_{\mu\nu} = -\frac{1}{2}\Box\bar{h}_{\mu\nu},$$

Now (1.2) implies[98],

$$(1.66) \qquad \Box\bar{h}_{\mu\nu} = -16\pi T_{\mu\nu},$$

and in vacuum, this can be written as,

$$(1.67) \qquad \Box\bar{h}_{\mu\nu} = 0.$$

This is in the form of a wave equation that admits homogenous solutions which are superposition of plane waves whose real part can be represented as,

$$(1.68) \qquad \bar{h}_{\mu\nu} = \mathscr{R}e\int A(k)e^{i(\mathbf{k.x}-\omega t)}d^3k,$$

where $\mathbf{k}$ is the propagation vector and ω corresponds to the frequency. The equation (1.67), can be written as,

$$(1.69) \qquad \eta_{\mu\nu}\bar{h}_{\mu\nu}^{,\mu\nu} = 0,$$

along with (1.68) implies that,

$$(1.70) \qquad k^\mu k_\mu = 0,$$

which means that the emanated waves travels with the speed of light. If we denote the perturbation $\bar{h}_{\mu\nu}$ in the Transverse Traceless(TT)

gauge[97] as $h_{\mu\nu}^{TT}$, relation between Riemann curvature tensor and metric perturbation can be written as,

$$(1.71) \qquad\qquad R_{\mu t \nu t} = -\frac{1}{2}\ddot{h}_{\mu\nu}^{TT},$$

where t is the time and $\ddot{h}_{\mu\nu}^{TT}$ is the second derivative of $h_{\mu\nu}^{TT}$ with respect to t. Consider a monochromatic plane wave traveling in the z direction,

$$(1.72) \qquad\qquad h_{\mu\nu}^{TT} = h_{\mu\nu}^{TT}(t-z).$$

(1.72) will be a solution to the wave equation $\Box h_{\mu\nu}^{TT} = 0$. The Lorentz gauge condition demands $h_{\mu\nu}^{TT}(t-z)$ to be a constant, ie.,

$$(1.73) \qquad\qquad h_{\mu\nu}^{TT}(t-z) = \; constant,$$

and for the wave propagating along the z direction, the constant is zero if $\mu = 0$ or $\mu = z$. This, in turn implies that the wave will be transverse in nature and hence will have two polarizations. Since $h_{\mu\nu}^{TT}(t-z) = 0$, the independent polarizations, taking into account the symmetry and trace-free condition, can be written as,

$$(1.74) \qquad\qquad h_{xx}^{TT} \;\; = \;\; -h_{yy}^{TT} \equiv h_+(t-z),$$

$$(1.75) \qquad\qquad h_{yy}^{TT} \;\; = \;\; h_{xx}^{TT} \equiv h_\times(t-z).$$

Thus, h_+ and $h_\times$ are the two waveforms of the GWs called as 'Plus' and 'Cross' polarizations respectively.

The calculation of gravitational waves in GTR was firstly done by Einstein. Einstein's calculation result stands today as the leading-order "quadrupole formula" for gravitational waves. This formula

plays a key role in gravitation analogous to the dipole formula for electromagnetic radiation, showing that gravitational waves arise from accelerated masses in the same way as electromagnetic waves arise from accelerated charges. From the quadrupole formula it can be understood that it is difficult to produce GWs in the laboratory since large masses moving at relativistic speeds are needed for its production. This is due to the weakness of the gravitational interaction. A consequence of this is that only astrophysical objects that are massive and relativistic enough can generate detectable GWs[99].

Indirect evidence for GWs has been obtained earlier since the discovery of *Hulse-Taylor* pulsar, but it took almost a century to detect the GWs based on GTR directly. The first detection has been reported from binary black hole merger by Advanced LIGO[100]. A second detection has also been reported from black hole merger much more stronger than the first one by LIGO[101]. LIGO serves as the center of attraction for future research in Gravitational Wave astronomy. LIGO has got three specialized Michelson interferometers located at two sites a) Hanford, 4km-long H1 and 2km long H2 detector b) at Livingston, a 4km long L1 detector. There are, however other detectors built around the globe such as VIRGO (Italy), GE600 (Germany), TAMA (Japan) etc which are laser interferometers and also antenna detectors such as *Explorer*, *Nautilus* etc. The VIRGO detector in Italy has a sensitivity[102] of 10^{-19} and LIGO in USA has reached a linearly polarized strain amplitude of the order[103] of 10^{-24}. The sensitivity of LIGO is at least 10 times better than a resonant bar.

However, the resonant bar observatory can play a significant role when the more sensitive network of interferometric detectors fails to make a detection by itself. "Spherical antenna detectors" are an improved version of their resonant bar detectors where the bars are replaced by solid spheres. They were proposed in the 1970s by Weber [104] and are useful to study the interaction of GWs with matter. The theoretical frame work for the detection of GWs using spherical antenna had already been developed[105–107]. Interest in experimental research in resonant spheres has been increased over the past years and today spherical antenna is recognized as the new generation of gravitational resonant detectors to complement the existing cylindrical antenna. Spherical detectors have the following properties: (1) relatively large energy cross section, (2) isotropic sky coverage and (3) directional sensitivity [108].

Nevertheless, GTR is still not adequate since it could not explain the cosmological late time-acceleration of the universe and the unification of gravity with quantum theory still remains as a problem with GTR. ETG form the future hope in directing the research in unifying gravity and quantum theory. GWs form one of the most important phenomena where one could check the validity of a new theory of gravity. However, currently LIGO is not designed to detect any polarization other than $+$ and $\times$ or their mixture. No studies were done aimed at constraining parameters corresponding to any alternative theories of gravity associated with the discovery of GWs due to the lack of predictions for what the inspiral-merger-ringdown GW signal

should look like in those cases. For these reasons, the generation of GWs based on ETG are catching interests of researchers.

1.8 Outline of the Thesis

General theory of relativity put forward by Einstein could not explain the recent late-time acceleration of the universe. Hence there is a strong motivation for the development of a modification of the GTR. And a plethora of works has been going on in this direction. The theories are generally called 'Extended Theories of Gravity' or Modified Theories of Gravity. One of these modifications to GTR are done by adding higher order invariants to the Einstein-Hilbert action. Of the so called Extended theories of gravity the class of gravity called 'Massive Gravity' gains more attention nowadays. In massive gravity theories, the action contains a term having a massive graviton.

These theories are found The best testing ground for massive gravity or any modified gravity would be a black hole. Just like the GTR, modified theories also provide black hole solutions. To check the validity of such theories it is worth looking for the existence of the black holes proposed by the theory. One way to check for the existence of black holes is to search for its Quasi Normal Modes (QNMs). Black holes can be detected by observing the QNMs through gravitational waves. The analogy of black hole mechanics with the classical thermodynamics also emerging as a new area of interest. Accordingly the thermodynamics of black holes show different behavior for different theories of gravity. Study of thermodynamics of black holes may help in constructing the theory of quantum gravity . Another way to check

the validity of such theories would be to check for the additional polarizations that the theory suggest in the Gravitational waves emanated from cosmic events such as black hole collision, supernovae explosion etc. With the discovery of GWs from black hole collision recently, this method offers a direct way to check such theories.

In this thesis, the studies on some of the aspects of GWs and black holes in Massive Gravity are done. The QNMs, the thermodynamic behavior and the holographic entanglement entropy of $(3+1)$ dimensional black hole solutions in dRGT massive gravity are studied. The thermodynamical aspects and behavior of QNMs are then studied for $(2+1)$ dimensional black hole solution in massive gravity. The QNMs are calculated numerically using The Improved Asymptotic Iteration Method (Improved AIM). The possibilities of phase transition of such black holes are also explored in detail under a massless scalar perturbation of black hole space-time. The important aspect of any theory of gravity, namely, the GW solution is found for an $f(R)$ theory of gravity. The existence of an additional massive polarization is found. The detection possibility of such a mode is also dealt with in this thesis. Accordingly the sensibility of Spherical antenna towards such a mode is calculated. Also, the detection possibility of such a mode by the LIGO detectors are studied in this thesis.

2

QUASI NORMAL MODES AND THERMODYNAMICS OF BLACK HOLES IN DRGT MASSIVE GRAVITY

2.1 Introduction

The importance of the study of black holes and their properties such as Quasi Normal (QN) frequencies and thermodynamics for any theory of gravity have been described in Chapter 1. As discussed there, dRGT massive gravity forms the class of massive gravity where all the ghosts have been eliminated and is one of the most recently researched alternative theories of gravity. The graviton mass is directly included in to the action[38]. At large scale the theory recovers the solution in which the graviton mass plays the role of cosmological constant to drive the late-time acceleration of the universe[109]. The

theory also leads to many black hole solutions. One obvious and important way of realizing the existence of black hole space-time is by studying its QNMs[67]. Therefore, it is worthwhile to look into the black hole solution of dRGT massive gravity and study its QNMs. An important factor is that the results should reproduce that from GTR when the graviton mass goes to zero. In relation to this, it will also be worthy to study the black hole thermodynamics to check for interesting results like phase transition of black holes and the Entanglement Entropy.

The QNMs depend only on the black hole parameters and will be characterized by complex frequencies[66]. The real part describes the actual oscillation frequency and the imaginary part gives the decay rate of the particular oscillation. In order to get the QNMs, the space-time around the black hole has to be perturbed and the resulting radial part of the wave equation has to be solved for the QN frequencies with the help of boundary conditions. The resulting equation will be complicated and hence an analytical solution is difficult to obtain. Therefore, numerical methods must be employed to calculate the QN frequencies. One of the semi-analytical method that gain recent attraction is the Asymptotic Iteration Method (AIM). The Improved AIM has been used in the case of different black hole space-times for finding the QNMs and has been proved to be effective[78].

2.2 Improved Asymptotic Iteration Method

Asymptotic Iteration Method(AIM) was proposed initially for finding the solutions of the second order differential equations of the form [77, 110],

$$(2.1) \qquad y''(x) - \lambda_0(x)y'(x) - s_0(x)y(x) = 0,$$

where $\lambda_0(x)$ and $s_0(x)$ are coefficients of the differential equation and are well defined functions and sufficiently differentiable. By differentiating (2.1) with respect to x gives,

$$(2.2) \qquad y'''(x) - \lambda_1(x)y'(x) - s_1(x)y(x) = 0,$$

where the new coefficients are, $\lambda_1(x) = \lambda_0' + \lambda_0^2 + s_0$ and $s_1(x) = s_0' + s_0\lambda_0$. Differentiating (2.1) twice with respect to x leads to,

$$(2.3) \qquad y''''(x) - \lambda_2(x)y'(x) - s_2(x)y(x) = 0,$$

where the new coefficients are, $\lambda_2(x) = \lambda_1' + \lambda_1\lambda_0 + s_1$ and $s_2(x) = s_1' + s_0\lambda_1$. Thus the $(n+1)^{th}$ and $(n+2)^{th}$ derivatives, with $n = 1, 2, ..$, can be respectively written as,

$$(2.4) \qquad y^{n+1}(x) = \lambda_{n-1}(x)y' + s_{n-1}(x)y,$$

$$(2.5) \qquad y^{n+2}(x) = \lambda_n(x)y' + s_n(x)y,$$

where the new coefficients are related to the older ones through the following expressions,

$$\lambda_n(x) = \lambda_{n-1}' + \lambda_{n-1}\lambda_0 + s_{n-1},$$

$$(2.6) \qquad s_n(x) = s_{n-1}' + s_0\lambda_{n-1},$$

where $n = 1, 2, 3, \ldots$. The ratio of $(n+2)^{th}$ derivative and $(n+1)^{th}$ derivative can be obtained from (2.4) and (2.5) as,

$$\frac{y^{(n+2)}(x)}{y^{(n+1)}(x)} = \frac{d}{dx}(ln\,y^{n+1})$$

(2.7)

$$= \frac{\lambda_n[y'(x) + \frac{s_n}{\lambda_n}y(x)]}{\lambda_{n-1}[y'(x) + \frac{s_{n-1}}{\lambda_{n-1}}y(x)]}.$$

Now, by introducing the asymptotic concept that for sufficiently large values of n,

(2.8)
$$\frac{s_n}{\lambda_n} = \frac{s_{n-1}}{\lambda_{n-1}} \equiv \alpha,$$

where α is a constant will immediately lead to the quantization condition[77],

(2.9)
$$\lambda_n(x)s_{n-1}(x) - \lambda_{n-1}(x)s_n(x) = 0.$$

We can now write (2.7) as,

(2.10)
$$\frac{d}{dx}(\ln y^{n+1}) = \frac{\lambda_n}{\lambda_{n-1}},$$

which gives,

$$y^{n+1}(x) = C_1 \exp\left(\int^x \frac{\lambda_n(t)}{\lambda_{n-1}(t)}dt\right),$$

(2.11)

$$= C_1 \lambda_{n-1} \exp\left(\int^x (\alpha + \lambda_0)dt\right),$$

where C_1 is the integration constant. Substituting (2.11) in (2.4), we get,

(2.12)
$$y' + \alpha y = C_1 \exp\left(\int^x \int^x (\alpha + \lambda_0)dt\right),$$

which leads to the general solution,

(2.13)

$$y(x) = \exp\left(-\int^x \alpha\,dt\right)\left[C_2 + C_1 \int^x \exp\left(\int^t (\lambda_0(\tau) + 2\alpha(\tau))d\tau\right)dt\right],$$

thereby proving the following theorem[77]:

40

Theorem: *Given λ_0 and s_0 in $C_\infty(a,b)$, then the differential equation*

$$(2.14) \qquad y'' = \lambda_0(x)y' + s_0(x)y,$$

has a general solution given by (2.14) if for some $n > 0$,

$$(2.15) \qquad \frac{s_n}{\lambda_n} = \frac{s_{n-1}}{\lambda_{n-1}} \equiv \alpha,$$

where,

$$(2.16) \qquad \lambda_k(x) = \lambda'_{k-1} + \lambda_{k-1}\lambda_0 + s_{k-1},$$

$$(2.17) \qquad s_k(x) = s'_{k-1} + s_0\lambda_{k-1},$$

for $k = 1,2,3,.....,n$.

The roots of this equation are used to obtain the eigenvalues of (2.1). The energy eigenvalues will be contained in the coefficients. To get the eigenvalues, each derivative of λ and s are found out and expressed in terms of the previous iteration. Then by applying the quantization condition given by (2.9), a general expression for the eigenvalue can be arrived at. Cifti et al.[111] first noted that this procedure has a difficulty that, the process of taking the derivative of s and λ terms of the previous iteration at each step can consume time and also affect the numerical precision of calculations. To overcome this difficulty, an improved version of AIM has been proposed that by-passes the need to take derivative at each iteration. This is shown to improve both accuracy and speed of the method. For that, λ_n and s_n are expanded in a Taylor series around the point x' at which AIM is performed and

41

can be written as,

$$\lambda_n(x') = \sum_{i=0}^{\infty} c_n^i (x - x')^i, \tag{2.18}$$

$$s_n(x') = \sum_{i=0}^{\infty} d_n^i (x - x')^i, \tag{2.19}$$

where c_n^i and d_n^i are the ith Taylor coefficients of $\lambda_n(x')$ and $s_n(x')$ respectively. Substitution of (2.18) and (2.19) in (2.6) leads to the recursion relations for the coefficients as,

$$c_n^i = (i + 1)c_{n-1}^{i+1} + d_{n-1}^i + \sum_{k=0}^{i} c_0^k c_{n-1}^{i-k}, \tag{2.20}$$

$$d_n^i = (i + 1)d_{n-1}^{i+1} + \sum_{k=0}^{i} d_0^k c_{n-1}^{i-k}, \tag{2.21}$$

Applying (2.20) and (2.21) in (2.9), the quantization condition can be re-written as,

$$d_n^0 c_{n-1}^0 - d_{n-1}^0 c_n^0 = 0. \tag{2.22}$$

This gives a set of recursion relations that do not require any derivatives. The coefficients given by (2.20) and (2.21) can be computed by starting at $n = 0$ and iterating up to $(n + 1)$ until the desired number of recursions are reached. The quantization condition given by (2.22) contains only $i = 0$ term. So, only the coefficients with $i < N - n$ where N is the maximum number of iterations to be performed needs to be determined. The radial part of the wave equation of a perturbed black hole space-time can be written in the form of a second order differential equation similar to (2.1) with the coefficients containing their QN frequencies and the condition given by (2.22) can be employed to extract the QNMs of the black hole[78, 79].

2.3 Quasi Normal Modes of a dRGT Black Hole

The basic ideas of massive gravity are given in chapter 1.2.2. In this section of this chapter we consider both the cases of neutral and charged black hole solutions in dRGT massive gravity and calculate their QNMs and then see the differences in their behavior in the de Sitter (dS) space-time.

2.3.1 Neutral dRGT black hole

In the standard formalism of dRGT massive gravity theory, the Einstein-Hilbert action is given by [59, 112],

$$S = \int d^4x \sqrt{-g} \frac{1}{2\kappa^2} \left[R + m_g^2 U(g,\phi) \right],$$

where g is the metric tensor, R is the Ricci scalar, m represents the graviton mass and U is the effective potential for the graviton and is given by [60],

$$U(g,\phi) = U_2 + \alpha_3 U_3 + \alpha_4 U_4,$$

where α_3 and α_4 are two free parameters. These parameters are redefined by introducing two new parameters α and β as[113],

$$\alpha_3 = \frac{\alpha - 1}{3}, \tag{2.23}$$

$$\alpha_4 = \frac{\beta}{4} + \frac{1 - \alpha}{12}, \tag{2.24}$$

the resulting action is varied with respect to the metric leading to the field equation,

$$G_{\mu\nu} = -m^2 X_{\mu\nu}, \tag{2.25}$$

43

where,

$$X_{\mu\nu} = \mathscr{K}_{\mu\nu} - \mathscr{K} g_{\mu\nu} - \alpha\{\mathscr{K}_{\mu\nu}^2 - \mathscr{K}\mathscr{K}_{\mu\nu} + \frac{[\mathscr{K}]^2 - [\mathscr{K}^2]}{2} g_{\mu\nu}\}$$

(2.26) $$3\beta[\mathscr{K}_{\mu\nu}^3 - \mathscr{K}\mathscr{K}_{|mu\nu}^2 + \frac{1}{2}\mathscr{K}_{\mu\nu}\{[\mathscr{K}]^2 - [\mathscr{K}^2]\}$$

$$-\frac{1}{6}g_{\mu\nu}\{[\mathscr{K}]^3 - 3[\mathscr{K}][\mathscr{K}^2] + 2[\mathscr{K}^2]\}\}],$$

The constraints of this field equation (2.25) can be obtained by using
the Bianchi identity,

(2.27) $$\nabla^{\mu\nu} X_{\mu\nu} = 0.$$

We are interested in a static and spherically symmetric space-time
whose metric can be expressed as[109, 114, 115],

(2.28) $$ds^2 = g_{tt}(r)dt^2 + 2g_{tr}(r)dtdr + g_{rr}(r)dr^2 + h(r)^2 d\Omega^2,$$

with $g_{tt}(r) = -\eta(r)$, $g_{rr} = \frac{1}{f(r)}$ and $h(r) = h_0 r$ where h_0 is a constant in
terms of α and β . Most of the black hole solutions are asymptotically
dS or AdS. The exact solution for the above ansatz is complicated. For
simplicity, we choose $g_{tr}(r) = 0$. It is further simplified by choosing
specific relations for the parameters. For that, we take $\alpha = -3\beta$ follow-
ing Ghosh et al.[113]. Since the fiducial metric acts like a Lagrangian
multiplier to eliminate the BD ghost, to simplify the calculations, we
choose the fiducial metric as[116],

(2.29) $$f_{\mu\nu} = (0, 0, c^2, c^2 \sin^2\theta),$$

where c is a constant. Then (2.28) becomes,

(2.30) $$ds^2 = -\eta(r)dt^2 + \frac{dr^2}{f(r)} + r^2 d\Omega^2,$$

44

The non-zero components of the Einstein tensor are obtained as,

$$(2.31) \qquad G^t_t = \frac{f'}{r} + \frac{f}{r^2} - \frac{1}{r^2},$$

$$(2.32) \qquad G^r_r = \frac{f(r\eta' + \eta)}{\eta r^2} - \frac{1}{r^2},$$

$$(2.33) \qquad G^\theta_\theta = G^\phi_\phi,$$

$$(2.34) \qquad = f'\left(\frac{\eta'}{4\eta} + \frac{1}{2r}\right) + f\left(\frac{\eta''}{2\eta} + \frac{\eta'}{2\eta r} - \frac{(\eta')^2}{4\eta^2}\right),$$

and the energy-momentum tensor $X_{\mu\nu}$ as,

$$(2.35) \qquad X^t_t = -\left(\frac{\alpha(3r - c)(r - c)}{r^2} + \frac{3\beta(r - c)^2}{r^2} + \frac{3r - 2c}{r}\right),$$

$$(2.36) \qquad X^r_r = -\left(\frac{\alpha(3r - c)(r - c)}{r^2} + \frac{3\beta(r - c)^2}{r^2} + \frac{3r - 2c}{r}\right),$$

$$(2.37) \qquad X^\theta_\theta = X^\phi_\phi,$$

$$(2.38) \qquad = \frac{\alpha(2c - 3r)}{r} + \frac{3\beta(c - r)}{r} + \frac{c - 3r}{r},$$

Substituting the components of Einstein tensor and energy-momentum tensor into (2.25) we find,

$$(2.39) \qquad \begin{aligned} \frac{f'}{r} + \frac{f}{r^2} - \frac{1}{r^2} &= \\ & m^2\left(\frac{\alpha(3r - c)(r - c)}{r^2} + \frac{3\beta(r - c)^2}{r^2} + \frac{3r - 2c}{r}\right), \end{aligned}$$

$$(2.40) \qquad \begin{aligned} \frac{f(r\eta' + \eta)}{\eta r^2} - \frac{1}{r^2} &= \\ & m^2\left(\frac{\alpha(3r - c)(r - c)}{r^2} + \frac{3\beta(r - c)^2}{r^2} + \frac{3r - 2c}{r}\right), \end{aligned}$$

$$(2.41)$$

$$f'\left(\frac{\eta'}{4\eta} + \frac{1}{2r}\right) + f\left(\frac{\eta''}{2\eta} + \frac{\eta'}{2\eta r} - \frac{(\eta')^2}{4\eta^2}\right) = $$
$$ -m^2\left(\frac{\alpha(2c - 3r)}{r} + \frac{3\beta(c - r)}{r} + \frac{c - 3r}{r}\right).$$

45

Solving (2.39) gives the form for the metric function as,

$$(2.42) \qquad f(r) = 1 - \frac{2M}{r} + \frac{\Lambda}{3}r^2 + \gamma r + \zeta,$$

where,

$$(2.43) \qquad \Lambda = 3m_g^2\left(1 + \alpha + \beta\right),$$

$$(2.44) \qquad \gamma = -cm_g^2\left(1 + 2\alpha + 3\beta\right),$$

$$(2.45) \qquad \zeta = c^2 m_g^2\left(\alpha + 3\beta\right).$$

From (2.39) and (2.40) one can arrive at the relation,

$$(2.46) \qquad \eta' f = f' \eta,$$

which implies that the functions η and f differs only by a constant and hence we are free to choose the constant in such a way that $\eta = f$.

Then, the metric given by (2.30) reads as,

$$(2.47) \qquad ds^2 = -f(r)dt^2 + \frac{dr^2}{f(r)} + r^2 d\Omega^2$$

Now, when $\gamma = \zeta = 0$, α and β will determine the nature of the solution. ie., if $(1 + \alpha + \beta) < 0$ we get a Schwarzschild dS type solution, if $(1 + \alpha + \beta) > 0$, we will get a Schwarzschild AdS type solution and when $m \to 0$ we get a Schwarzschild black hole. The dRGT solution described here contains Schwarzschild ($m = 0$), dS/AdS, global monopole of GTR and thus also contains the monopole-dS-Schwarzschild solution[113].

For a static spherically symmetric space-time background with vanishing energy-momentum tensor, the field perturbations are not coupled

to the perturbations of the metric and therefore are equivalent to test field in black hole background. A massless scalar field satisfies the Klein-Gordon equation in curved space-time as given by,

$$(2.48) \qquad \frac{1}{\sqrt{-g}} \frac{\partial}{\partial x^a} g^{ab} \sqrt{-g} \frac{\partial}{\partial x^b} \Phi = 0,$$

$$(2.49) \qquad ie., \frac{1}{f(r)} \frac{\partial^2 \Phi}{\partial t^2} - \frac{\partial}{\partial r} f(r) \frac{\partial \Phi}{\partial r} - \frac{\Delta_{\theta,\phi} \Phi}{r^2} = 0,$$

where,

$$(2.50) \qquad \Delta_{\theta,\phi} = \frac{1}{\sin\theta} \frac{\partial}{\partial \theta} (\sin\theta) + \frac{1}{\sin^2\theta} \frac{\partial^2}{\partial\phi^2}.$$

For finding the QNMs, the radial part has to be extracted from (2.49). For this purpose, the radial and angular parts has to be separated. Hence we choose the variable separable form for the field as,

$$(2.51) \qquad \Phi = \sum_{l=0}^{\infty} \sum_{m=0}^{l} \frac{R(r)}{r} e^{-i\omega t} Y_{l,m}(\theta,\phi),$$

where ω gives the frequency of the oscillations corresponding to the black hole perturbation, $Y_{l,m}(\theta,\phi)$ are the spherical harmonics and,

$$(2.52) \qquad \Delta_{\theta,\phi} Y_{l,m}(\theta,\phi) = -l(l+1) Y_{l,m}(\theta,\phi).$$

Substituting (2.51) in (2.49) and using (2.50) and (2.52) we get the radial part of the equation,

$$(2.53) \qquad \frac{d^2 R}{dr^2} + \frac{f'(r)}{f(r)} \frac{dR}{dr} + \left[\frac{\omega^2}{f(r)^2} - \frac{(\frac{2M}{r^3} + \frac{\gamma}{r} + \frac{2\Lambda}{3} + \frac{l(l+1)}{r^2})}{f(r)} \right] R = 0.$$

By using tortoise coordinate $x = \int \frac{dr}{f(r)}$, the above equation can be brought into the standard form[117],

$$(2.54) \qquad \frac{d^2 R}{dx^2} + [\omega^2 - V(r)]R = 0,$$

47

where,

$$(2.55) \qquad V(r) = f(r)\left(\frac{l(l+1)}{r^2} + \frac{f'(r)}{r}\right).$$

The SdS black hole has three singularities given by the roots of $f(r) = 0$, which are the event horizon, r_1, the cosmological horizon, r_2 and at $r_3 = -(r_1 + r_2)$. The QNMs are defined as solutions of (2.54) with boundary conditions: $R(x) \to e^{i\omega x}$ as $x \to \infty$ and $R(x) \to e^{-i\omega x}$ as $x \to -\infty$ for an $e^{-i\omega t}$ time dependence that corresponds to ingoing waves at the horizon and out going waves at infinity. The surface gravity κ_i at these singular points are defined as,

$$(2.56) \qquad \kappa_i = \frac{1}{2}\frac{\partial f}{\partial r}\Big|_{r \to r_i}.$$

Before calculating the QNMs using Improved AIM, it is needed to make a change of variable as $\xi = 1/r$ in (2.53) leading to,

$$(2.57) \qquad \frac{d^2R}{d\xi^2} + \frac{p'}{p}\frac{dR}{d\xi} + \left[\frac{\omega^2}{p^2} - \frac{l(l+1) + (2M\xi + \gamma/\xi + \frac{2\Lambda}{3\xi^2})}{p}\right]R = 0,$$

where,

$$(2.58) \qquad p \;=\; -2M\xi^3 + \xi^2(1+\zeta) + \gamma\xi + \frac{\Lambda}{3},$$

$$(2.59) \qquad p' \;=\; -6M\xi^2 + \gamma + 2\xi(1+\zeta).$$

In de Sitter space-time, the radial black hole solution has got 3 singularities and these are represented as ξ_1 (Event horizon), ξ_2 (Cosmological horizon) and $\xi_3 = -\left(\frac{\xi_1\xi_2}{\xi_1+\xi_2}\right)$ and hence we can write [78, 118],

$$(2.60) \qquad e^{i\omega\xi} = (\xi - \xi_1)^{\frac{i\omega}{2\kappa_1}}(\xi - \xi_2)^{\frac{i\omega}{2\kappa_2}}(\xi - \xi_3)^{\frac{i\omega}{2\kappa_3}}.$$

The idea is to scale out the divergent behavior at the cosmological horizon first and then re-scale at the event horizon for a convergent

solution. Now to scale out the divergent behavior at cosmological horizon, we take,

$$(2.61) \qquad R(\xi) = e^{i\omega\xi} u(\xi).$$

The master equation given by (2.57) then takes the form,

$$(2.62) \qquad pu'' + (p' - 2i\omega)u' - \left[l(l+1) + \left(2M\xi + \gamma/\xi + \frac{2\Lambda}{3\xi^2} \right) \right] u = 0.$$

The correct scaling condition of QNM at the event horizon implies,

$$(2.63) \qquad u(\xi) = (\xi - \xi_1)^{-\frac{i\omega}{2\kappa_1}} \chi(\xi).$$

(2.63) then can be viewed of the form as,

$$(2.64) \qquad \chi'' = \lambda_0(\xi)\chi' + s_0(\xi)\chi,$$

where λ_0 and s_0 are the coefficients of the second order differential equation. After being written in the form of a second order differential equation, we now are in a position to calculate the QNMs using Improved AIM. It can be seen from (2.62) that the coefficient of u' includes the frequency ω. Therefore the quantization condition given by (2.22) can be used to find out ω of (2.62) by iterating to some n maximum. For calculating the QNMs, we have used the MATHEMATICA NOTEBOOK given in the reference [119] after modifying it to employ for the case of massive gravity.

Table 2.1 shows the QN frequencies obtained through improved AIM method for a static spherically symmetric neutral black hole spacetime in dRGT massive gravity defined by the metric function (2.42). The values of α and β are so chosen that Λ remains negative such that

the space-time is dS. The parameters are chosen as $M = c = 1$ in these
calculations. The table shows the quasinormal modes calculated for
$m = 0.8$ and $m = 1$ respectively for the same range of α and β values. It
can be seen that increasing the value of m increases the magnitude of
the cosmological constant, which is obvious. Also, as m increases, the
QN frequencies are seen to be increasing in magnitude for both $l = 2$
and $l = 3$ modes. As for every m, both the real and imaginary parts of
the quasinormal frequencies are seen to be continuously increasing
in magnitude as Λ increases. 50 iterations have been executed for
calculating the QNMs. We have taken $(1 + \alpha + \beta) < 0$ while calculating
the QNMs so that the results of the calculations will correspond to
that in the de Sitter space-time.

If we take $\gamma = \zeta = 0$ the space-time becomes SdS. The QN frequen-
cies calculated for this case and the comparison of those results with
the results calculated using WKB Method taken from Table 1 of
Zhidenko[120, 121] is shown in Table 2.2. The table also shows the
accurateness of the Improved AIM. Comparing these QN frequencies
with Table 2.1, it can be seen that the values of the QN frequencies,
when m takes a finite value, are higher in magnitude than when
$m = 0$, which corresponds to SdS space-time. It will be interesting to
check the QNM behavior of the black hole if it carries the parameter
charge, in addition to mass and is done below.

Table 2.1: *QNMs of dRGT black hole under massless scalar perturbations calculated by Improved AIM (with 50 iterations) for l = 2 and l = 3 modes.The α and β values are kept the same while QNMs are calculated by varying the m values*

$m = 0.8$				
Λ	γ	ζ	$\omega(l = 2)$	$\omega(l = 3)$
-0.080	-0.80	1.9840	$1.15155 - 0.348046\,i$	$1.62914 - 0.341517\,i$
-0.088	-0.80	1.9904	$1.15615 - 0.350418\,i$	$1.63572 - 0.343749\,i$
-0.096	-0.80	1.9968	$1.16081 - 0.352759\,i$	$1.64237 - 0.346001\,i$
-0.104	-0.80	2.0032	$1.16552 - 0.355121\,i$	$1.64910 - 0.348271\,i$
-0.112	-0.80	2.0096	$1.17030 - 0.357501\,i$	$1.65590 - 0.350560\,i$
-0.120	-0.80	2.0160	$1.17512 - 0.359902\,i$	$1.66278 - 0.352868\,i$
-0.128	-0.80	2.0224	$1.18001 - 0.362322\,i$	$1.66974 - 0.355195\,i$
$m = 1.0$				
Λ	γ	ζ	$\omega(l = 2)$	$\omega(l = 3)$
-0.100	-1.00	3.1000	$2.81587 - 1.049800\,i$	$3.90051 - 1.026860\,i$
-0.110	-1.00	3.1100	$2.83013 - 1.057140\,i$	$3.91984 - 1.033950\,i$
-0.120	-1.00	3.1200	$2.84445 - 1.064510\,i$	$3.93924 - 1.041070\,i$
-0.130	-1.00	3.1300	$2.85881 - 1.071910\,i$	$3.95870 - 1.048210\,i$
-0.140	-1.60	3.1400	$2.87322 - 1.079340\,i$	$3.97823 - 1.055380\,i$
-0.150	-1.75	3.1500	$2.88768 - 1.086800\,i$	$3.99781 - 1.062580\,i$
-0.160	-1.90	3.1600	$2.90220 - 1.094280\,i$	$4.10746 - 1.069800\,i$

2.3.2 Charged dRGT black hole

The metric function for a charged black hole from the class of dRGT massive gravity can be obtained following section 2.3.1 as,

$$(2.65) \qquad f(r) = 1 - \frac{2M}{r} + \frac{Q^2}{r^2} + \frac{\Lambda}{3}r^2 + \gamma r + \zeta,$$

where Q corresponds to the charge. Proceeding as above, the radial part of the wave equation can be found as,

$$(2.66) \qquad \frac{d^2R}{d\xi^2} + \frac{p'}{p}\frac{dR}{d\xi} + \left[\frac{\omega^2}{p^2} - \frac{(2M\xi - 2Q^2\xi^4 + \gamma/\xi + \frac{2\Lambda}{3\xi^2})}{p}\right]R = 0,$$

51

Table 2.2: Column 2 shows QNMs calculated using Improved AIM
for $\gamma = \zeta = 0$ for different values of Λ shown in column 1. These are
compared with the SdS case calculated in [120] shown in column 4.
The results are found to agree quite well.

Λ(dRGT)	ω_{AIM}	Λ(SdS)	ω_{WKB}
0	$0.483644 - 0.0967588\ i$	0	0.48364 - 0.09677 i
-0.02	$0.434585 - 0.0885944\ i$	0.02	0.43461 - 0.08858 i
-0.04	$0.380784 - 0.0787610\ i$	0.04	0.38078 - 0.07876 i
-0.06	$0.320021 - 0.0668449\ i$	0.06	0.32002 - 0.06685 i
-0.08	$0.247470 - 0.0519043\ i$	0.08	0.24747 - 0.05197 i
-0.09	$0.202960 - 0.0425584\ i$	0.09	0.20296 - 0.04256 i
-0.10	$0.146610 - 0.0306869\ i$	0.10	0.14661 - 0.03069 i
-0.11	$0.0461689 - 0.0063134\ i$	0.11	0.04617 - 0.00963 i

where,

$$(2.67) \qquad p \;=\; Q^2\xi^4 - 2M\xi^3 + \xi^2(1+\zeta) + \gamma\xi + \frac{\Lambda}{3},$$

$$(2.68) \qquad p' \;=\; 4Q^2\xi^3 - 6M\xi^2 + \gamma + 2\xi(1+\zeta).$$

Scaling out the divergent behavior at the event horizon leads to the
master equation,

$$(2.69) \quad pu'' + (p' - 2i\omega)u' - \left[l(l+1) + \left(2M\xi - 2Q^2\xi^2 + \gamma/\xi + \frac{2\Lambda}{3\xi^2} \right) \right] u = 0.$$

Again, the correct scaling condition of QNMs at the event horizon
implies,

$$(2.70) \qquad u(\xi) = (\xi - \xi_1)^{-\frac{i\omega}{2\kappa_1}} \chi(\xi),$$

where,

$$(2.71) \qquad \begin{aligned} \kappa_1 &= \frac{1}{2}\frac{\partial f}{\partial r}\big|_{r\to r_1}, \\ &= M\xi^2 - Q^2\xi^3 + \frac{\Lambda}{3}\xi + \frac{\gamma}{2}. \end{aligned}$$

The master equation is now in the form of (2.1) so that the quantization condition given by (2.22) can be employed to find out the QNMs.

Table 2.3 shows the QNMs calculated using the improved AIM method for different values of α and β. We have chosen the values $M = c = 1$ and $Q = 0.5$ in these calculations. The QNMs are studied as in the previous subsection by varying the m values while keeping the values of α and β the same. It can be seen that as m increases, the real part of the quasi normal frequency deceases while the magnitude of the imaginary part increases. For each m, the QN frequencies vary continuously. A black hole is stable only when the imaginary part in its QN spectrum is negative[122]. It is noted while calculating the QNMs that the roots of the frequency, ω give positive as well as negative imaginary parts. Here we are interested in the stable modes and therefore have considered only the negative imaginary parts of ω. 50 iterations have been taken for calculating the QNMs.

2.4 Thermodynamics and P-V Criticality of Black Holes in dRGT Massive Gravity in de Sitter Space-time

It is seen in the previous section that the black hole solutions, both neutral and charged ones, in dS space-time have got 2 horizons. A black hole with more than one horizon or multiple horizons will correspond to different thermodynamical systems. Hence it will be interesting to study the thermodynamics of those black holes.

Table 2.3: *The QNMs obtained under massless scalar perturbations of a charged dRGT black hole having charge Q = 0.5 for l = 2 and l = 3 modes. The α and β values are kept the same while QNMs are calculated by varying the m values*

$m = 0.8$				
Λ	γ	ζ	$\omega(l=2)$	$\omega(l=3)$
-0.080	-0.80	1.9840	$2.43544 - 0.523799\,i$	$1.67618 - 0.168257\,i$
-0.088	-0.80	1.9904	$2.43455 - 0.535763\,i$	$1.67635 - 0.180489\,i$
-0.096	-0.80	1.9968	$2.43252 - 0.547233\,i$	$1.67351 - 0.195613\,i$
-0.104	-0.80	2.0032	$2.42939 - 0.558215\,i$	$1.67069 - 0.209057\,i$
-0.112	-0.80	2.0096	$2.42523 - 0.568718\,i$	$1.66693 - 0.222338\,i$
-0.120	-0.80	2.0160	$2.42021 - 0.578624\,i$	$1.66230 - 0.235427\,i$
-0.128	-0.80	2.0224	$2.41399 - 0.588313\,i$	$1.65677 - 0.248391\,i$
$m = 1.0$				
Λ	γ	ζ	$\omega(l=2)$	$\omega(l=3)$
-0.10	-1.00	3.1000	$0.304084 - 2.99974\,i$	$0.9866449 - 4.93190\,i$
-0.11	-1.00	3.1100	$0.342169 - 3.05263\,i$	$1.0195500 - 5.01834\,i$
-0.12	-1.00	3.1200	$0.378347 - 3.10442\,i$	$1.0531600 - 5.10348\,i$
-0.13	-1.00	3.1300	$0.413140 - 3.15511\,i$	$1.0872800 - 5.18734\,i$
-0.14	-1.60	3.1400	$0.446882 - 3.20472\,i$	$1.1219000 - 5.26998\,i$
-0.15	-1.75	3.1500	$0.479812 - 3.25326\,i$	$1.1570200 - 5.35141\,i$
-0.16	-1.90	3.1600	$0.512100 - 3.30072\,i$	$1.1926600 - 5.43168\,i$

2.4.1 Thermodynamics of neutral dRGT black holes

The basis of black hole thermodynamics have been dealt with in detail in chapter 1.5. Generally, the cosmological constant, Λ, is treated as representing a negative pressure [123] as,

$$\Lambda = -8\pi P. \tag{2.72}$$

For $\gamma = \zeta = 0$, the metric function (2.42) would lead to the case of a dS space-time provided Λ is negative. Keeping this in mind we take,

$$(2.73) \qquad\qquad \Lambda = 8\pi P,$$

where P is the pressure. The boundary of the black hole is described by the black hole horizon, r_h and is determined by the condition, $f(r)|_{r_h} = 0$. From this condition, the mass of the black hole can be expressed in terms of r_h as,

$$(2.74) \qquad\qquad M = \frac{1}{6} r_h (3 + 3 r_h \gamma + 3\zeta + r_h^2 \Lambda),$$

and the black hole mass is considered to be the enthalpy of the system. The thermodynamic volume, V is given by[124, 125],

$$(2.75) \qquad\qquad V = \frac{\partial M}{\partial P}.$$

Varying (2.75) partially with respect to the pressure P, we get

$$(2.76) \qquad\qquad V = \frac{4}{3} \pi r_h^3.$$

The temperature of the black hole, described by the metric in (2.42), given by the Hawking temperature can be written as [126],

$$(2.77) \qquad \begin{aligned} T &= \frac{1}{4\pi} f'(r_h), \\ &= \frac{1}{4\pi r_h} \left[\frac{2M}{r_h} + \gamma r_h + 2\frac{\Lambda}{3} r_h^2 \right]. \end{aligned}$$

Substituting M from (2.74) in (2.77) and rearranging it we get an expression for the cosmological constant,

$$(2.78) \qquad\qquad \Lambda = \frac{4\pi T - 2\gamma}{r_h} - \frac{(1+\zeta)}{r_h^2}.$$

But from (2.73), the cosmological constant can be related to the pressure as $\Lambda = 8\pi P$. Therefore (2.78) can be written in terms of P as,

$$P = \frac{\Lambda}{8\pi},$$

(2.79)
$$= \left(\frac{T}{2} - \frac{\gamma}{4\pi}\right)\frac{1}{r_h} - \left(\frac{1}{8\pi} + \frac{\zeta}{8\pi}\right)\frac{1}{r_h^2},$$

or,

(2.80)
$$P = \frac{w_1}{r_h} + \frac{w_2}{r_h^2},$$

where,

(2.81)
$$w_1 = \left(\frac{T}{2} - \frac{\gamma}{4\pi}\right),$$

(2.82)
$$w_2 = -\left(\frac{1}{8\pi} + \frac{\zeta}{8\pi}\right).$$

From (2.81), w_1 can be treated as a shifted temperature. From (2.76) it can be seen that, thermodynamic volume, V, is a monotonic function of the horizon radius r_h and hence r_h can be used instead of V in the analysis. (2.80) can be treated as the equation of state describing the thermodynamic state of the black hole. The critical point is then determined by the simultaneous satisfaction of the conditions,

(2.83)
$$\frac{\partial P}{\partial r_h}\bigg| r_h = r_{hc}, T = T_c = 0,$$

and

(2.84)
$$\frac{\partial^2 P}{\partial^2 r_h}\bigg|_{r_h=r_{hc},T=T_c} = 0.$$

Substituting for P in the above differential equation it is found that the conditions given by (2.83) and (2.84) are not simultaneously satisfied. However, the condition,

(2.85)
$$\frac{\partial P}{\partial r_h}\bigg|_{r_h=r_{hc},T=T_c} = 0,$$

gives the critical horizon,

$$(2.86) \qquad r_{hc} = -\frac{2w_2}{w_1}.$$

Evaluation of $\left.\frac{\partial^2 P}{\partial^2 r_h}\right|_{r_h=r_{hc}, T=T_c}$ gives a non-zero value which can imply either a local maximum or a local minimum depending on whether the value is greater than or less than zero. The critical pressure is found out by substituting (2.86) in to (2.80) which gives,

$$(2.87) \qquad P_c = -\frac{w_1^2}{4w_2}.$$

This critical point corresponds to a physically feasible one if P_c is positive [126]. It can be seen that this happens only if w_2 is negative irrespective of the sign of w_1. The relation between shifted temperature, w_1, critical pressure, P_c and horizon radius r_h can be found out from (2.86) and (2.87) as,

$$(2.88) \qquad \frac{P_c r_{hc}}{w_1} = \frac{1}{2}.$$

This ratio is called the 'Compressibility Ratio'. The value of compressibility ratio for a Van der Waals gas is 0.375. Hence, the black hole system, with the Compressibility Ratio given by (2.88), can be thought of as behaving like a near Van der Waals system. The P-r_h diagram plotted for different shifted temperature is shown in Fig.2.1. In the first figure, the curves are plotted for $w_2 = 1$, the curves are seen to show critical behavior but it likely does not correspond to a physical one because, from (2.87), for the above said values of w_1 and w_2 the critical pressure P_c turns out to be negative for these curves. The second figure plotted for $w_2 = -0.5$, show inflection point but there is no phase transition.

57
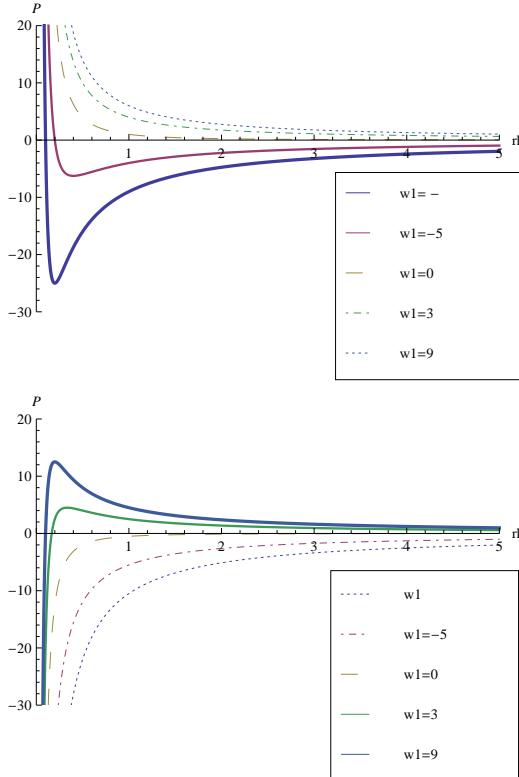
Figure 2.1: First figure shows P-r_h diagram for the value $w_2 = 1$ which exhibits critical behavior and the second figure shows the plot for the value $w_2 = -0.5$ which exhibits an inflection.

2.4.2 Thermodynamics of charged dRGT black holes

Consider a charged black hole with the metric of the form (2.65). The Hawking Temperature for this metric function can be found out as,

(2.89)
$$T = \frac{1}{4\pi} f'(r_h),$$
$$= \frac{1}{4\pi r_h} \left[\frac{2M}{r_h} - \frac{2Q^2}{r_h^2} + \gamma r_h + 2\frac{\Lambda}{3} r_h^2 \right].$$

From the above equation, the equation of state can be obtained proceeding as described in the previous subsection. The mass, M of the black hole can be written in terms of the horizon radius r_h as,

$$(2.90) \qquad M = \frac{1}{6r_h}(3Q^2 + 3r_h^2(1+\zeta) + 3r_h^3\gamma + r_h^4\Lambda),$$

Substituting for M in (2.89) and rearranging we get,

$$(2.91) \qquad \Lambda = \frac{4\pi T - 2\gamma}{r_h} - \frac{(1+\zeta)}{r_h^2} + \frac{Q^2}{r_h^4}.$$

Writing this equation in terms of P,

$$(2.92) \qquad \begin{aligned} P &= \frac{\Lambda}{8\pi}, \\ &= \left(\frac{T}{2} - \frac{\gamma}{4\pi}\right)\frac{1}{r_h} - \left(\frac{1}{8\pi} + \frac{\zeta}{8\pi}\right)\frac{1}{r_h^2} + \frac{Q^2}{8\pi r_h^4}, \end{aligned}$$

or,

$$(2.93) \qquad P = \frac{w_1}{r_h} + \frac{w_2}{r_h^2} + \frac{w_3}{r_h^4},$$

where,

$$(2.94) \qquad w_1 = \left(\frac{T}{2} - \frac{\gamma}{4\pi}\right),$$

$$(2.95) \qquad w_2 = -\left(\frac{1}{8\pi} + \frac{\zeta}{8\pi}\right),$$

$$(2.96) \qquad w_3 = \frac{Q^2}{8\pi}.$$

(2.93) describes the equation of state. The critical point is then determined by the simultaneous satisfaction of (2.83) and (2.84). Unlike in the case of a neutral black hole, it is found that (2.83) and (2.84) are simultaneously satisfied which gives the solutions, for critical horizon as,

$$(2.97) \qquad r_{hc} = \sqrt{-\frac{6w_4}{w_2}},$$

and for the critical temperature as,

$$(2.98) \qquad w_{1c} = \frac{2}{3}\sqrt{-\frac{2w_2^3}{w_3}}.$$

Using (2.93), (2.97) and (2.98), an expression for the critical pressure
can be arrived at as,

$$(2.99) \qquad P_c = \frac{w_2^2}{12w_3}.$$

The relation connecting shifted temperature w_{1c}, critical pressure, P_c
and critical horizon radius r_{hc} are found as,

$$(2.100) \qquad \frac{P_c r_{hc}}{w_{1c}} = \frac{3}{8},$$

which is exactly the same as in the case for a Van der Waals system.
The P-V diagram plotted for different shifted temperature is shown
in Fig.2.2. In the first figure, the curves are plotted for $w_2 = -10$ and
$w_3 = 1$. The second figure is plotted for $w_2 = 6$ and $w_3 = 1$. The first
figure shows an inflection point and a phase transition, but the second
one does not, as is obvious due to the sign change of w_2.

2.5 Holographic Entanglement Entropy in dS Space-time

Study on Entanglement Entropy (EE) of the black hole system pro-
vides a link to the relation between the classical black hole thermody-
namics and quantum effect as discussed in chapter 1.6. This may help
in paving way to a quantum explanation for gravitation and hence
gains importance. For a given quantum field theory described by a
density matrix ρ, the entanglement entropy for a region A and its
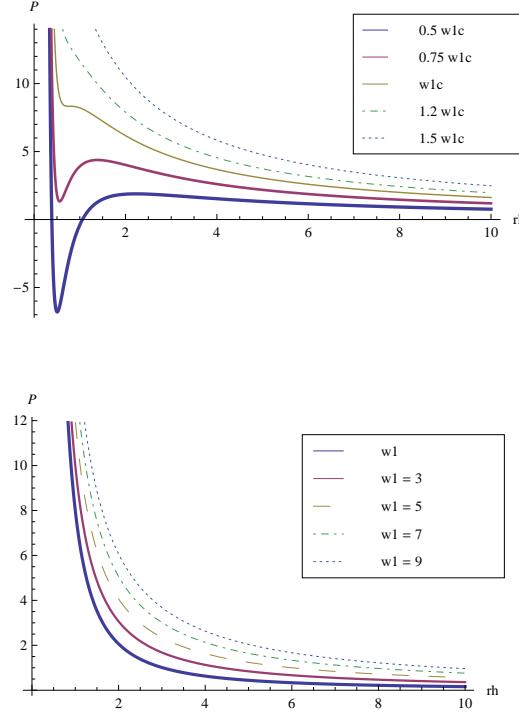
Figure 2.2: In the first figure P-r_h diagram is plotted for the value $w_2 = -10$ and $w_3 = 1$ which exhibits a phase transition and the second figure shows plots for the value $w_2 = 6$ and $w_3 = 1$ which does not exhibit any phase transition.

compliment B is defined as[127],

$$(2.101) \qquad\qquad S_A = -\mathrm{Tr}_A(\rho_A \ln \rho_A),$$

where $\rho_A = \mathrm{Tr}_B(\rho)$ is the reduced density matrix. This provides us with a convenient way to measure how closely entangled a given system B is. Here, the total system is divided into sub systems A and B. S_A can be computed, geometrically, in terms of the bulk minimal

61

surface enclosed on ∂A as given by[93],

$$(2.102) \qquad\qquad S_A = \frac{\text{Area } \gamma}{4},$$

where γ is the co-dimensional minimal surface with the boundary condition $\partial \gamma = \partial A$ and G is taken here as unity. For computing the entanglement entropy, A is parameterized by a shape in (θ, ϕ). The profile in the bulk will then be given by $r(\theta, \phi)$. The surface is completely characterized by the induced metric[94],

$$(2.103) \qquad\qquad h_{ab} = g_{\mu\nu} \partial_a x^\mu(\sigma^a) \partial_b x^\nu(\sigma^a),$$

with coordinates $a, b = 0, 1$, $\sigma^0 = \tau$ (time part) and $\sigma^1 = \sigma$ (space part). Then the minimum area will correspond to,

$$(2.104) \qquad\qquad A = -\frac{1}{2} \int_{\phi=0}^{2\pi} (-\det h)^{1/2} d\theta d\phi,$$

which gives,

$$(2.105) \qquad\qquad A = \int r \sin\theta \left[f(r)^{-1} \left(\frac{dr}{d\theta} \right) + r^2 \right]^{1/2} d\theta.$$

The non-trivial embedding function $x^\mu(\sigma^a)$ is now given by $r(\theta)$ and the Lagrangian given by the integrand of (2.105) can be treated as a classical mechanics problem with θ as the time parameter and treat the problem for solving $r(\theta)$ as that of a particle. Thus, the effective Lagrangian is given by,

$$(2.106) \qquad\qquad L = r \sqrt{\frac{r'^2}{f(r)} + r^2}.$$

In this work, we consider the surface bounded by the line of latitude

$\theta = \theta_0$ which has got the topology of a disc. The minimum area can then be written as,

$$(2.107) \qquad A = \int_{\theta=0}^{\theta=\theta_0} r \sin\theta \left[f(r)^{-1}(\frac{dr}{d\theta}) + r^2 \right]^{1/2} d\theta.$$

For a black hole, to avoid the entanglement entropy be affected by the surface that wraps the boundary, we take a cap shaped small area. To deal with the UV divergence it is assumed that the area sites on a slice and $r = \frac{1}{\epsilon}$, $\epsilon \to 0$ gives the UV cut off. Rather, A starts from $x = -\frac{l}{2}$, $r = \frac{1}{\epsilon}$, extends in to the bulk and reaches a minimum r and then returns back to the boundary $r = \frac{1}{\epsilon}$ at $x = +\frac{l}{2}$. Then the area to be minimized becomes,

$$(2.108) \qquad A = \int_{-l/2}^{l/2} r \left[\sqrt{\frac{r'(\theta)^2}{f(r)} + r(\theta)^2} \right]^{1/2} d\theta.$$

The area above will be divergent. So it is regularized by subtracting off the pure dS area with the same entangling surface. The area corresponding to pure dS can be found from the metric and the metric function with $m_0 \to 0$ and $Q \to 0$. Then the regularized entropy is given by,

$$(2.109) \qquad S_{ent} = S - S_0,$$

where S_0 is of the pure dS space-time and S is given by (34). With the Lagrangian at hand, the equation of motion can be found out from which we get an expression for $r(\theta)$. This procedure is rather complicated to do analytically and hence it is done numerically. The equation of motion corresponding to the Lagrangian in (2.108) is given by,

$$(2.110) \qquad 4f(r)^2 r^2 - r f(r) \dot{r}^2 + 2f(r)(\dot{r}^2 + r\ddot{r}) = 0.$$

This equation of motion is solved for the value of $r(\theta)$ numerically with $l = 2.2$, with the boundary condition $r(0) = 2.19$, $r'(0) = 0$ and with the parameter values $m = 1$, $\Lambda = 0.1$, $\alpha = 1$, $c = 1$, $c_1 = 1$ and $Q = 0.25$. The $r(\theta)$ and $r'(\theta)$ are inserted back into (2.108). The integral is minimized to find A corresponding to the minimal surface. This area is then used in (2.102) to calculate the entanglement entropy over the small area ∂A. The entanglement entropy corresponding to pure dS space-time is also evaluated in a similar manner.

Here, we are interested in the behavior of entanglement entropy with the black hole temperature. The entropy of the black hole can be evaluated from

(2.111)
$$S = \int \frac{1}{T} \frac{\partial M}{\partial r},$$
$$= 4\pi r_h.$$

Taking r_h from (2.77) and substituting in (2.111), for a neutral black hole, the Temperature-Entropy relation is obtained as,

(2.112)
$$T = \frac{4(1+\zeta)\pi S + 8\gamma\sqrt{\pi}S^{3/2} + 4S^2\Lambda}{16\pi^{3/2}S^{3/2}}.$$

Similarly for a charged black hole, the Temperature-Entropy relation is obtained as,

(2.113)
$$T = \frac{-\pi^2 Q^2 + 4(1+\zeta)\pi S + 8\gamma\sqrt{\pi}S^{3/2} + 4S^2\Lambda}{16\pi^{3/2}S^{3/2}}.$$

To compare the thermodynamic entropy with entanglement entropy, the regularized entanglement entropy calculated from the above procedure is substituted in the temperature-entropy relation and then plotted in Fig.2.3. The figure on top shows the behavior of entanglement entropy of a neutral dRGT black hole while the figure on bottom
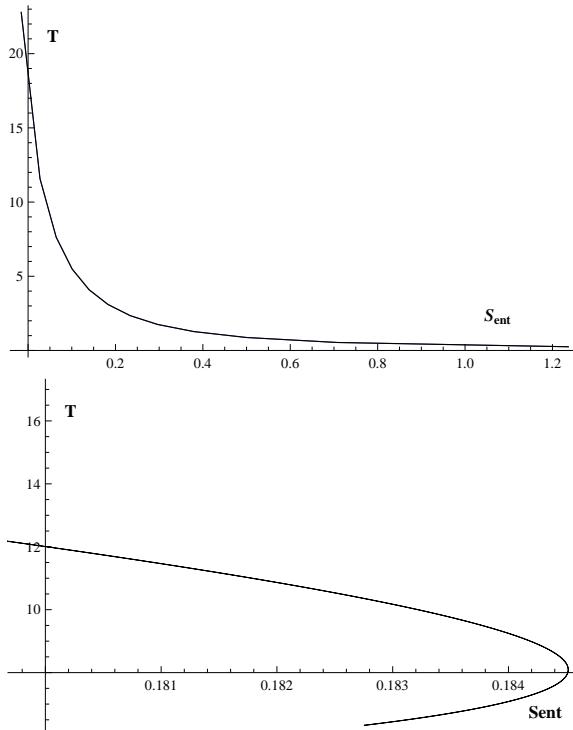
Figure 2.3: Regularized entanglement entropy versus temperature for neutral dRGT black hole (top) and charged dRGT black hole (bottom) with the massive parameter value $m = 1$.

shows the behavior of entanglement entropy of a charged dRGT black hole with the parameter values $m = c = c_1 = 1$ and $Q = 0.25$. From the figure it can be clearly understood that there is no phase transition for a neutral black hole while it shows a phase transition for a charged black hole. These results are thus in accordance with the results from thermodynamics studies discussed in the previous section of this chapter.

65

2.6   Summary of the Chapter

In this chapter, studies on the QNMs coming out of massless scalar perturbations in black hole space-time in a class of dRGT massive gravity, is presented. We have used the Improved AIM to calculate the QNMs in the de Sitter space-time with 50 iterations. The QNMs are studied by varying the massive parameter, m. It is found that as m increases the magnitudes of the QN frequencies increase for neutral black hole. These QNMs are also higher in magnitude compared to the SdS case meaning that such black holes decay fast. It is also found that as γ and ζ tend to zero, the results converge to the SdS case. For a charged black hole, the real part of the quasi normal frequency decreases and the magnitude of imaginary part increases as m is increased.

We have also presented in this chapter, the P-V criticality in the extended phase space of the aforesaid black holes. The neutral black holes show a near Van der Waals behavior with the compressibility ratio of 0.5. But it does not show any physically feasible phase transition for the dS space-time. The charged black hole on the other hand exactly shows a Van der Waals behavior and clearly exhibits a phase transition. Study on the holographic entanglement entropy of a neutral and charged black hole shows results in accordance with the thermodynamical studies.

Studies on the black hole QNMs, thermodynamics and phase transition of a linearly charged BTZ black hole done is presented in the following Chapter.

3

QUASI NORMAL MODES AND THERMODYNAMICS OF LINEARLY CHARGED BTZ BLACK HOLES IN MASSIVE GRAVITY

The study of black holes in AdS space-time is gaining much importance mainly due to its correspondence with Conformal Field Theory (CFT). For the study of such correspondences, the $(2+1)$ dimensional BTZ black hole solutions form the appropriate candidates. BTZ solutions thus gains importance as a testing ground of any theory of gravity for a deeper understanding. In the case of massive gravity also studies in that direction should be exploited to get a deeper understanding of the theory.

3.1 Introduction

Recently there has been a growing interest in the asymptotically Anti-de Sitter(AdS) space-time. The black hole solution proposed by Banados-Teitelboim-Zanelli (BTZ) in $(2+1)$ dimensions deals with asymptotically AdS space-time and has got well defined charges at infinity, mass, angular momentum and makes a good testing ground especially when one would like to go beyond the asymptotic flatness[128]. Another interesting aspect of the black hole solution is related to the AdS/CFT correspondence. In $(2+1)$ dimensions, the BTZ black hole solution is a space-time of constant negative curvature and it differs from the AdS space-time in its global properties[129].

As discussed before, QNMs form the testing ground for the existence of black holes in any theory of gravity. The study of QNMs in AdS space-time was initiated by Horowitz and Hubeny[130]. It was Cardoso and Lemos who first calculated the exact QNMs of the BTZ black holes[131]. They have found out both analytical and numerical solutions to the BTZ black hole perturbation for non-rotating BTZ black holes. It is interesting to note that they got exact analytical solutions to the wave equation that made the BTZ black hole space-time an important one where one can prove or disprove the conjectures relating to QNMs, critical phenomena or area quantization. This work was then extended to the case of a rotating black hole space-time by Birmingham[132]. The QNMs are also studied for charged dilaton black holes in $(2+1)$ dimensions[133].

Another important aspect of black holes is, as earlier discussed, the

black hole thermodynamics. There has been growing interests in this aspect among researchers. The black hole thermodynamics plays a crucial role in the non-perturbative aspects of quantum gravity. Among the thermodynamical aspects, the thermal stability of a black hole holds a significant position. A black hole has to be thermally stable. A thermally unstable solution may lead to a phase transition of black hole from a thermally unstable to a stable state. The thermodynamic phase transitions and area spectra of the BTZ black holes are studied in the literature[91, 134, 135]. The charged BTZ black hole solutions are also studied for the phase transition in references [136, 137]

Understanding that electromagnetic field can be a good choice of source for getting deep insights into the 3 dimensional massive gravity, we concentrate on the QNMs, the associated phase transition and thermodynamics of linearly charged BTZ black hole in massive gravity in the presence of Maxwell's field.

3.2 Quasi Normal Modes for Scalar Perturbations

For a linearly charged black hole, the Einstein-Maxwell action in $(2+1)$ dimension is given by[138],

$$(3.1) \qquad S_{EM} = \frac{1}{16\pi G} \int d^3x \sqrt{-g} \left[R + \frac{2}{l^2} - 4\pi G F_{\mu\nu} F^{\mu\nu} \right],$$

where R is the Ricci scalar, $F_{\mu\nu} = \partial_\mu A_\nu - \partial_\nu A_\mu$ is the Faraday tensor, A_μ is the gauge potential, and $F^{\mu\nu} F_{\mu\nu}$ is the Maxwell invariant. The action given above can be generalized to include the massive gravity

for the dS space-time as[139],

$$S = \frac{-1}{16\pi} \int d^3x \sqrt{-g} [R + 2\Lambda + L(\mathscr{F}) +$$

(3.2)

$$m^2 \sum_i^4 c_i \mathscr{U}_i(g, f)],$$

where $\mathscr{F} = F^{\mu\nu}F_{\mu\nu}$, L is an arbitrary Lagrangian of electrodynamics, $\frac{1}{l^2} = \Lambda$, the cosmological constant in the dS space-time, $\mathscr{U}_i$s are the effective potentials, m is the massive parameter and c_is are constants. By varying (3.2) with respect to the metric $g_{\mu\nu}$, one can obtain the gravitational field equation as,

(3.3) $\qquad G_{\mu\nu} + \Lambda g_{\mu\nu} - \frac{1}{2}g_{\mu\nu}L(\mathscr{F}) - 2L_{\mathscr{F}}F_{\mu\rho}F_\nu^\rho + m^2\mathscr{K}_{\mu\nu} = 0,$

where, $\quad G_{\mu\nu} = R_{\mu\nu} - \frac{1}{2}g_{\mu\nu}R$, $L_{\mathscr{F}} = \frac{dL(\mathscr{F})}{d\mathscr{F}}$, $\mathscr{K}_\nu^\mu = \sqrt{g^{\mu\alpha}f_{\alpha\nu}}$,

and,

$$\mathscr{K}_{\mu\nu} = \frac{-c_1}{2}\left(\mathscr{U}g_{\mu\nu} - \mathscr{K}_{\mu\nu}\right) - \frac{c_2}{2}\left(\mathscr{U}_2 g_{\mu\nu} - 2\mathscr{U}_1\mathscr{K}_{\mu\nu} + 2\mathscr{K}_{\mu\nu}^2\right) -$$

(3.4) $\qquad \frac{c_3}{2}\left(\mathscr{U}_3 g_{\mu\nu} - 3\mathscr{U}_2\mathscr{K}_{\mu\nu} + 6\mathscr{U}_1\mathscr{K}_{\mu\nu}^2 - 6\mathscr{K}_{\mu\nu}^3 + 24\mathscr{K}_{\mu\nu}^4\right) -,$

$$\frac{c_4}{2}\left(\mathscr{U}_4 g_{\mu\nu} - 4\mathscr{U}_3\mathscr{K}_{\mu\nu} + 12\mathscr{U}_2\mathscr{K}_{\mu\nu}^2 - 24\mathscr{U}_1\mathscr{K}_{\mu\nu}^3 + 24\mathscr{K}_{\mu\nu}^4\right)$$

where $\mathscr{K}$ has got the same definition as in the previous chapters. To obtain a static charged black hole solution we consider the 3 dimensional metric with the space-time signature as, $(-++)$,

(3.5) $\qquad ds^2 = -f(r)dt^2 + f^{-1}(r)dr^2 + r^2 d\theta^2,$

where $f(r)$ is an arbitrary function of the radial coordinate. To get an exact solution for this metric, the following ansatz for the fiducial metric is employed[116],

(3.6) $\qquad f_{\mu\nu} = \text{diag}(0, 0, c^2 h_{ij}),$

70

where c is a positive constant. Using the above metric ansatz the effective potential terms are obtained as,

$$(3.7) \qquad \mathscr{U}_1 = \frac{(d-2)c}{r},$$

$$(3.8) \qquad \mathscr{U}_2 = \mathscr{U}_3 = \mathscr{U}_4 = 0,$$

which tells that since we are dealing with 3 dimensions, the only contribution of massive gravity comes from $\mathscr{U}_1$. The Lagrangian of the Maxwell field is chosen as, $L(\mathscr{F}) = -\mathscr{F}$ since we are dealing with linearly charged BTZ solution. Here, we are also interested in electrically charged black hole solution and hence the radial electric field is chosen as,

$$(3.9) \qquad h(r) = \sqrt{Q}\,\ln\left(\frac{r}{\alpha}\right),$$

where Q is an integration constant which is related to the electric charge and α is an arbitrary constant that has got the dimension of length. Using (3.3) and (3.5) for getting exact solution for the metric function leads to the set of differential equations, corresponding to the 'tt' (or 'rr'') and '$\phi\phi$' components respectively, given by,

$$(3.10) \qquad rf'(r) + 2r^2\Lambda + 2Q - m^2 cc_1 r = 0,$$

$$(3.11) \qquad \frac{r^2}{2}f''(r) + \Lambda r^2 - Q = 0.$$

Solving these equations will lead to the metric function, in the dS space-time as[138, 139],

$$(3.12) \qquad f(r) = \Lambda r^2 - m_0 - 2Q\ln\frac{r}{\alpha} + m^2 cc_1 r,$$

where m_0 is related to the mass of the black hole, α is an arbitrary constant and c and c_1 are constants. For an AdS, Λ will take negative

71

values. From the metric function, it can be understood that the contribution of the massive term depends on the sign of c_1.

For finding the QNMs, the black hole space-time described by the metric function (3.12) has to be perturbed. Here a massless scalar field perturbation in this space-time is considered and in that case the black hole space-time satisfies the Klein-Gordon equation,

$$(3.13) \qquad \frac{1}{\sqrt{-g}} \frac{\partial}{\partial x^a} \left(g^{ab} \sqrt{-g} \frac{\partial}{\partial x^b} \right) \Phi = 0,$$

which on expanding gives,

$$(3.14) \qquad \frac{1}{f(r)} \frac{\partial^2 \Phi}{\partial t^2} - \frac{\partial}{\partial r} f(r) \frac{\partial \Phi}{\partial r} - \frac{1}{r^2} \frac{\partial^2 \Phi}{\partial \phi^2} = 0.$$

To separate the radial and angular variables, we make use of the ansatz,

$$(3.15) \qquad \Phi = \frac{R(r)}{r} e^{-i\omega t} e^{im_l \phi},$$

where ω is the frequency, m_l is the angular momentum quantum number. Using the above ansatz, the radial part of the Klein-Gordon equation can be written as,

$$(3.16) \qquad \frac{d^2 R}{dr^2} + \frac{f'(r)}{f(r)} \frac{dR}{dr} + \left[\frac{\omega^2}{f(r)^2} - \frac{\left(\frac{m_l^2}{r^2} - \frac{2Q}{r^2} + \frac{cc_1 m}{r} \right)}{f(r)} \right] R = 0.$$

Quasi normal modes are ingoing waves at the event horizon and outgoing waves at the cosmological horizon, leading to the boundary condition,

$$(3.17) \qquad R \to \begin{cases} e^{i\omega r}, & \text{as } r \to \infty \\ e^{-i\omega r}, & \text{as } r \to -\infty \end{cases}$$

Making a variable change $r \to 1/\xi$, the equation (3.16) becomes,

(3.18)
$$\frac{d^2R}{d\xi^2} + \frac{p'}{p}\frac{dR}{d\xi} + \left[\frac{\omega^2}{p^2} - \frac{2Q + \frac{2\Lambda}{\xi^2} - \frac{cc_1m}{\xi} - m_l^2}{p}\right]R = 0,$$

where,

(3.19)
$$p = M\xi^2 - cc_1m\xi + 2Q\xi^2\ln\left(\frac{1}{\alpha\xi}\right) + \Lambda,$$

(3.20)
$$p' = 2(M - Q)\xi - cc_1m + 4Q\xi\ln\left(\frac{1}{\alpha\xi}\right).$$

The equation given by (3.18) has got the singularities at the event horizon and at an outer horizon. In order to solve the equation, the singularities have to be scaled out. Here, we first scale out the divergent behavior at the outer horizon and then re-scale to avoid the event horizon. To scale out the divergence at outer horizon, we take[118],

(3.21)
$$R(\xi) = e^{i\omega\xi}u(\xi),$$

where,

(3.22)
$$e^{i\omega\xi} = (\xi - \xi_1)^{\frac{i\omega}{2\kappa_1}}(\xi - \xi_2)^{\frac{i\omega}{2\kappa_2}},$$

and,

(3.23)
$$\kappa_i = \frac{1}{2}\frac{\partial f}{\partial r}|_{r \to r_i},$$

is the surface gravity at each horizon. The master equation then will take the form,

(3.24)
$$pu'' + (p' - 2i\omega)u' - \left(2Q - \frac{2\Lambda}{\xi^2} - \frac{cc_1m}{\xi} - m_l^2\right)u = 0.$$

This can be viewed as of a second order differential equation of the form,

(3.25)
$$u'' = \lambda_0(\xi)u' + s_0(\xi)u,$$

73

with,

$$(3.26) \qquad \lambda_0 \;=\; -\frac{(p' - 2i\omega)}{p},$$

$$(3.27) \qquad s_0 \;=\; \frac{\left(2Q - \frac{2\Lambda}{\xi^2} - \frac{cc_1 m}{\xi} - m_l^2\right)}{p}.$$

The Improved AIM discussed in the previous chapter is employed to find out the QNMs. In Table 3.1 we list the QN frequencies of the black hole in the dS space-time for $m = 1$, $m = 1.05$ and $m = 1.1$ for different values of the cosmological constant, calculated using the improved AIM. We have used the parameter values: $Q = 0.25$, $m_l = 1$, $\alpha = 1$, $c = 1$ and $c_1 = 1$. In the numerical calculations we have used 15 iterations. It is observed that the behavior of the QN frequencies, ie., the way by which QN frequencies vary with Λ, change after a particular Λ value. This change in behavior is shown in the table by a horizontal line as a separator. This sudden change in behavior happens at $\Lambda = 0.1$ for $m = 1$, at $\Lambda = 0.21$ for $m = 1.05$ and at $\Lambda = 0.28$ for $m = 1.1$. This behavior of the QNMs, ω_R versus ω_I, are plotted in Fig.3.1. From the figures it can be clearly seen that the slope of the curve changes suddenly at some transition point for $m = 1, 1.05, 1.1$ and can be treated as a clear indication of a phase transition. However for the same values of the constant parameters this phase transition occurs at different values of Λ for the different m values. The higher the value of m, the higher the value of Λ at which the phase transition occurs. As an example, the variation of the QN frequencies (ω_R and ω_I) with Λ for the massive parameter $m = 1.1$ is shown in Fig.3.2.

In Table 3.2, we have shown the QN frequencies, calculated for $Q =$
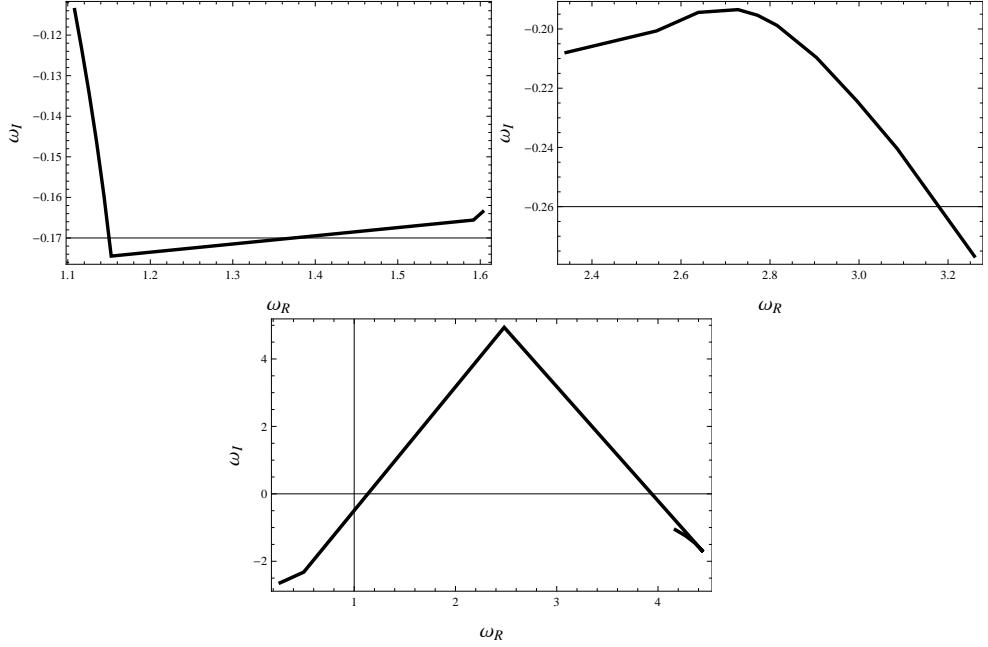
Figure 3.1: QNM behavior of linearly charged BTZ black hole for the massive parameter values $m = 1, 1.05, 1.1$ (from top left) and $Q = 0.25$. The sudden change in the slope can be treated as an indicative of a possible phase transition.

0.35 for the massive parameter values, $m = 0.9$, $m = 0.95$ and $m = 1.0$ with $m_l = c = c_1 = 1$. The behavior of these QNMs (ω_R versus ω_I) are shown in Fig.3.3. Just like in the case where $Q = 0.25$, here also there is a sudden change in the slope of the curve after a particular Λ indicating that of a possible phase transition. Thus, for both values of Q, the black hole shows phase transition for the dS space-time. We can see from Tables 3.1 and 3.2 that for the value $m = 1.0$ the phase transition occurs at different values of Λ for the $Q = 0.25$ and $Q = 0.35$ cases.

75
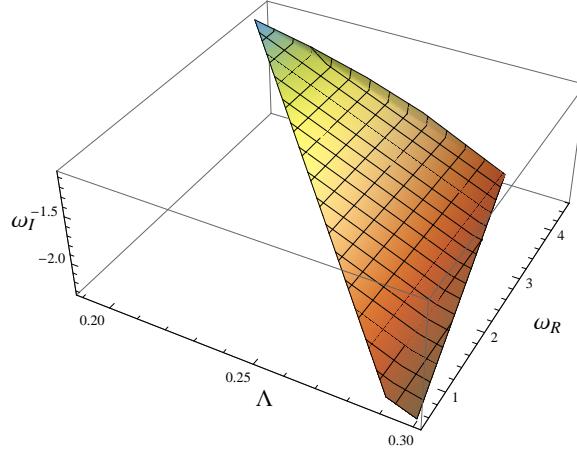
Figure 3.2: The behavior of QNMs with Λ calculated in Table 3.1 for
$m = 1.1$ for the dS space-time

Table 3.1: QNMs of linearly charged BTZ black hole for different
values of the massive parameter for dS space-time with $Q = 0.35$

	$m = 0.9$		$m = 0.95$		$m = 1.0$
Λ	$\omega = \omega_R + \omega_I$	Λ	$\omega = \omega_R + \omega_I$	Λ	$\omega = \omega_R + \omega_I$
0.09	.898571 - .0783066i	0.05	1.16072 - .0686295i	0.01	1.68971 - .172263i
0.10	.901026 - .0798863i	0.06	1.18398 - .0690504i	0.015	1.69779 - .581786i
0.11	.902855 - .0851571i	0.07	1.20614 - .0630027i	0.02	1.70293 - .198065i
0.12	.902565 - .0947457i	0.08	1.21651 - .0514301i	0.025	1.70506 - .214255i
0.13	1.03909 - .107478i	0.09	1.21431 - .0415960i	0.03	1.70405 - .232616i
0.14	1.01865 - .0859070i	0.10	1.20180 - .0347956i	0.04	1.69178 - .27573i
0.15	1.00159 - .0683552i	0.11	1.17941 - .0303883i	0.05	1.66379 - .327079i
0.16	.983281 - .0666629i	0.12	1.14639 - .0274678i	0.06	1.61649 - .386106i
0.17	.961166 - .0464981i	0.13	1.10110 - .0251206i	0.07	1.54442 - .451769i
0.18	.933873 - .0396936i	0.14	1.04093 - .0224859i	0.08	1.43902 - .521872i

In Table 3.3 we show the QNMs calculated for an AdS space-time
for the massive parameter values $m = 1, 1.05, 1.1$ with $Q = 0.1$, $\alpha = 1$,
$c = 1$, $c_1 = 1$. From Table 3.3, it can be observed that the ω_R and ω_I
continuously decrease and after reaching a particular Λ, the real and
imaginary parts suddenly increase and then continuously decrease.
This jump can be treated as an indication of an inflection point and is
shown in Fig.3.4.
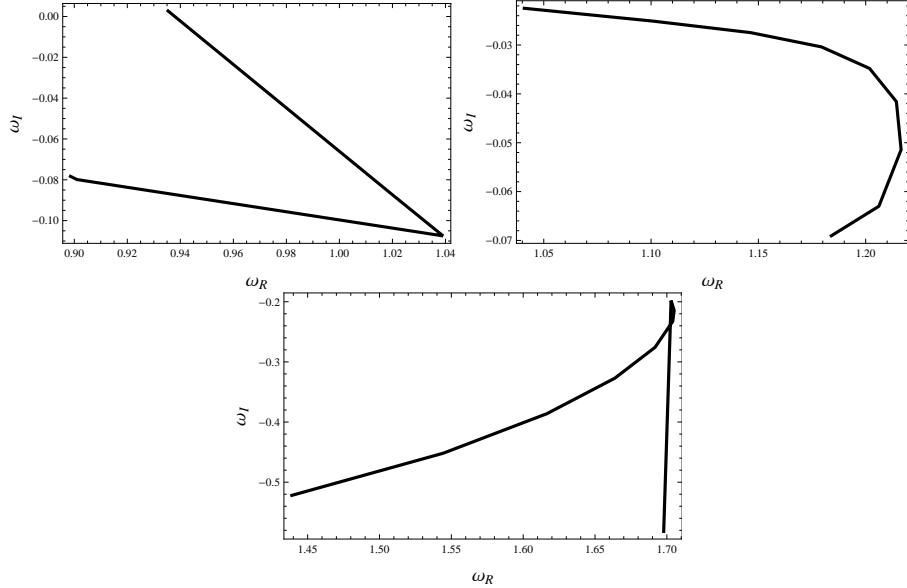
Figure 3.3: QNM behavior of linearly charged BTZ black hole for dS space-time with $Q = 0.35$ for the massive parameter values $m = 0.9, 0.95, 1.0$ (from top left). The sudden change in the slope can be treated as an indicative of a possible phase transition.

Table 3.2: QNMs of linearly charged BTZ black hole for different values of the massive parameter for dS space-time with $Q = 0.35$

	$m = 0.9$		$m = 0.95$		$m = 1.0$
Λ	$\omega = \omega_R + \omega_I$	Λ	$\omega = \omega_R + \omega_I$	Λ	$\omega = \omega_R + \omega_I$
0.09	.898571 - .0783066i	0.05	1.16072 - .0686295i	0.01	1.68971 - .172263i
0.10	.901026 - .0798863i	0.06	1.18398 - .0690504i	0.015	1.69779 - .581786i
0.11	.902855 - .0851571i	0.07	1.20614 - .0630027i	0.02	1.70293 - .198065i
0.12	.902565 - .0947457i	0.08	1.21651 - .0514301i	0.025	1.70506 - .214255i
0.13	1.03909 - .107478i	0.09	1.21431 - .0415960i	0.03	1.70405 - .232616i
0.14	1.01865 - .0859070i	0.10	1.20180 - .0347956i	0.04	1.69178 - .27573i
0.15	1.00159 - .0683552i	0.11	1.17941 - .0303883i	0.05	1.66379 - .327079i
0.16	.983281 - .0666629i	0.12	1.14639 - .0274678i	0.06	1.61649 - .386106i
0.17	.961166 - .0464981i	0.13	1.10110 - .0251206i	0.07	1.54442 - .451769i
0.18	.933873 - .0396936i	0.14	1.04093 - .0224859i	0.08	1.43902 - .521872i

It can be seen that there is no drastic change in the slope and the behavior of the QNMs are similar for all values of m. Hence it can be inferred that there will be no phase transition. In Table

Table 3.3: QNMs of linearly charged BTZ black hole for different
values of the massive parameter for AdS space-time with $Q = 0.1$

	$m = 1.0$		$m = 1.05$		$m = 1.1$
Λ	$\omega = \omega_R + \omega_I$	Λ	$\omega = \omega_R + \omega_I$	Λ	$\omega = \omega_R + \omega_I$
-0.06	1.83077 - 5.78701 i	-0.05	1.39873 - 7.68495 i		
-0.07	1.70014 - 5.33444 i	-0.06	1.29210 - 7.27705 i	-0.04	0.75408 - 9.41718 i
-0.08	1.53828 - 4.92198 i	-0.07	1.14457 - 6.93423 i	-0.05	0.63741 - 9.08170 i
-0.09	1.34563 - 4.54476 i	-0.08	0.95604 - 6.62556 i	-0.06	0.48892 - 8.73203 i
-0.10	1.11762 - 4.20206 i	-0.09	0.72592 - 6.35819 i	-0.07	0.21318 - 8.39613 i
-0.11	0.84041 - 3.89983 i	-0.95	0.58718 - 6.23146 i		
-0.12	0.48197 - 3.66706 i	-0.10	0.40624 - 6.12793 i		
-0.13	0.81813 - 4.06506 i	-0.11	1.57334 - 7.10865 i	-0.08	2.18254 - 10.2207 i
-0.135	0.75562 - 3.41486 i	-0.13	1.12639 - 5.99601 i	-0.09	1.44272 - 10.1043 i
-0.14	0.32251 - 2.91165 i	-0.14	0.86214 - 5.07753 i	-0.10	1.41871 - 9.40952 i

Table 3.4: QNMs of linearly charged BTZ black hole for different
values of the massive parameter for AdS space-time with $Q = 0.25$

	$m = 0.95$		$m = 1.0$		$m = 1.05$
Λ	$\omega = \omega_R + \omega_I$	Λ	$\omega = \omega_R + \omega_I$	Λ	$\omega = \omega_R + \omega_I$
0.01	.292587 - 9.19482i	0.13	.820054 - 4.96149i	0.29	1.01098 - .0351877i
0.02	.772162 - 8.39220i	0.15	.431983 - 3.38060i	0.31	1.02868 - .0148701i
0.03	.844245 - 7.75702i	0.17	.00879691 - .0348464i	0.32	1.04119 - .00215093i
0.04	.820904 - 7.24016i	0.19	1.72429 - .0660172i	0.33	1.62431 - .102106i
0.05	.759655 - 6.75177i	0.20	1.73419 - .0561830i	0.34	1.62400 - .083530i
0.07	.551068 - 5.89321i	0.21	1.74461 - .043151i	0.35	1.61905 - .067770i
0.09	.390010 - 4.86350i	0.22	1.75581 - .0330092i	0.36	1.60957 - .060276i
0.11	.243717 - 3.77402i	0.23	1.76769 - .0186321i		

3.4 we have calculated the QNMs for the AdS space-time for the
massive parameter values $m = 0.95, 1, 1.05$ with $Q = 0.25$, $\alpha = 1$, $c = 1$,
$c_1 = 1$. Fig.3.5 shows the behavior of QN frequencies, ω_R versus ω_I,
for the above case. It can be seen that there is a sudden change in the
slope of the curve after reaching a particular Λ indicating a possible
phase transition. For $Q = 0.1$ the AdS black hole space-time does not
show any phase transition behavior but for $Q = 0.25$ it is found to be
showing a phase transition behavior. Thus it can be inferred that the
phase transition behavior depends on the charge Q.

Now, it would be interesting to check the variation of QNMs with Q.
Table 3.5 shows the QN frequencies calculated for different charges Q
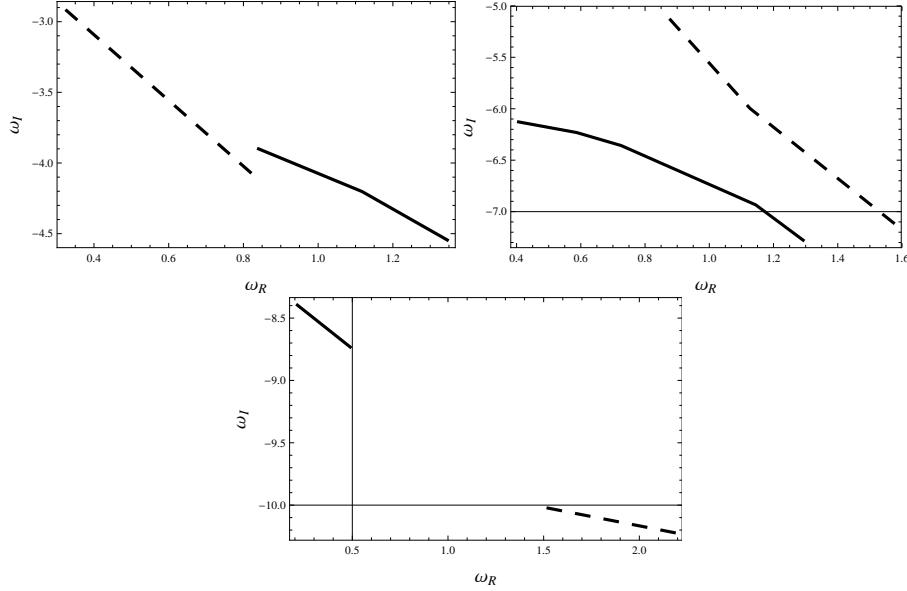
Figure 3.4: QNM behavior of linearly charged BTZ black hole with charge Q =0.1 for AdS space-time for the massive parameter value $m = 1, 1.05, 1.1$ (from top left). The bold lines represent the behavior of QNMs before the inflection point and the dotted lines line represent the behavior of QNMs after the inflection point. The behavior of QNMs are seen to be the similar in the plots. There is no much difference in the slope of the curves

in dS space-time for a fixed Λ. It can be seen that the behavior of QN frequency changes frequently. The phase transition behavior is highly dependent on the charge. The phase does not remain the same for a wide range of charge and hence phase transition is found to happen frequently over a range of charges. This variation is plotted in Fig.3.6.

The variation of QNMs with charge calculated for a fixed Λ in the AdS case is shown in Table 3.6. It can be seen that compared to the dS case the phases remain the same for most of the values of charge in AdS space-time This behavior is plotted in Fig.3.7.

79
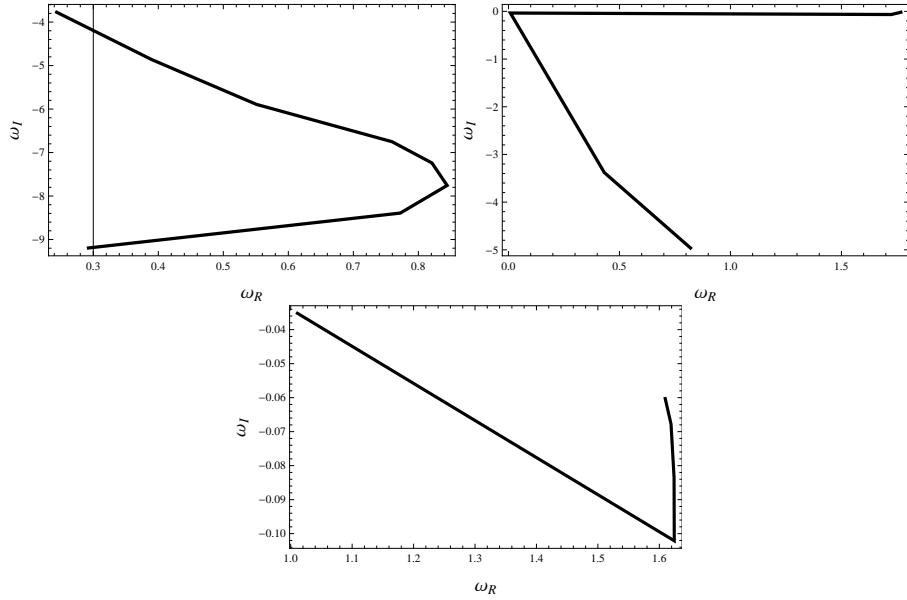
Figure 3.5: QNM behavior of linearly charged BTZ black hole with
$Q = 0.25$ for the massive parameter values $m = 0.95, 1.0, 1.05$ (from
top left).

Table 3.5: Table showing the variation of QNMs with Q in the dS
space-time

Q	ω
0.15	4.47348 - 0.19884 i
0.20	4.33915 - 0.108836 i
0.25	0.0930679 - 0.0668980 i
0.30	1.54638 - 0.132502 i
0.35	1.68971 - 0.172263 i
0.40	0.0325096 - 0.466834 i

Thus, the variation of QNMs with Λ for a linearly charged black

hole in massive gravity is calculated for the dS and AdS space-times

and compared for different values of the massive parameter m. We

have also studied the variation of QNMs with charge. For the dS

80

Table 3.6: Table showing the variation of QNMs with Q in the AdS space-time

Q	ω
0.05	1.12930 - 9.66585 i
0.10	1.14048 - 9.54589 i
0.15	2.42998 - 12.8629 i
0.20	3.49176 - 14.0316 i
0.25	3.64711 - 13.9835 i
0.30	0.294699 - 9.56518 i
0.35	0.557735 - 9.42807 i
0.40	0.792729 - 9.21181 i
0.45	0.940783 - 9.04476 i
0.50	1.03930 - 8.88485 i
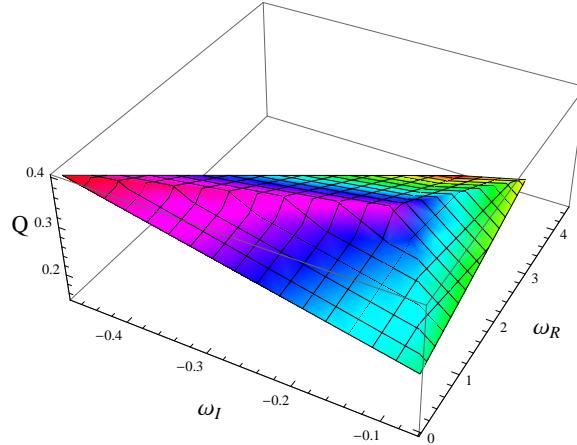
Figure 3.6: Variation of QNMs with charge Q for the dS space-time

space-time, the QNMs for the charges, $Q = 0.25$ and $Q = 0.35$ showed phase transition behavior, but the value of Λ at which the phase transition occurs are different for the two charges. For the AdS space-time also the variation of QNMs with Λ is looked into for the charge values, $Q = 0.1$ and $Q = 0.25$. It is found that for the case of $Q = 0.1$ no phase transition behavior is observed whereas, for $Q = 0.25$ the
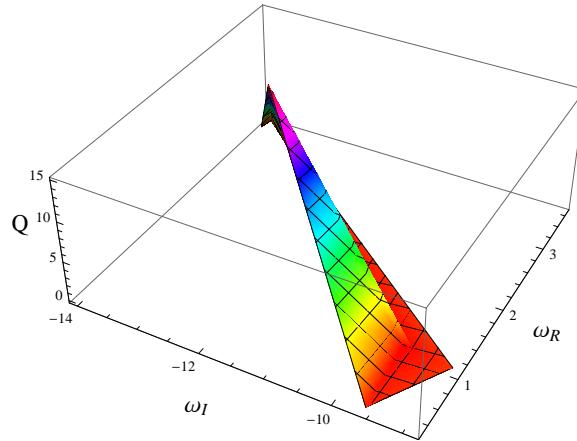
Figure 3.7: Variation of QNMs with charge Q for AdS space-time

black hole shows a phase transition behavior. These results prompted
to check the variation of QNMs with Q for some fixed Λ for the dS
and AdS space-times. It shows that phase transition happens for a
large range of charges for the dS space-time whereas phase transition
happens only for certain values of charge in the AdS space-time. Now,
having these results at hand, it would be interesting to study the
thermodynamics.

3.3 Thermodynamics of the Black Hole

From the laws of black hole thermodynamics discussed in chapter 1.5,
the mass of the black hole, m_0, is obtained from the solution of the
condition, $f(r)|_{r \to r_h} = 0$ as,

$$(3.28) \qquad m_0 = m^2 c c_1 r_h + \Lambda r_h^2 - 2Q \ln(\frac{r_h}{\alpha}).$$

The temperature of the black hole is given by,

(3.29)
$$T = \frac{\kappa}{2\pi}$$
$$= \frac{1}{4\pi} f'(r)\bigg|_{r \to r_h}.$$

Employing (3.12) one gets the expression for the temperature as,

(3.30)
$$T = \frac{cc_1 m^2}{4\pi} - \frac{Q}{2\pi r_h} + 4Pr_h,$$

where $P = \frac{\Lambda}{8\pi}$. Finally, the entropy is evaluated as,

(3.31)
$$S = \int_0^{r_h} \frac{1}{T} \frac{\partial m_0}{\partial r} dr$$
$$= 4\pi r_h.$$

The equation of state, $P(V, T)$ can be obtained from (3.30) as,

(3.32)
$$P = \frac{Q}{8\pi r_h^2} + \frac{-cc_1 m^2 + 4\pi T}{16\pi r_h}.$$

For $(2 + n)$ dimensional massive gravity, the volume is given by[126], $V = (\frac{\partial H}{\partial P})_{S,Q} = \frac{V_n}{n+1} r^{n+1}$. With $n = 1$, the calculation gives the horizon radius in terms of its volume as, $r_h = (\frac{V}{8\pi})^{1/2}$.

To specify the phase transition it will be useful to introduce the Gibbs free energy as a Legendre transformation of enthalpy as,

(3.33)
$$G = H - TS,$$

where H is the enthalpy, T is the temperature given by (3.29) and S is the entropy given by (3.31). We use the black hole mass m_0 as the enthalpy since $H \equiv m_0$ rather than the internal energy of the gravitational system[140]. Substituting (3.28), (3.30) and (3.31) in (3.33), we get an expression for the Gibbs free energy as,

(3.34)
$$G(T, \Lambda) = 2Q + \Lambda r_h^2 - 2Q \ln(\frac{r_h}{\alpha}).$$

83

Or in terms of P,

$$(3.35) \qquad G(T, \Lambda) = 2Q + 8\pi P r_h^2 - 2Q \ln(\frac{r_h}{\alpha}).$$

A parametric plot can be made between G and T using (3.30) and
(3.35) for a constant P. Fig.3.8 shows the variations of Gibbs free
energy with temperature. Top of the figure shows the G-T plot for
$P = 0.001$. It can be seen that the upper branch which lies in the posi-
tive Gibbs free energy region moves towards the lower branch which
lies in the 'positive temperature-negative Gibbs free energy' region
which indicates a possible phase transition. The bottom plot shows
variation of G with T for $P = -0.001$. The plot lies in the positive
Gibbs free energy region and shows a cusp like behavior.

Fig.3.9 shows the variation of pressure, P and temperature, T with
the horizon radius, r_h, for fixed values of temperature and pres-
sure plotted using (3.30) and (3.32) respectively. Top of the Fig.3.9,
shows the variation of temperature with r_h for the pressure values
$P = -0.003, -0.002, -0.001, 0.001$, and 0.002. The bottom of the
Fig.3.9 shows the variation of pressure with r_h for the fixed values of
temperature, $T = -0.3, -0.2, -0.1, 0.1$, and 0.2.

More details regarding the phase transition can be extracted from
the entropy of the system. Hence the temperature-entropy relation
would be worth looking at. For that, r_h from (3.31) is substituted for
r_h in (3.30) so that we get an expression relating the entropy and
temperature as,

$$(3.36) \qquad T = -\frac{2Q}{S} + \frac{2\pi c c_1 m^2 + \Lambda S}{8\pi^2}.$$
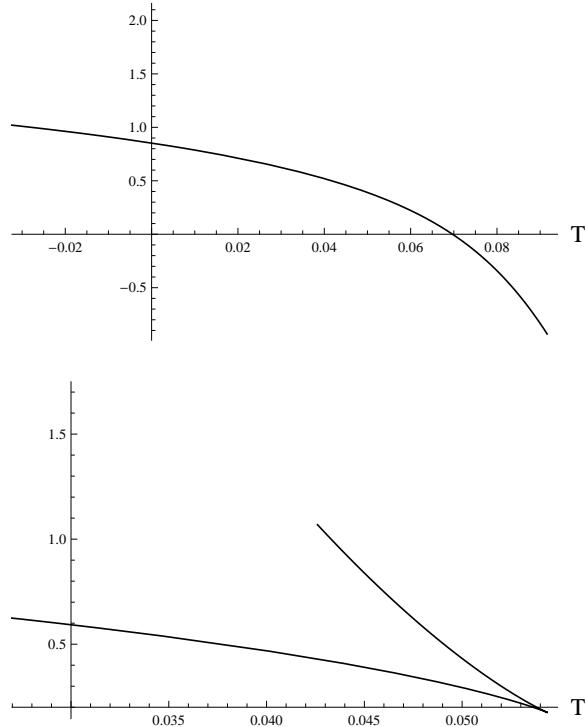
Figure 3.8: Variation of Gibbs free energy with temperature for the dS space-time (top) and AdS space-time (bottom).

To understand the behavior of entropy, the variation of entropy with temperature is plotted in Fig.3.10 for the values $\Lambda = 0.1$ and $\Lambda = -0.1$, with the parameter values $m_0 = c = c_1 = 1$, $\alpha = 1$, $Q = 0.25$ and $m = 1$. It can be seen that S remains positive only for a small range of temperature and both of them show phase transition behavior.

As discussed earlier, knowing the stability of black hole phases are important for understanding their phase transition behavior. Now, in order to study the stability of the phases or the feasibility of the above phase transitions, it may be worth looking at the behavior of
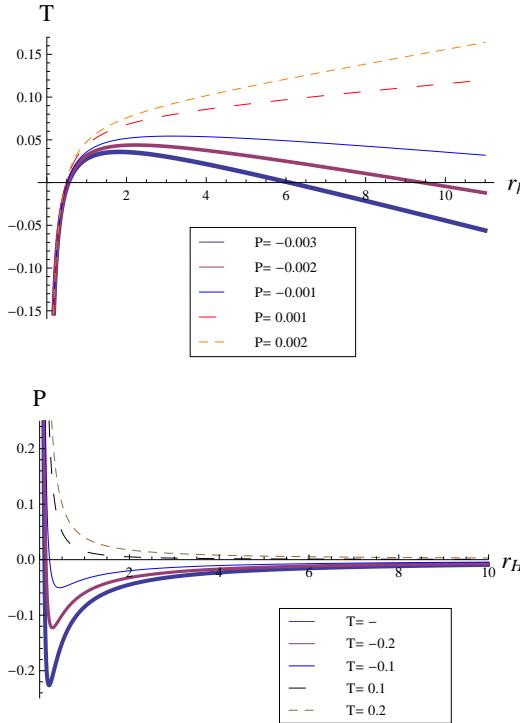
Figure 3.9: **Top :** Variation of T with r_h. **Bottom :** Variation of P
with r_h.

specific heat with temperature. If the heat capacity makes a transition
from negative values to positive values as the temperature varies,
the system undergoes a phase transition. Negative heat capacity
represents unstable state while positive value implies a stable state.
The specific heat capacity is given by the expression,

$$
(3.37) \qquad C_Q = \frac{T}{\left(\frac{\partial T}{\partial S}\right)_Q},
$$

Substituting the expression for T from (3.30) leads to,

$$
(3.38) \qquad C_Q = 2\pi r_h \left(\frac{-2Q + r_h \left(m^2 + 2 r_h \Lambda \right)}{Q + r_h^2 \Lambda} \right).
$$
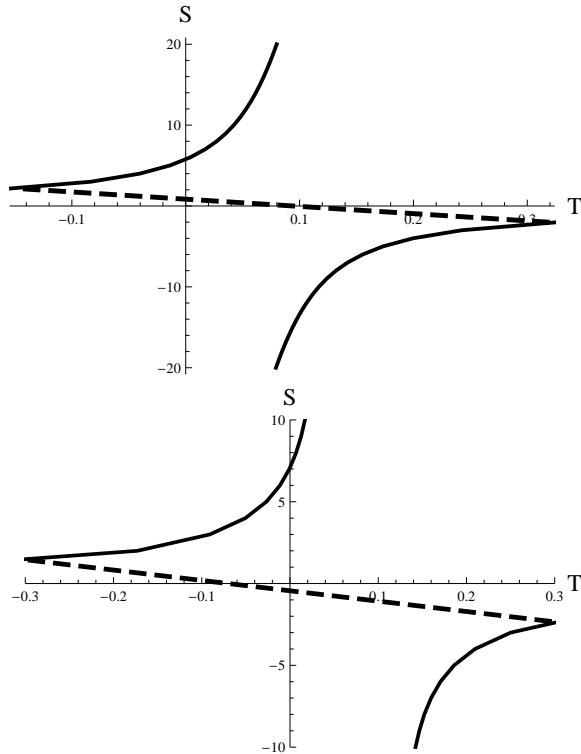
Figure 3.10: The variation of entropy with temperature for $\Lambda = 0.1$(top) and -0.1(bottom) in dS space-time

The plots of specific heat versus temperature for $\Lambda = 0.1$ and $\Lambda = -0.1$ are given in Fig.3.11 for the parameter values $m = c = c_1 = 1$ and $Q = 0.25$. From the plot it can be clearly understood that for $\Lambda = 0.1$, the specific heat changes from negative to positive values indicating a phase transition from unstable to stable configuration. For $\Lambda = -0.1$, from the figure we can say that it somewhat shows a phase transition behavior. However, it is observed that for given constant parameter values, the black holes in AdS space-time show the phase transition behavior only for a very small range of Λ values whereas in dS space-time it shows phase transition for a wide range of Λ values.

87

It would also be worth noting the variation of the behavior of specific
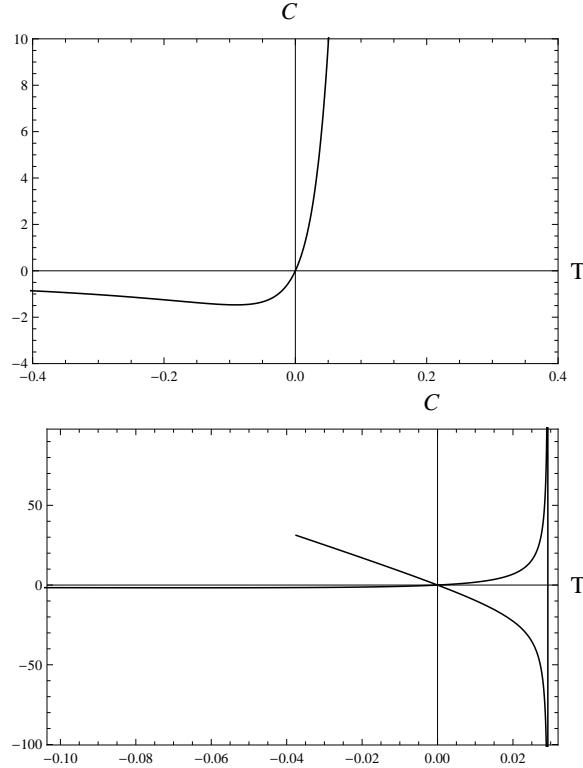
Figure 3.11: Figure showing the variation of specific heat with temperature for $\Lambda = 0.1$ (top) and $\Lambda = -0.1$ (bottom).

heat with charge, Q. For this, we have plotted variation of specific heat with temperature for $Q = 0.1, 0.25, 0.5, 0.6$ for dS space-time; the other parameters remaining the same and is shown in Fig.3.12. It can be seen that upto $Q = 0.5$ it shows a phase transition and then after reaching $Q = 0.6$, no more phase transition is seen. Also it is found that above this value no phase transition is observed.

The variation of the behavior of specific heat with Q for the AdS space-time for the values $Q = 0.1, 0.25, 0.3, 0.4$ is shown in Fig.3.13. It
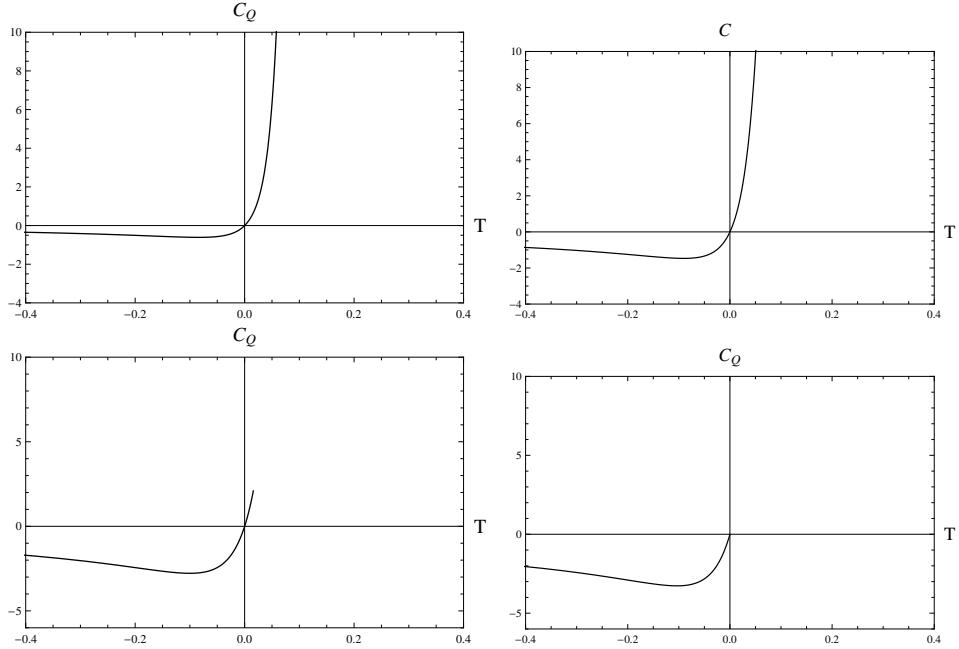
Figure 3.12: The variation of specific heat with temperature for $Q = 0.1, 0.25, 0.5, 0.6$ respectively from top left in dS space-time

can be seen that for $Q = 0.1$ it does not show any phase transition and for $Q = 0.25$ and $Q = 0.3$ it shows a phase transition and then after reaching $Q = 0.4$, no phase transition is seen. Also, it is found that above this value no phase transition is observed. From this it can also be concluded that AdS space-time shows phase transition only for a small range of Q when compared with the dS space-time.

Thus from the specific heat plots phase transition is observed in the dS space-time for the values of charge $Q = 0.1$ to $Q = 0.5$ and no phase transition is observed for values above $Q = 0.6$. In the AdS case, the phase transition is not observed for $Q = 0.1$ and values above $Q = 0.4$ and shows a phase transition for $Q = 0.25$ and $Q = 0.3$. These results
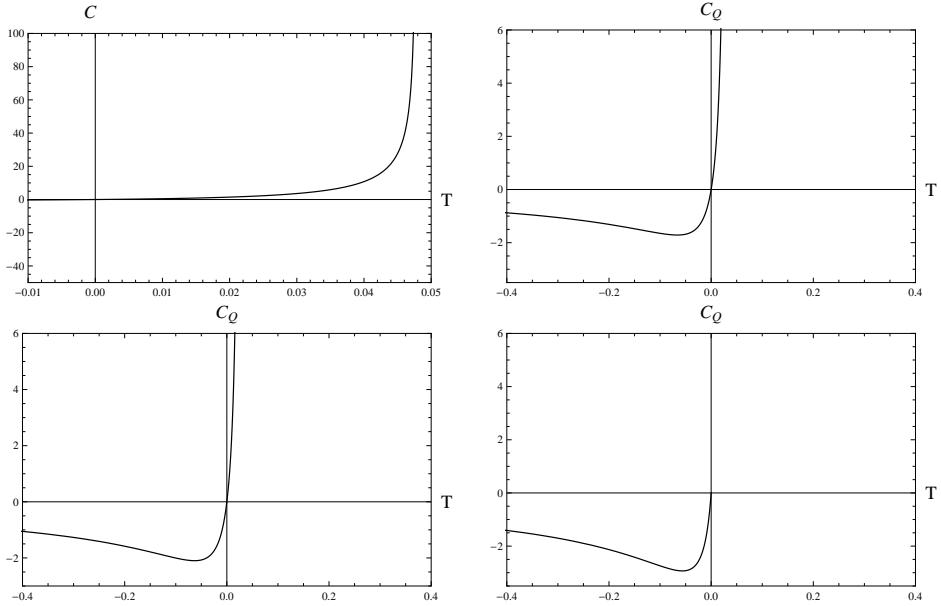
Figure 3.13: The variation of specific heat with temperature for $Q = 0.1, 0.25, 0.3, 0.4$ respectively from top left in AdS space-time

are in accordance with the results obtained from QNM study.

3.4 Summary of the Chapter

In this chapter, the QNMs are calculated for a linearly charged BTZ black hole in massive gravity. The values of the parameters are so chosen that in the metric function, the massive parameter dominates. It is found that in the dS space-time, as the cosmological constant Λ is increased, the QN frequencies varied continuously and then after reaching a particular value of $\Lambda(= 0.1)$, their behavior is found to be abruptly changing afterwards. This is shown in the ω_I-ω_R plot This can be seen as a strong indication of a possible phase transition occurring in the system. When the massive parameter m is increased,

a similar behavior is found but the Λ at which the change of behavior of QNMs takes place is found to be shifted to a higher value($\Lambda = 0.28$). Also, it can be inferred that the variation of the massive parameter will only alter the point at which the phase transition happens. For different values of Q the phase transition occurs for different values of Λ.

The QNMs for an AdS space-time is also calculated and the behavior of their quasi normal frequencies are analyzed. For $Q = 0.1$ the behavior of QNMs showed an inflection point but no phase transition. However for $Q = 0.25$ it showed a phase transition. It is seen that the phase transition behavior is found dependent on Q. It is also observed by studying the variation of QNMs with Q that AdS space-time shows phase transition only for certain limited ranges of Q compared to the dS case. The thermodynamics of such black holes in the dS space-time is then looked into. The behavior of specific heat showed phase transition for the dS case for a wide range of Q whereas for AdS space-time phase transition is shown only for a limited range of Q.

MASSIVE GRAVITATIONAL WAVES AND ITS DETECTION USING SPHERICAL ANTENNA

4.1 Introduction

Another important aspect of any theory of gravity is the study of Gravitational Waves. It came out as one of the important results of GTR. Therefore massive gravity theories are also expected to give GW solutions for making itself eligible for replacing or modifying GTR. The GWs produced must also be detected. The path breaking discovery of GWs was made recently by LIGO from black hole collisions. The discovery indicates the accuracy in the prediction of GWs based on the well celebrated GTR theory. While analyzing the GWs, the deviations from GTR can also be studied. From the discovery, a phenomenological limit to the mass of the graviton for GTR deviations was more accurately done as $m < 1.2 \times 10^{-22} eV/c^2$ at 90%

confidence[100]. However the presence of additional modes of polarizations, that could possibly come from a modified theory such as scalar mode (basis of this work), could not be detected or in other words, the detector orientations of LIGO as such will not be capable of detecting a massive graviton. Hence more research has to be done to explore the ways in which additional polarization mode could be detected. Expecting that the response of a spherical antenna can be omnidirectional in nature towards a scalar mode that may possibly come from a modified gravity theory, it will be good to exploit the detection possibility via spherical antenna.

Antennae form the primitive, yet effective method for detecting GWs. The first antenna detector was proposed by Weber. This cylindrical antenna consists of an elastic body which may become deformed by the dynamic derivatives of the gravitational potentials, and its normal modes get excited. Such an antenna measures, precisely, the Fourier transform of certain components of the Riemann curvature tensor, averaged over its volume[104].

GW astronomy has two goals :

1. To verify the existence of GWs (which is detected now),
2. Use GW as a tool for astronomical observation.

The former requires a detector of high sensitivity and the latter imposes the additional requirement that the detectors have good direction resolution and a broad bandwidth.

Antennae may be of two kinds, Cylindrical or Spherical. Cylindrical antenna forms the primitive of its kind. Theoretical interests in

spherical GW antennae dates back to the 1970s. Spherical antennae have a greater cross section than bar detectors of similar dimensions. More importantly, they have both omnidirectional and omnipolarization sensitivity, and also the potential to detect the direction of wave provenance. It was in 1971 that Forward[141] proposed the initial spherical antenna detector for GW detection. He proposed that by suitably positioning transducers on the sphere one could determine the direction, polarization and amplitude of the wave. Johnson and Merkowitz[142] proposed a method of positioning six radial transducers on a truncated icosahedral to construct a nearly spherical detector. They showed that a spherical detector cooled to ultra low temperature can have sensitivity comparable to or even better than the first generation LIGO detectors in the frequency range around 1 KHz. Zhou and Michelson in 1994[143] showed that a spherical detector has a reasonable direction resolution even at relatively low signal-to-noise ratio (S/N = 10), while an interferometer network requires a much higher S/N for direction estimation. A spherical detector has isotropic direction resolution independent of the source direction and polarization, in contrast to the interferometer network, which can only partially cover the sky.

In order to study the production of GWs from a massive theory of gravity, the class $f(R)$ theory of gravity is chosen. It comes about as a toy model that could be used as an easy one to study the deviation from GTR and also understand the relevant issues.

4.2 Generation of Massive GWs in f(R) Theory of Gravity

We will first obtain the field equation for $f(R)$ theory by varying the modified action given by (1.4) with respect to the metric $g_{\mu\nu}$. Then, the field equation is found as,

$$(4.1) \qquad f'(R)R_{\mu\nu} - \frac{1}{2}f(R)g_{\mu\nu} - (\nabla_\mu\nabla_\nu - g_{\mu\nu}\square)f'(R) = \kappa T_{\mu\nu}.$$

Taking $f(R)$ to be of the specific form,

$$(4.2) \qquad f(R) = R + aR^2.$$

we get,

$$(4.3) \quad (R_{\mu\nu} - \frac{1}{2}Rg_{\mu\nu}) + 2aRR_{\mu\nu} - \frac{1}{2}aR^2 g_{\mu\nu} - 2a(\nabla_\mu\nabla_\nu - g_{\mu\nu}\square)R = \kappa T_{\mu\nu}.$$

Then taking the trace of this equation we get,

$$(4.4) \qquad 6a\square R - R = \kappa T.$$

Now, as a step towards linearization, we can write the metric as[98]

$$(4.5) \qquad g_{\mu\nu} = \eta_{\mu\nu} + h_{\mu\nu},$$

where $\eta_{\mu\nu}$ is the metric of the flat space-time and $h_{\mu\nu}$, a small perturbation where $\|h_{\mu\nu}\| \ll 1$. The Riemann tensor, after neglecting terms containing higher orders of h, takes the form,

$$(4.6) \qquad R^a_{bcd} = \partial_c\Gamma^a_{bd} - \partial_d\Gamma^a_{bc}.$$

The Ricci tensor is then given by,

$$(4.7) \qquad R_{\mu\nu} = \frac{1}{2}(\partial\nu\partial^\alpha h_{\mu\alpha} + \partial\mu\partial^\alpha h_{\nu\alpha} - \square h_{\mu\nu} - \partial_\mu\partial_\nu h),$$

96

and the Ricci scalar as

$$R = \eta^{\mu\nu} R_{\mu\nu} = (h^{,\alpha\beta}_{\alpha\beta} - \Box h).$$
(4.8)

Substituting (4.7) in the trace equation (4.8), we obtain,

$$6a\Box\partial^\alpha\partial^\beta h_{\alpha\beta} - 6a\Box^2(\eta^{\alpha\beta} h_{\alpha\beta}) - \partial^\alpha\partial^\beta h_{\alpha\beta} + \Box(\eta^{\alpha\beta} h_{\alpha\beta}) = \kappa T.$$
(4.9)

(4.9) is not in the form of a wave equation. To make it in the form of a wave equation, we employ the trace reversed perturbation given by[144],

$$\bar{h}_{\alpha\beta} = h_{\alpha\beta} - \frac{1}{2}\eta_{\alpha\beta}h,$$
(4.10)

instead of $h_{\alpha\beta}$ and the De Donder gauge[144], given by

$$\partial^\beta \bar{h}_{\alpha\beta} = 0.$$
(4.11)

We can see that (4.9) now takes the form,

$$\Box^2 \bar{h}_{\mu\nu} - m^2 \Box \bar{h}_{\mu\nu} = 0,$$
(4.12)

where,

$$m^2 = \frac{1}{6a}.$$
(4.13)

(4.12) can be solved by means of factorization[145] to obtain,

$$\Box \bar{h}_{\mu\nu} = 0,$$
(4.14)

and

$$\Box \bar{h}_{\mu\nu} - m^2 \bar{h}_{\mu\nu} = 0.$$
(4.15)

The general solution of (4.14) is given by,

$$(4.16) \qquad \bar{h}_{\mu\nu} = \int A(k)\exp(-i(k.r - \omega t))dk,$$

while that of (4.15) is given by,

$$(4.17) \qquad \bar{h}_{\mu\nu} = \int A(k)\exp(-i(k.r - \omega_m t))dk,$$

where $\omega \neq \omega_m$.

Thus, the solution of (4.12) is given by the sum of (4.16) and (4.17). (4.16) is the one that we usually have in GTR. That is, the general solution of the wave equation contains the usual general relativity solution and an additional solution containing the term m^2. From (4.14) one can get,

$$(4.18) \qquad \eta_{\alpha\beta}\bar{h}_{\mu\nu}^{\ ,\alpha\beta} = 0,$$

which implies,

$$(4.19) \qquad \eta_{\alpha\beta}k^\alpha k^\beta = k^\alpha k_\alpha = 0,$$

where k^α is the propagation vector. Here the propagation vector is a null vector which means that the corresponding wave travels with the speed of light. From (4.15) one gets,

$$(4.20) \qquad \eta_{\alpha\beta}k^\alpha k^\beta = m^2 = k^\alpha k_\alpha.$$

Here k^α is not a null vector which in turn implies that the wave is massive and that it travels with a speed less than that of light. Thus it can be seen that the GW obtained from $f(R)$ gravity allows two solutions and thereby the polarizations + and × corresponding to the

massless solution and s, scalar polarization, corresponding to the massive solution that can be identified with the massive polarization[146]. Thus we can have two independent polarizations h_+ and $h_\times$ from (4.16) and a scalar mode h_s from (4.17) so that the GW solution to (4.12) can be written as,

$$h_{\mu\nu} = h_+ e^{(+)}_{\mu\nu} + h_\times e^{(\times)}_{\mu\nu} + h_s e^{(s)}_{\mu\nu}, \tag{4.21}$$

where $e_{\mu\nu}$s are the basis vectors and are given by,

$$e^{(+)}_{\mu\nu} = \frac{1}{\sqrt{2}} \begin{pmatrix} 1 & 0 & 0 \\ 0 & -1 & 0 \\ 0 & 0 & 0 \end{pmatrix}, \quad e^{(\times)}_{\mu\nu} = \frac{1}{\sqrt{2}} \begin{pmatrix} 0 & 1 & 0 \\ 1 & 0 & 0 \\ 0 & 0 & 0 \end{pmatrix}, \tag{4.22}$$

$$e^{(s)}_{\mu\nu} = \frac{1}{\sqrt{2}} \begin{pmatrix} 0 & 0 & 0 \\ 0 & 0 & 0 \\ 0 & 0 & 1 \end{pmatrix}. \tag{4.23}$$

During detection, the GW will be showing one polarization mode at a time. Hence for studying the massive scalar mode of the gravitational waveform, it is sufficient to check the detectability of the massive polarization alone which is done below.

4.3 Detection of Massive Gravitational Waves using Spherical Antenna

In this section of this chapter, we will discuss how the massive mode given in (4.12) can be detected using a spherical antenna. Spherical antennae are considered by many to be the natural next step in the

development of resonant GW detectors. This is because of the improved sensitivity shown by a sphere and its capability for detection of multimodes. As discussed earlier in this chapter, the antenna measures, precisely the Fourier transformed components of the Riemann curvature tensor averaged over its volume.

The calculations are done following Lobo[147] and Gasparini[106]. We assume that the antenna is a solid elastic body that responds to GW perturbations through the equations of classical non-relativistic linear elasticity theory. This assumption is valid since any GW induced displacements will be small the speed of such displacements will be lower than that of light for any foreseen frequencies. Let **u(r, t)** be the displacement vector of the infinitesimal mass element at point **r** relative to the solid's center of mass in its unperturbed state, whose density distribution in that state is $\rho(r)$. Let a volume force density **F(r, t)** acts on such a solid. If a GW hits the detector at the time $t = 0$, the equation of motion for a solid sphere of density ρ is given by,

$$(4.24) \quad \rho \frac{\partial^2 \vec{u}(\vec{r},t)}{\partial t^2} - v\nabla^2 \vec{u}(\vec{r},t) - (\gamma + v)\vec{\nabla}(\vec{\nabla} \cdot \vec{u}(\vec{r},t)) = \vec{F}(\vec{r},t),$$

where v and γ are the Lame coefficients. The driving force **F(r,t)** is of the separable type,

$$(4.25) \qquad \mathbf{F}(\mathbf{r},t) = \mathbf{F}(\mathbf{r})g(t).$$

An incoming GW manifests itself as a tidal force density and is given by,

$$(4.26) \qquad F^j(\bar{r},t) = \rho R^j_{0k0} x^k(\bar{r},t),$$

where R^{j}_{0k0} is the Riemann curvature tensor. The tidal forces are refined to the antenna's center of mass and thus x^k is a vector originating there. Now, for a resonant mass detector the spatial dependence of the Riemann tensor need not be considered since the tidal forces are referred to the antenna's center of mass and $\mathbf{r}$ is a vector originating there. Then the Riemann tensor, to the first order in h, is given as,

$$(4.27) \qquad\qquad R_{i0k0}(t) = \frac{1}{2}\ddot{h}_{ij}(t).$$

This symmetric tensor can be decomposed into basis of $M^{(\mathrm{m})}_{ij}$ and $M^{(\alpha)}_{ij}$ where $M^{(\alpha)}_{ij}$ are five linearly independent symmetric traceless tensors and $M^{(\mathrm{m})}_{ij}$ is a multiple of the unit tensor δ_{ij}. With a real basis, these base matrices can be written with as,

$$M^{(\mathrm{m})}_{ij} = \sqrt{\frac{1}{4\pi}} \begin{pmatrix} 1 & 0 & 0 \\ 0 & 1 & 0 \\ 0 & 0 & 1 \end{pmatrix},$$

$$M^{1c}_{ij} = \sqrt{\frac{15}{16\pi}} \begin{pmatrix} 0 & 0 & 1 \\ 0 & 0 & 0 \\ 1 & 0 & 0 \end{pmatrix},$$

$$M^{2c}_{ij} = \sqrt{\frac{15}{16\pi}} \begin{pmatrix} 1 & 0 & 0 \\ 0 & -1 & 0 \\ 0 & 0 & 0 \end{pmatrix},$$

$$M^{1s}_{ij} = \sqrt{\frac{15}{16\pi}} \begin{pmatrix} 0 & 0 & 0 \\ 0 & 0 & 1 \\ 0 & 1 & 0 \end{pmatrix},$$

$$M_{ij}^{2s} = \sqrt{\frac{15}{16\pi}} \begin{pmatrix} 0 & 1 & 0 \\ 1 & 0 & 0 \\ 0 & 0 & 0 \end{pmatrix},$$

$$M_{ij}^{0} = \sqrt{\frac{5}{16\pi}} \begin{pmatrix} -1 & 0 & 0 \\ 0 & -1 & 0 \\ 0 & 0 & 2 \end{pmatrix}.$$

With this choice, we can write the tidal force density as

(4.28)
$$\vec{F}(\vec{r},t) = f^{\text{m}}(\vec{x})g^{(\text{m})}(t) + \sum_{\alpha} f^{\alpha}(\vec{x})g^{\alpha}(t)$$

$$= \sum f^{S}(\vec{x})g^{(S)}(t),$$

$S = \text{m},\alpha$ where α corresponds to the five quadrupole modes and,

(4.29)
$$f^{S}(\vec{x}) = \rho M_{ij}^{S} r_j,$$

(4.30)
$$g^{(\text{m})}(t) = \frac{4\pi}{3} M_{ij}^{(\text{m})} R_{i0j0}(t),$$

(4.31)
$$g^{\alpha}(t) = \frac{8\pi}{15} M_{ij}^{(\alpha)} R_{i0j0}(t).$$

$g^{S}(t)$ is the mode amplitude and is equal to $\ddot{h}^{S}(t)$, where $S = \text{m},\alpha$.
Thus,

$$\ddot{h}^{(\text{m})}(t) = \frac{4\pi}{3} M_{ij}^{(\text{m})} R_{i0j0},$$

(4.32)
$$\ddot{h}^{\alpha}(t) = \frac{8\pi}{15} M_{ij}^{\alpha} R_{i0j0}.$$

This decomposition displays the monopole-quadrupole structure of the
Riemannian tensor where m denotes the vibrational mode correspond-
ing to the monopole mode $l = 0$ and $\alpha = 0, 1c, 1s, 2c, 2s$ corresponds
to quadrupole mode, $l = 2$. Its six independent components can thus

be expressed in terms of one monopole amplitude $\ddot{h}^{(\text{m})}(t)$ and five quadrupole amplitudes $\ddot{h}^\alpha(t)$. The form of the force density given in (4.25) allows us to express the displacement $\overrightarrow{u}(\overrightarrow{r},t)$ as a Green's function integral. The corresponding solution then can be written by the series expansion:

$$(4.33) \qquad \overrightarrow{u}(\overrightarrow{r},t) = \sum_S \sum_N \omega_N^{-1} f_N^S g_N^S(t) \Phi_N(\overrightarrow{r}),$$

where,

$$f_N^S \ = \ M^{-1} \int_{solid} \overrightarrow{\Phi}_N(\overrightarrow{r}).\overrightarrow{f}^S(\overrightarrow{r})\mathrm{d}^3 r,$$

$$(4.34) \qquad g_N^S(t) \ = \ \int_0^t \ddot{h}^S(t')\sin\omega_N(t-t')\mathrm{d}t'.$$

$\Phi_N(\overrightarrow{r})$ are the normalized eigen-solutions of the corresponding homogenous equation:

$$\rho\omega_N^2\Phi_N + v\nabla^2\Phi_N + (\gamma+v)\nabla(\nabla.\Phi_N) = 0,$$

with suitable boundary conditions. M is the normalization factor and N denotes a set of indices labelling the eigenmode of frequency ω_N. Writing the solution given by (4.33) as,

$$\overrightarrow{u}(\overrightarrow{r},t) = \sum_N B_N(t)\Phi_N(\overrightarrow{r}),$$

where $B_N = \sum_\infty \omega_N^{-1} f_N^S g_N^S(t)$, satisfies the equation,

$$\ddot{B_N}(t) + \omega_N^2 B_N(t) \ = \ \sum_\infty \sum_S f_N^S \ddot{h}^S(t),$$

$$= \ \sum_\infty \sum_S M^{-1} \int_{solid} \overrightarrow{\Phi}_N(\overrightarrow{r}).\overrightarrow{f}^S(r)\ddot{h}^S(t)\mathrm{d}^3 r,$$

$$(4.35) \qquad = \ M^{-1}\rho(\overrightarrow{r})R_{joko}(t)r_k\Phi_{N,j}(\overrightarrow{r}).$$

103

Each mode is then equivalent to a one dimensional harmonic oscillator
with frequency ω_N, driven by a force per unit mass,

$$(4.36) \qquad F_N = \sum_\infty f_N^S \ddot{h}^S(t).$$

For such a system, the energy per mass unit adsorbed from the driving
force is given by

$$(4.37) \qquad E_s(n,l,S) = \frac{1}{2} \left| \int F_N(t) e^{-i\omega_N t} dt \right|^2.$$

For the specific case of a sphere, the normal modes are given by
spheroidal and toroidal ones. For these modes f_N^S can be written as,

$$
\begin{aligned}
f_{nlS\prime}^{Ssp} &= M^{-1} \int_{sphere} \overrightarrow{\Phi}_{nlS\prime}^{sp}(\overrightarrow{r}) . \overrightarrow{f}^S(\overrightarrow{r}) \mathrm{d}^3 r \\
&= a_n \delta_{l,0} \delta_{m,0}, \\
&= b_n \delta_{l,2} \delta_{\alpha,\alpha\prime}, \\
f_{nl\alpha\prime}^{\alpha T} &= M^{-1} \int_{sphere} \overrightarrow{\Phi}_{nl\alpha\prime}^{T}(\overrightarrow{r}) . \overrightarrow{f}^\alpha(\overrightarrow{r}) \mathrm{d}^3 r \\
(4.38) \qquad &= 0,
\end{aligned}
$$

where $a_n = -\frac{1}{M} \int_0^R \rho r^3 A_{n0}(r)\mathrm{d}r$ and $b_n = -\frac{1}{M} \int_0^R \rho r^3 (A_{n2}(r) + 3B_{n2}(r))\mathrm{d}r$.

A_{nl}, B_{nl} are scalar functions of r given by [106],

$$
\begin{aligned}
(4.39) \qquad A_{nl}(r) = C(n,l)[&\beta_3(k_{nl}R)j_l\prime(q_{nl}r) - \\
&l(l+1)\frac{q_{nl}}{k_{nl}}\beta_1(q_{nl}R)\frac{j_l(k_{nl}r)}{k_{nl}r}],
\end{aligned}
$$

$$
\begin{aligned}
(4.40) \qquad B_{nl}(r) = C(n,l)[&\beta_3(k_{nl}R)\frac{j_l(q_{nl}r)}{q_{nl}r} - \\
&\frac{q_{nl}}{k_{nl}}\beta_1(q_{nl}R)\frac{[k_{nl}rj_l(k_{nl}r)]\prime}{k_{nl}r}],
\end{aligned}
$$

where the j_l are spherical Bessel functions,

$$\beta_0(x) = \frac{j_l(x)}{x^2}, \quad \beta_1(x) = \frac{d}{dx}\frac{j_l(x)}{x}, \quad \beta_2(x) = \frac{d^2}{dx^2}j_l(x),$$

$$\beta_3(x) = \frac{1}{2}\beta_2(x) + \left[\frac{l(l+1)}{2} - 1\right]\beta_0(x),$$

k and q are given by

$$k_{nl}^2 = \frac{\rho\omega_{nl}^2}{\nu}, \quad q_{nl}^2 = \frac{\rho\omega_{nl}^2}{\gamma + 2\nu}.$$

Each mode characterized by n, l, α corresponds to the generic N. n is a positive integer which represents the energy level for a fixed angular momentum l. Thus, on interaction of the spherical detector with a GW, the toroidal modes do not contribute. The contribution comes only from the spheroidal modes. F_N for a sphere can now be found from (4.33) and (4.35) with which the energy stored in the modes is obtained as,

$$E_s(n,0,m) = \frac{1}{2}a_n^2\delta_{l,0}\left|\int \ddot{h}^m(t)e^{-i\omega_{n0}t}dt\right|^2,$$

(4.41) $$E_s(n,2,\alpha) = \frac{1}{2}b_n^2\delta_{l,2}\left|\int \ddot{h}^\alpha(t)e^{-i\omega_{n2}t}dt\right|^2.$$

With these results in hand, the energy stored in each quadrupole mode of the sphere for the GW from our modified theory may be found from the description given below. Riemann tensor from the modified theory can be written as

(4.42) $$R_{i0j0} = \frac{1}{2}\begin{pmatrix} \ddot{h}_+ & \ddot{h}_\times & 0 \\ \ddot{h}_\times & -\ddot{h}_+ & 0 \\ 0 & 0 & m^2\ddot{h}_s \end{pmatrix}_{ij},$$

where h_+ and $h_\times$ are the massless polarizations from the GTR and h_s is the massive scalar polarization coming by employing the modification.

105

Let $(\hat{x}, \hat{y}, \hat{z})$ be the detector frame basis. Let θ be the angle from the $\hat{z}$ axis and ϕ the angle between $\hat{x}$ and the projection into the $(\hat{x}, \hat{y})$ plane. Now, for a generic arrival direction given by the angle (θ, ϕ), we have to perform a rotation in order to obtain Riemann tensor in the antenna frame. This can be achieved as [148]:

$$(4.43) \qquad R_{i0j0} = \frac{1}{2}\left(C\begin{pmatrix} \ddot{h}_+ & \ddot{h}_\times & 0 \\ \ddot{h}_\times & -\ddot{h}_+ & 0 \\ 0 & 0 & m^2 h_s \end{pmatrix}C^T\right)_{ij},$$

$$\text{with,} \qquad C = \begin{pmatrix} \cos\theta\cos\phi & -\sin\phi & \sin\theta\cos\phi \\ \cos\theta\sin\phi & \cos\phi & \sin\theta\sin\phi \\ -\sin\theta & 0 & \cos\theta \end{pmatrix}.$$

The components of $\ddot{h}^S(t)$ can be obtained using (4.32) as,

$$\ddot{h}^{\mathrm{m}}(t) = \frac{\sqrt{4\pi}}{3}m^2 h_s,$$

$$\ddot{h}^0(t) = \sqrt{\frac{\pi}{5}}\left(\sin^2\theta\ddot{h}_+ + \frac{1}{3}m^2\cos^2\theta h_s\right),$$

$$\ddot{h}^{1c}(t) = \sqrt{\frac{4\pi}{15}}\left(-\sin\theta\cos\theta\cos\phi\ddot{h}_+ + \sin\theta\sin\phi\ddot{h}_\times - \frac{1}{2}m^2\sin\theta\cos\theta\cos\phi h_s\right),$$

$$\ddot{h}^{1s}(t) = \sqrt{\frac{4\pi}{15}}\left(\sin\theta\cos\theta\sin\phi\ddot{h}_+ - \sin\theta\cos\phi\ddot{h}_\times + \frac{1}{2}m^2\sin\theta\cos\theta\sin\phi h_s\right),$$

$$\ddot{h}^{2c}(t) = \sqrt{\frac{4\pi}{15}}\left(\cos^2\theta\cos^2\phi\ddot{h}_+ - 2\cos\theta\sin\phi\cos\phi\ddot{h}_\times\right),$$

$$\ddot{h}^{2s}(t) = \sqrt{\frac{4\pi}{15}}\left(\cos^2\theta\sin^2\phi\cos^2\phi\ddot{h}_+ - \cos\theta\sin^2\phi\ddot{h}_\times\right).$$

Using these equations the energy stored for each mode is obtained

from (4.41) as,

$$E_s(n,0,\mathbb{m}) = \frac{4\pi}{9}a_n^2 m^4 \left|\tilde{h}_s(\omega_{n0})\right|^2,$$

$$E_s(n,2,0) = \frac{\pi}{10}b_n^2[\sin^4\theta\,\omega_{n2}^4\left|\tilde{h}_+(\omega_{n2})\right|^2 + \frac{1}{9}m^4\cos^4\theta\left|\tilde{h}_s(\omega_{n2})\right|^2],$$

$$E_s(n,2,1c) = \frac{2\pi}{15}b_n^2[\omega_{n2}^4((\cos^2\theta\sin^2\theta\cos^2\phi\left|\tilde{h}_+(\omega_{n2})\right|^2 + \sin^2\theta\sin^2\phi\left|\tilde{h}_\times(\omega_{n2})\right|^2 -$$
$$\cos\theta\sin^2\theta\sin^2\phi Re(\tilde{h}_+\tilde{h}_\times^*)) + \frac{1}{4}(m^4\sin^2\theta\cos^2\theta\cos^2\phi\left|\tilde{h}_s(\omega_{n2})\right|^2)],$$

$$E_s(n,2,1s) = \frac{2\pi}{15}b_n^2[\omega_{n2}^4(\cos^2\theta\sin^2\theta\sin^2\phi\left|\tilde{h}_+(\omega_{n2})\right|^2 + \sin^2\theta\cos^2\phi\left|\tilde{h}_\times(\omega_{n2})\right|^2 -$$
$$\cos\theta\sin^2\theta\sin 2\phi Re(\tilde{h}_+\tilde{h}_\times^*)) + \frac{1}{4}(m^4\sin^2\theta\cos^2\theta\sin^2\phi\left|\tilde{h}_s(\omega_{n2})\right|^2],$$

$$E_s(n,2,2c) = \frac{2\pi}{15}b_n^2[\omega_{n2}^4((1+\cos^2\theta)^2(\cos^2\phi - \frac{1}{2})^2\left|\tilde{h}_+(\omega n2)\right|^2 + 4\cos^2\theta\sin^2\phi$$
$$\cos^2\phi\left|\tilde{h}_\times(\omega_{n2})\right|^2 - 4\cos\theta\sin\phi\cos\phi(1+\cos^2\theta)(\cos^2\phi -$$
$$\frac{1}{2})Re(\tilde{h}_+\tilde{h}_\times^*)),$$

(4.44)

$$E_s(n,2,2s) = \frac{2\pi}{15}b_n^2[\omega_{n2}^4((1+\cos^2\theta)^2\cos^2\phi\sin^2\phi\left|\tilde{h}_+(\omega_{n2})\right|^2 + \cos^2\theta(\cos^2\phi -$$
$$\sin^2\phi)^2\left|\tilde{h}_\times(\omega_{n2})\right|^2 + 2\cos\theta\sin\phi\cos\phi(1+\cos^2\theta)(\cos^2\phi -$$
$$\sin^2\phi)Re(\tilde{h}_+\tilde{h}_\times^*)).$$

It is assumed that h_+ and $h_\times$ decrease fast enough as $t \to \pm\infty$ to allow integration by parts and $\tilde{h}_+(\omega)$, $\tilde{h}_\times(\omega)$ and $\tilde{h}_s(\omega)$ stands for the Fourier transform of $+$, $\times$ and scalar polarizations respectively. If the source emits randomly polarized radiation we can re-write h_+, $h_\times$ and h_s in terms of one possible intrinsic polarization with as[149],

(4.45)

$$h_+ = \cos(\psi)e_+ + \sin(\psi)e_\times, \quad h_\times = -\sin(\psi)e_+ + \cos(\psi)e_\times, \quad h_s = e_s.$$

Since h_s has no ψ dependence, averaging (4.41) over ψ will not make any change in the h_s term. Then, for a source emitting randomly polarized radiation, the average energy for each mode can be written as,

$$\bar{E}_s(n,0,\mathbb{m}) = \frac{4\pi}{9} a_n^2 m^4 |\tilde{e}_s|^2 ,$$

$$\bar{E}_s(n,2,0) = \frac{\pi}{15} b_n^2 [\frac{3}{4}\sin^4\theta\,\omega_{n2}^4(|\tilde{e}_+|^2 + |\tilde{e}_\times|^2) + \frac{1}{6} m^4 \cos^4\theta\,|\tilde{e}_s|^2],$$

$$\bar{E}_s(n,2,1c) = \frac{\pi}{15} b_n^2 [\omega_{n2}^4(\sin^2\theta(\cos^2\theta\cos^2\phi + \sin^2\phi)(|\tilde{e}_+|^2 + |e_\times|^2) +$$
$$\frac{1}{4}(m^4\sin^2\theta\cos^2\theta\cos^2\phi\,|\tilde{e}_s|^2)],$$

$$\bar{E}_s(n,2,1s) = \frac{\pi}{15} b_n^2 [\omega_{n2}^4(\cos^2\theta\sin^2\phi)(|\tilde{e}_+|^2 + |\tilde{e}_\times|^2) +$$
$$\frac{1}{4}(m^4\sin^2\theta\cos^2\theta\sin^2\phi\,|\tilde{e}_s|^2)],$$

$$\bar{E}_s(n,2,2c) = \frac{\pi}{15} b_n^2 [\omega_{n2}^4((1+\cos^2\theta)^2(\cos^2\phi - \frac{1}{2})^2 + 4\cos^2\theta\sin^2\phi\cos^2\phi))$$
$$(|\tilde{e}_+|^2 + |e_\times|^2)],$$

$$\bar{E}_s(n,2,2s) = \frac{\pi}{15} b_n^2 [\omega_{n2}^4((1+\cos^2\theta)^2\cos^2\phi\sin^2\phi + \cos^2\theta(\cos^2\phi - \sin^2\phi)^2)$$
$$(|\tilde{e}_+|^2 + |\tilde{e}_\times|^2)].$$

The average energy corresponding to the monopole mode does not involve any angular terms. It is also interesting to note that the massive wave does not contribute anything to the quadrupolar $2c$ and $2s$ modes. ie., only three of the five orthogonal modes are triggered by the massive wave. The energy sensitivity for the monopole and quadrupole modes respectively of the antenna for the massive wave are defined as,

$$\epsilon_{(m)} = \frac{\bar{E}_s(n,0,m)}{\frac{4\pi}{9} m^4 a_n^2 |\tilde{e}_s|^2},$$

$$(4.46) \qquad \epsilon_\alpha = \frac{\bar{E}_s(n,2,\alpha)}{\frac{\pi}{60} b_n^2 \omega^4 |\tilde{e}_s|^2}.$$

Calculation of the energy sensitivity for the monopole mode is direct. For calculating the energy sensitivity of quadrupole modes towards a massive GW, we first write the average energy stored for each mode for the massive wave alone by setting $e_+ = e_\times = 0$. The resulting equation for the average energy stored is substituted in (4.44). Since the energy sensitivity for the monopole mode does not involve any angular dependence, its value is a constant and is maximum. The energy sensitivity thus got is plotted and shown on the right hand side of each pair of figures in Fig.4.1. They show the energy transferred from massive GWs to the quadrupole modes of the sphere in the order of modes 0, $1c$ and $1s$. The corresponding sensitivity for the $+$ and $\times$ polarizations obtained by setting $e_s = 0$ is given on the left hand side of each pair of figures for the sake of comparison. Red color indicates a maximum and blue color indicates a minimum. It can be seen from the figure that in the massive case, the maximum has been shifted. The region where it showed a maximum for $+, \times$ polarizations is no more a region of maximum sensitivity.

From Fig.4.1 it can also be inferred that for massive waves, the detector becomes very directional. For a fixed source whose galactic coordinates (b, l_g) are known one can find the angles (θ, ϕ) of the source with respect to the detector frame[150]. Fig.4.2 gives the total sensitivity of the sphere towards a massive GW. However, Fig.4.3 shows how strong this directional dependence is. Those well defined peaks in the case of a massive wave clearly quantifies the strength
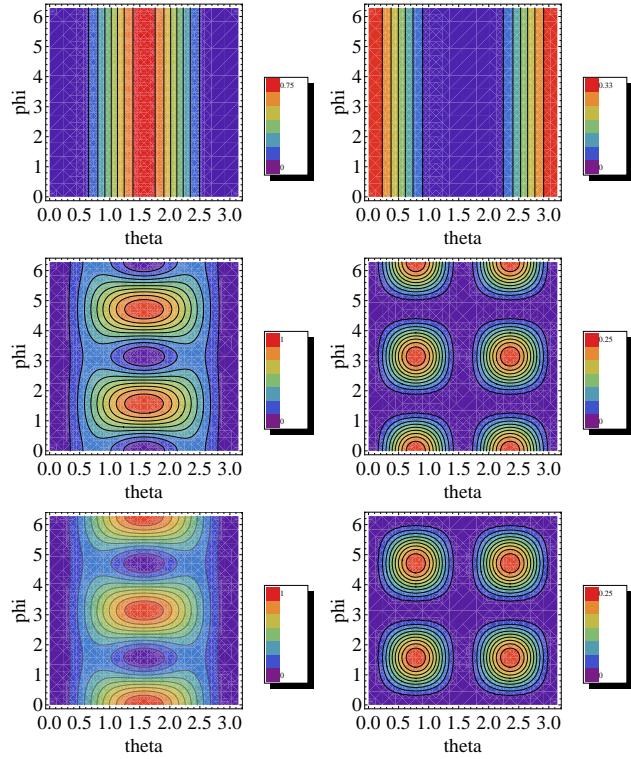
Figure 4.1: Comparison of ϵ_α: Each pair shows comparison of GR(left) with that of f(R)(right) for $\epsilon_0, \epsilon_{1c}, \epsilon_{1s}$ respectively from top

of the directional dependence of the antenna. Fig.4.4 displays the energy ϵ_α stored in the modes 0, 1c and 1s of a sphere near Leiden, Holland (latitude $l = 52.16°$N, longitude L $= 4.45°$E), as functions of Greenwich sidereal time (in sidereal hours) and of galactic longitude b for a randomly polarized source lying in the galactic plane ($l_g = 0$). Again, red color indicates the maximum and blue the minimum value. Fig.4.5 shows the energy sensitivity for the mode $\alpha = 0$ near the galactic center $b = 0$.

Figure 4.2: Total energy sensitivity as a function of θ and ϕ for the spherical antenna detector
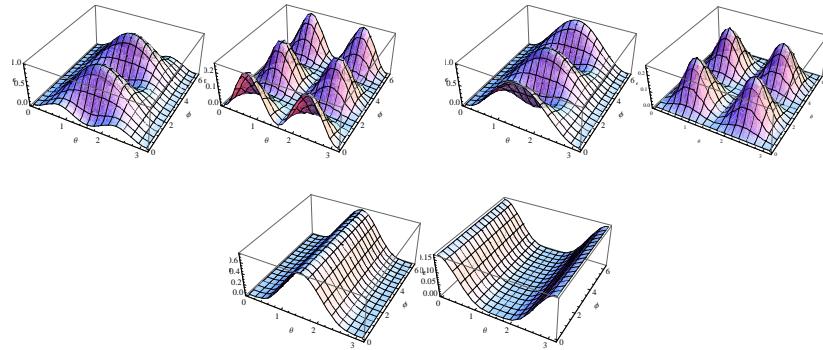
Figure 4.3: Figure showing the directionality of spherical antenna towards massless waves from GR (shown on the left of each pair) and towards massive wave (shown on the right side of each pair). Well defined peaks of massive GW quantifies the directional dependence of antenna towards such a wave

4.4 Modified TIGA Configuration for Detecting Massive Mode

A simple spherical antenna is not a good practical detector. When a sphere interacts with a massive wave, because of the smallness of h, the magnitude of the displacement of the detector will be very

111
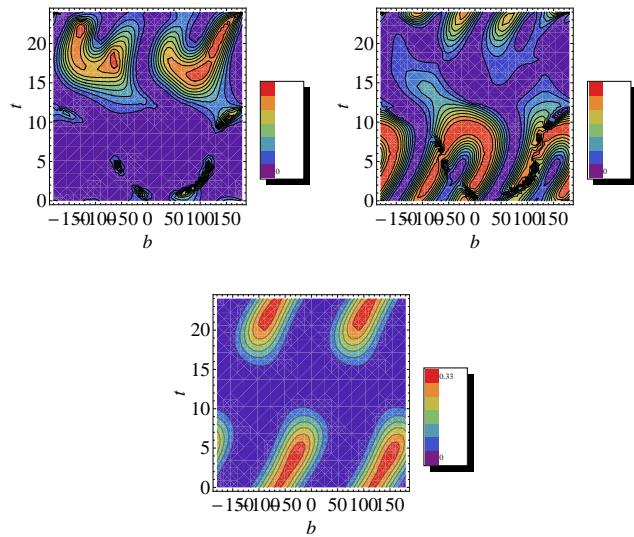
Figure 4.4: Sensitivity of the modes $1c, 1s$ and 0 as a function of the GW source position in the galactic plane
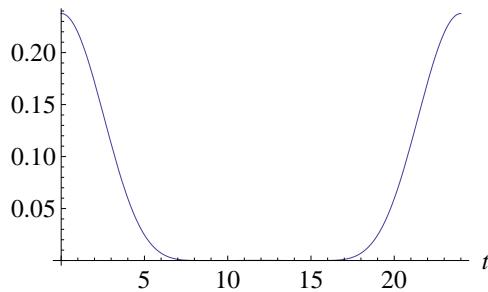

Figure 4.5: sensitivity of the mode $\alpha = 0$ as a function of sidereal time for a source at the galactic center

low, of the order of hL, L being the length of the detector. So, in order to amplify these displacements, a set of mechanical resonators are needed. One of the normal modes of each of these mechanical resonator is tuned to be resonant with the frequency of the antenna.

112

The motion of the surface of the antenna excites this mode and there is a resonant transfer of momentum between the resonator and the antenna. Frequencies other than the fundamental mode and nearby frequencies will not be amplified by the system[151]. Hence it acts as a resonant mechanical transformer, turning small motions of the large antenna into large motions of the small resonators. In the presence of the resonators, the equation of motion given by (4.24) gets modified as[143],

(4.47)
$$\rho \frac{\partial^2 \vec{u}(\vec{r}, t)}{\partial t^2} - v \nabla^2 \vec{u}(\vec{r}, t) - (\gamma + v) \vec{\nabla} (\vec{\nabla} \cdot \vec{u}(\vec{r}, t)) = \sum \vec{f}^{(\eta)}(\vec{r}) g^{(\eta)}(t),$$

where η is a parameter that takes the values $\mathtt{m}$, 0, $1c$, $1s$, $2c$, $2s$, 1, 2, 3, ... $= \{S, i\}$. It is clear that the first components of this force density,

(4.48)
$$\vec{F}_{GW} = \sum \vec{f}^S(\vec{r}) g^S(t) = \sum \vec{f}^S(\vec{r}) \ddot{h}^S(t),$$

are the usual ones attributable to GW while,

(4.49)
$$\vec{F}_{res} = \sum \vec{f}^i(\vec{r}) g^i(t),$$

are the new contributions given by the elastic terms of resonators. A minimum of five resonators are required to measure the five quadrupole modes of a sphere and one for the monopole mode.

Merkowitz and Johnson[142], in their paper, have proposed Truncated Icosahedral Gravitational wave Antenna (TIGA) for measuring the quadrupole modes of a sphere. It consists of a highly symmetric arrangement of six resonators. These resonators are tuned to the quadrupole frequency ω_{n2}. Each resonator is assumed identical,

and the mass of the resonator m_R and spring constant, k_R of each are tuned to match the frequency of the five sphere modes so that $k_R/m_R = \omega^2$. The quantity that is measurable is $q(t)$, the resonator amplitude which is the displacement of the resonator relative to the sphere surface. Since the resonators mimic the motion of the sphere, even when only one sphere mode is excited, most of the rest of the modes will also be excited. The fixed linear combination of the measured amplitudes $q(t)$ separates out each of the spherical amplitudes $h^\alpha(t)$ and serves as a direct way to determine the spherical amplitudes $h^\alpha(t)$. These linear combinations are called 'mode channels' to show that each one is coupled only to a single amplitude $h^\alpha(t)$ of the gravitational field. The mode channel is given by,

$$(4.50) \qquad\qquad \tilde{p}(\omega) = \mathbf{Y}\tilde{q}(\omega),$$

where $\tilde{q}(\omega)$ is the Fourier transform of $q(t)$ and $\mathbf{Y}$ is the pattern matrix. Pattern matrix is the collection of pattern vectors whose elements are the values of the relative radial displacements of the surface of the sphere at the resonator locations. In other words, (4.50) can be written as,

$$\tilde{p}_i(\omega) = Y_{\alpha i} q_i$$

where i is the number of resonators and the number α corresponds to the spherical modes present. In the case of $+$ and $\times$ polarizations, the spherical modes are the five quadrupole modes and for the TIGA, six resonators are used to detect the massless polarization. Therefore, with $i = 6$ and $\alpha = 5$ and the pattern matrix Y is given by[106],

(4.51)

$$
\begin{pmatrix}
\frac{1}{\sqrt{4\pi}} & \frac{1}{\sqrt{4\pi}} & \frac{1}{\sqrt{4\pi}} & -\frac{1}{\sqrt{4\pi}} & -\frac{1}{\sqrt{4\pi}} & -\frac{1}{\sqrt{4\pi}} \\[6pt]
\sqrt{\frac{3+\sqrt{5}}{6\pi}} & -\sqrt{\frac{3+\sqrt{5}}{24\pi}} & -\sqrt{\frac{3-\sqrt{5}}{24\pi}} & \sqrt{\frac{3+\sqrt{5}}{24\pi}} & -\sqrt{\frac{3-\sqrt{5}}{6\pi}} & \sqrt{\frac{3-\sqrt{5}}{24\pi}} \\[6pt]
0 & \sqrt{\frac{3+\sqrt{5}}{8\pi}} & -\sqrt{\frac{3+\sqrt{5}}{8\pi}} & \sqrt{\frac{3\sqrt{5}}{8\pi}} & 0 & -\sqrt{\frac{3\sqrt{5}}{8\pi}} \\[6pt]
\sqrt{\frac{3-\sqrt{5}}{6\pi}} & -\sqrt{\frac{3-\sqrt{5}}{24\pi}} & -\sqrt{\frac{3-\sqrt{5}}{24\pi}} & -\sqrt{\frac{3+\sqrt{5}}{24\pi}} & \sqrt{\frac{3+\sqrt{5}}{6\pi}} & -\sqrt{\frac{3+\sqrt{5}}{24\pi}} \\[6pt]
0 & -\sqrt{\frac{3-\sqrt{5}}{8\pi}} & \sqrt{\frac{3-\sqrt{5}}{8\pi}} & \sqrt{\frac{3+\sqrt{5}}{8\pi}} & 0 & -\sqrt{\frac{3+\sqrt{5}}{8\pi}}
\end{pmatrix},
$$

where, $Y = Y_{n,l,\alpha}(\theta_i,\phi_i) = Y_{1,2,\alpha}(\theta_i,\phi_i)$, $i = 6$ forms a 5×6 matrix and is the real spherical harmonics. Three of the resonators have the azimuth angles $\theta_1 = \theta_2 = \theta_3 = \theta_A$ and $\phi_1 = 0, \phi_2 = \frac{2\pi}{3}, \phi_3 = \frac{4\pi}{3}$ and the other three have $\theta_4 = \theta_5 = \theta_6 = \theta_B$ and $\phi_4 = \frac{\pi}{3}, \phi_5 = \pi, \phi_6 = \frac{5\pi}{3}$. The angles θ_A, θ_B lies between 0 and $\frac{\pi}{2}$ and are solutions of the equation,

$$
45\cos^4\theta - 30\cos^2\theta + 1 = 0.
$$

The above TIGA configuration can be extended to include the monopole mode $\alpha = 0$ by adding another resonant transducer to this arrangement [151, 152]. It is then tuned to the monopole frequency ω_{n0}. The pattern matrix will then look like,

(4.52)

$$
\begin{pmatrix}
\frac{1}{\sqrt{4\pi}} & \frac{1}{\sqrt{4\pi}} & \frac{1}{\sqrt{4\pi}} & \frac{1}{\sqrt{4\pi}} & \frac{1}{\sqrt{4\pi}} & \frac{1}{\sqrt{4\pi}} & \frac{1}{\sqrt{4\pi}} \\[6pt]
0 & \frac{1}{\sqrt{4\pi}} & \frac{1}{\sqrt{4\pi}} & \frac{1}{\sqrt{4\pi}} & -\frac{1}{\sqrt{4\pi}} & -\frac{1}{\sqrt{4\pi}} & -\frac{1}{\sqrt{4\pi}} \\[6pt]
0 & \sqrt{\frac{3+\sqrt{5}}{6\pi}} & -\sqrt{\frac{3+\sqrt{5}}{24\pi}} & -\sqrt{\frac{3-\sqrt{5}}{24\pi}} & \sqrt{\frac{3+\sqrt{5}}{24\pi}} & -\sqrt{\frac{3-\sqrt{5}}{6\pi}} & \sqrt{\frac{3-\sqrt{5}}{24\pi}} \\[6pt]
0 & 0 & \sqrt{\frac{3+\sqrt{5}}{8\pi}} & -\sqrt{\frac{3+\sqrt{5}}{8\pi}} & \sqrt{\frac{3\sqrt{5}}{8\pi}} & 0 & -\sqrt{\frac{3\sqrt{5}}{8\pi}} \\[6pt]
0 & \sqrt{\frac{3-\sqrt{5}}{6\pi}} & -\sqrt{\frac{3-\sqrt{5}}{24\pi}} & -\sqrt{\frac{3-\sqrt{5}}{24\pi}} & -\sqrt{\frac{3+\sqrt{5}}{24\pi}} & \sqrt{\frac{3+\sqrt{5}}{6\pi}} & -\sqrt{\frac{3+\sqrt{5}}{24\pi}} \\[6pt]
0 & 0 & -\sqrt{\frac{3-\sqrt{5}}{8\pi}} & \sqrt{\frac{3-\sqrt{5}}{8\pi}} & \sqrt{\frac{3+\sqrt{5}}{8\pi}} & 0 & -\sqrt{\frac{3+\sqrt{5}}{8\pi}}
\end{pmatrix},
$$

with $\mathbf{Y} = Y_{n,l,S}(\theta_i, \phi_i)$, $i = 7$, $l = 0, 2$ and $S = 6$ with one monopole and
five quadrupole modes. $\mathbf{Y}$ has now become a 6×7 matrix and $\tilde{p}(\omega)$ vec-
tor has six components meaning that there will be six mode channels,
one corresponding to the monopole and the other five corresponding
to the quadrupole modes. $\mathbf{Y}$ can be made a 7×7 by adding another
row of unity to the matrix which embraces the condition that the sum
of all the displacement corresponding to the quadrupole modes is zero
(in the case of a high SNR) and then can be inverted to find $\tilde{q}(\omega)$ as,

$$\mathbf{q} = \mathbf{Y}^{-1}\mathbf{p}.$$

with the mode channel given by,

$$\tilde{p}_m(\omega) = -\frac{7}{4\pi}\frac{Aam^4\tilde{h}^{(m)}(\omega)}{(\omega^2 - \omega_+^2)(\omega^2 - \omega_+^2)}, \quad l = 0,$$

(4.53)
$$\tilde{p}_\alpha(\omega) = -\frac{3}{2\pi}\frac{Ab\omega^4\tilde{h}^\alpha(\omega)}{(\omega^2 - \omega_+^2)(\omega^2 - \omega_+^2)}, \quad l = 2,$$

where a, b and A are the same constants a_n, b_n and A_{nl} of (4.38)
and explanations given there with $n = 1$ because it is at this mode
that the cross section is the most significant [106]. ω_+ and ω_- are
the upshifted and downshifted frequencies from their corresponding
fundamental frequencies respectively. The $\mathbf{q}$s are then obtained as,

$$\tilde{q}_m(\omega) = 2\sqrt{\pi}\tilde{p}_m(\omega),$$

$$\tilde{q}_1(\omega) = \frac{\sqrt{\pi}}{3}\tilde{p}_0(\omega) + \frac{\sqrt{3\pi}}{9}(\sqrt{5}+1)\tilde{p}_{1c}(\omega) + \frac{\sqrt{3\pi}}{9}(\sqrt{5}-1)\tilde{p}_{2c}(\omega),$$

$$\tilde{q}_2(\omega) = \frac{\sqrt{\pi}}{3}\tilde{p}_0(\omega) - \frac{\sqrt{3\pi}}{18}(\sqrt{5}+1)\tilde{p}_{1c}(\omega) + \frac{\sqrt{\pi}}{6}(\sqrt{5}+1)\tilde{p}_{1s}(\omega) -$$

$$\frac{\sqrt{3\pi}}{18}(\sqrt{5}-1)\tilde{p}_{2c}(\omega) - \frac{\sqrt{\pi}}{6}(\sqrt{5}-1)\tilde{p}_{2s}(\omega),$$

$$\tilde{q}_3(\omega) = \frac{\sqrt{\pi}}{3}\tilde{p}_0(\omega) - \frac{\sqrt{3\pi}}{18}(\sqrt{5}+1)\tilde{p}_{1c}(\omega) - \frac{\sqrt{\pi}}{6}(\sqrt{5}+1)\tilde{p}_{1s}(\omega) - $$
$$\frac{\sqrt{3\pi}}{18}(\sqrt{5}-1)\tilde{p}_{2c}(\omega) + \frac{\sqrt{\pi}}{6}(\sqrt{5}-1)\tilde{p}_{2s}(\omega),$$

$$\tilde{q}_4(\omega) = -\frac{\sqrt{\pi}}{3}\tilde{p}_0(\omega) + \frac{\sqrt{3\pi}}{18}(\sqrt{5}-1)\tilde{p}_{1c}(\omega) + \frac{\sqrt{\pi}}{6}(\sqrt{5}-1)\tilde{p}_{1s}(\omega) - $$
$$\frac{\sqrt{3\pi}}{18}(\sqrt{5}+1)\tilde{p}_{2c}(\omega) + \frac{\sqrt{\pi}}{6}(\sqrt{5}+1)\tilde{p}_{2s}(\omega),$$

$$\tilde{q}_5(\omega) = -\frac{\sqrt{\pi}}{3}\tilde{p}_0(\omega) - \frac{\sqrt{3\pi}}{9}(\sqrt{5}-1)\tilde{p}_{1c}(\omega) + \frac{\sqrt{3\pi}}{9}(\sqrt{5}+1)\tilde{p}_{2c}(\omega),$$

$$\tilde{q}_6(\omega) = -\frac{\sqrt{\pi}}{3}\tilde{p}_0(\omega) + \frac{\sqrt{3\pi}}{18}(\sqrt{5}-1)\tilde{p}_{1c}(\omega) - \frac{\sqrt{\pi}}{6}(\sqrt{5}-1)\tilde{p}_{1s}(\omega) - $$
$$\frac{\sqrt{3\pi}}{18}(\sqrt{5}+1)\tilde{p}_{2c}(\omega) - \frac{\sqrt{\pi}}{6}(\sqrt{5}+1)\tilde{p}_{2s}(\omega).$$

Taking the squared absolute value of these quantities, we can find the sensitivities. $\tilde{h}^\alpha(\omega)$ can be written in terms of $\tilde{h}_+$, $\tilde{h}_-$ and $\tilde{h}_s$. Here, in this calculation, like in the previous section of this Chapter, we take only the contribution from massive polarization $\tilde{h}_s$. Then the sensitivity of each resonator is given by the ratio,

$$(4.54) \qquad Q_m(\theta,\phi) = \frac{|\tilde{q}_i(\omega)|^2}{\beta(\omega)|\tilde{e}_s|^2},$$

$$(4.55) \qquad Q_i(\theta,\phi) = \frac{|\tilde{q}_i(\omega)|^2}{\beta(\omega)(|\tilde{e}_+|^2 + |\tilde{e}_\times|^2)}.$$

with,

$$\beta(\omega) = \frac{A^2 a^2 m^8}{\frac{7}{3}\left((\omega^2 - \omega_+^2)(\omega^2 - \omega_-^2)\right)^2}, \; l = 0,$$

$$(4.56) \qquad \beta(\omega) = \frac{A^2 b^2 \omega^8}{\frac{3}{5}\left((\omega^2 - \omega_+^2)(\omega^2 - \omega_-^2)\right)^2}, \; l = 2.$$

117

Each Q_i being,

$$Q_\mathrm{m} = 1, \tag{4.57}$$

$$Q_1 = (\frac{1}{3\sqrt{3}}\cos^2\theta - \frac{\sqrt{3}}{9}(\sqrt{5}+1)\cos\theta\sin\theta\cos\phi)^2, \tag{4.58}$$

$$Q_2 = (\frac{1}{3\sqrt{3}}\cos^2\theta + \frac{\sqrt{3}}{18}(\sqrt{5}+1)\cos\theta\sin\theta\cos\phi -$$
$$\frac{\sqrt{1}}{6}(\sqrt{5}+1)\cos\theta\sin\theta\sin\phi)^2, \tag{4.59}$$

$$Q_3 = (\frac{1}{3\sqrt{3}}\cos^2\theta + \frac{\sqrt{3}}{18}(\sqrt{5}+1)\cos\theta\sin\theta\cos\phi +$$
$$\frac{\sqrt{\pi}}{6}(\sqrt{5}+1)\cos\theta\sin\theta\sin\phi)^2, \tag{4.60}$$

$$Q_4 = (-\frac{1}{3\sqrt{3}}\cos^2\theta - \frac{\sqrt{3}}{18}(\sqrt{5}+1)\cos\theta\sin\theta\cos\phi -$$
$$\frac{\sqrt{1}}{6}(\sqrt{5}+1)\cos\theta\sin\theta\sin\phi)^2, \tag{4.61}$$

$$Q_5 = (-\frac{1}{3\sqrt{3}}\cos^2\theta + \frac{\sqrt{3}}{9}(\sqrt{5}-1)\cos\theta\sin\theta\cos\phi)^2, \tag{4.62}$$

$$Q_6 = (-\frac{1}{3\sqrt{3}}\cos^2\theta - \frac{\sqrt{3}}{18}(\sqrt{5}-1)\cos\theta\sin\theta\cos\phi +$$
$$\frac{\sqrt{\pi}}{6}(\sqrt{5}-1)\cos\theta\sin\theta\sin\phi)^2. \tag{4.63}$$

These Qs give the sensitivities of the seven resonators towards a massive GW. Again, the monopole mode has the maximum sensitivity towards the massive wave. Fig.4.6 shows the sensitivity plotted for the quadrupole modes. Here too, in the presence of mechanical resonators, the antenna shows directional dependence. Fig.4.7 shows the total sensitivity of the sphere with resonators for $l = 2$ modes. A comparison of the strength of the direction dependence of the massive wave with that of massless waves for the quadrupole modes is given in Fig.4.8.

118
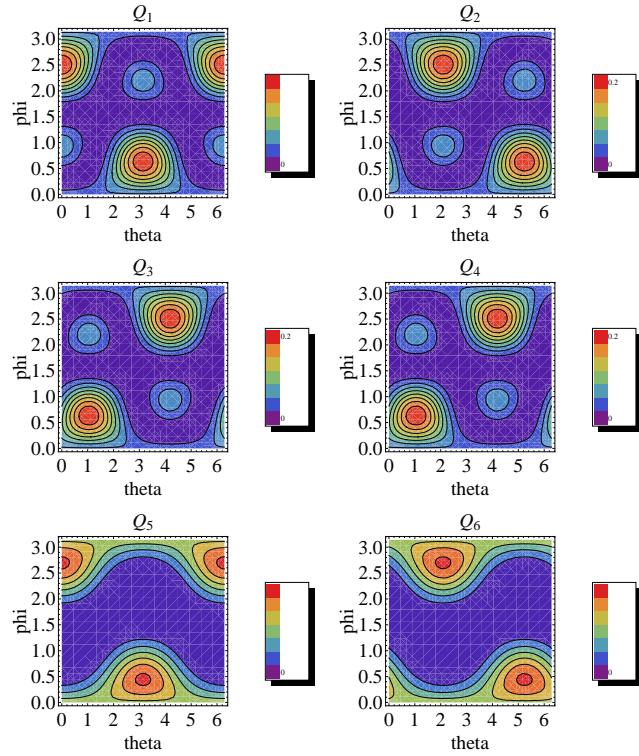
Figure 4.6: Sensitivity of six resonators as a function of θ and ϕ

4.5   Summary of the Chapter

In this chapter, GWs from $f(R)$ gravity with $f(R)$ of the form $R + aR^2$, a being some unknown constant, is studied using the simplest method. A massive mode in addition to the massless modes is also obtained. Thus $f(R)$ gravity produced gravitational waves with $+$, $\times$ and an additional scalar, s, polarizations. The sensitivity of the sphere modes of a spherical antenna detector towards such a massive wave is determined. It shows that massive scalar polarization can be detected using spherical antenna detectors .

119
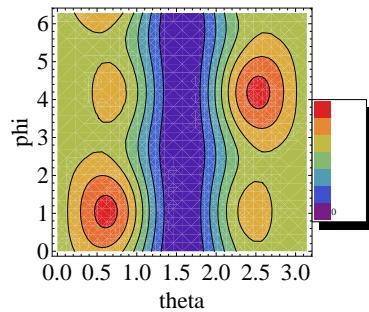
Figure 4.7: Total energy sensitivity as a function of θ and ϕ for a spherical antenna detector with resonators

The sensitivities of the monopole and quadrupole modes of a sphere towards an incoming massive GWs are calculated. The monopole mode shows the maximum sensitivity towards a massive GW. However, the massive wave is found to trigger only three of the five quadrupole modes of the sphere. If, in addition we know the galactic coordinates of the source, then the sensitivity of the antenna can be predicted exactly. Thus the massive component can be easily recognized and will be detected if ever possible. We have also found a modified TIGA configuration wherein an additional resonant transducer has been added to the six resonator TIGA configuration for detecting the monopole mode of the sphere. This $l = 0$ mode shows a maximum sensitivity towards a massive wave and hence its detection will be straightforward.

Now, it will be worth looking at the detection possibility of this massive mode in the interferometric detector LIGO since they grab the current relevance in GW detection. This is done in next chapter.
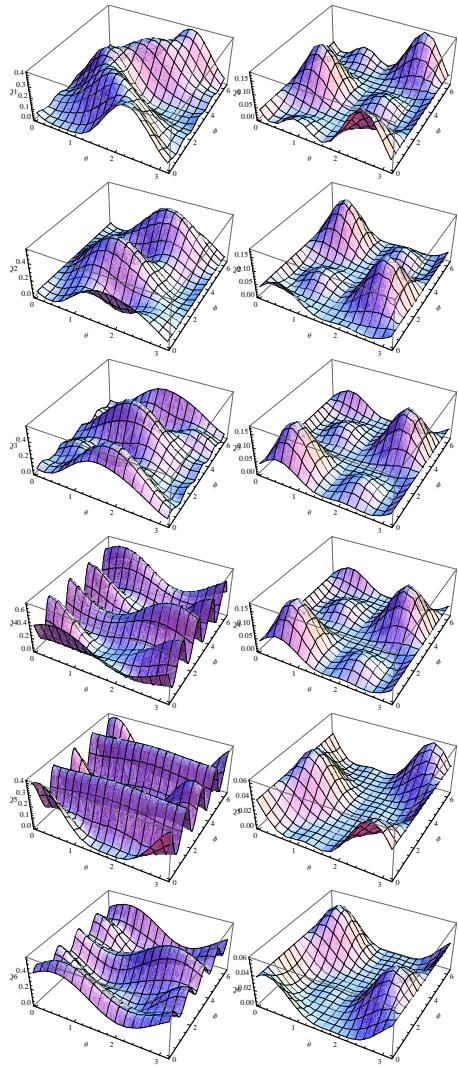
Figure 4.8: Figure showing the directionality of spherical antenna in the presence of resonators towards massless waves from GR (shown on the left of each pair) and towards massive wave (shown on the right side of each pair).

Massive Gravitational Waves and its Detection using Laser Interferometers

5.1 Introduction

As discussed in the previous chapter, the existence of Gravitational Waves (GWs) is a natural outcome of GTR. With the path breaking discovery of GWs, LIGO serves as the center of attention for future research in Gravitational Wave Astronomy. Gravitational waves from binary black hole merger was detected by the LIGO detector. A laser interferometer defines its own coordinate system so that the x and y axes run along the two interferometer arms and the origin is at the beam-splitter. The Fig.5.1 shows an indicative picture of LIGO oriented towards GW source.
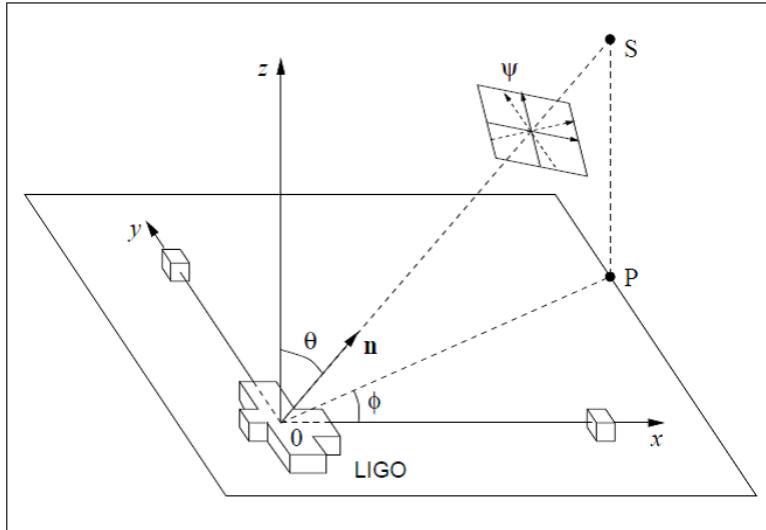
Figure 5.1: Orientation of the LIGO detector with respect to the source of gravitational waves

The arrangement consists of two beam lines of 4 km length which form a power-recycled Michelson interferometer with Gires-Tournois etalon arms. A pre-stabilized 1064 nm Nd:YAG laser emits a beam with a power of 20 W that passes through a power recycling mirror. The mirror fully transmits light incident from the laser and reflects light from the other side increasing the power of the light field between the mirror and the subsequent beam splitter to 700 W. From the beam splitter the light travels along two orthogonal arms. By the use of partially reflecting mirrors, Fabry-Perot cavities are created in both arms that increase the effective path length of laser light in the arm. The gravitational waves will interact hardly at all with the light. Instead, they will push the end mirrors back and forth relative to the

coordinate system, thereby lengthening one arm while shortening the other. These changing arm lengths will cause a changing interference of the light returning to the beam splitter from the two arms, and that changing interference will produce the fluctuating light intensity $I_{out}(t) \propto h(t)$ measured by the photodetectors[153].

The gravitational sources producing detectable GWs are astrophysical in nature. Of the different GW sources present, Gamma Ray Bursts (GRBs) form an important class. GRBs are intense flashes of γ-rays which occur approximately once per day and are isotropically distributed over the sky [154, 155]. They are grouped into two broad classes by their characteristic duration and spectral hardness: a) short GRB, the progenitors of which are thought to be mergers of neutron star binaries or neutron-star black hole binaries and b) long GRB which are associated with core-collapse supernovae. Both mergers and supernovae scenarios result in the formation of stellar-mass black holes with accretion disk and the emission of GWs is expected in this process.

GWs are considered to be one of the promising tools to probe the early Universe. The detection of GWs involves the statistical analysis of the observed data. It should tell whether the data contain the signal or not or whether the data supports a certain theoretical model or not with reliability. Statistical analysis can follow one of the two perspectives[156]: 1) Frequentist/Classical analysis and 2) Bayesian analysis. In a frequentist analysis, the probabilities are viewed in terms of the frequencies of random repeatable events whereas proba-

bilities in Bayesian analysis provide a quantification of uncertainty.
From a Bayesian perspective, we can use the machinery of probability
theory to describe the uncertainty in model parameters or in the
choice of the model itself. Bayesian analysis can be *parametric* or *non-parametric*. Non-parametric models constitute an approach to model
selection and adaptation where sizes of models are allowed to grow
with data size whereas in parametric models, a fixed number of para-
meters are used. A Bayesian formulation of non-parametric problem
is non trivial since a Bayesian model defines the prior and posterior
distribution on a single fixed parameter space, but the dimension of
this parameter space in a non parametric approach changes with the
sample size [157].

In the recent studies on the discovery of GWs, it is noted that no
studies were done aiming at constraining parameters corresponding
to any of the alternative theories of gravity due to lack of predictions
for what the inspiral-merger-ringdown GW signal would look like in
those cases. Also the *Fermi* Gamma-ray Burst Monitor (GBM) obser-
vations at the time of the LIGO event GW150914 reveal the presence
of a weak transient source above 50 KeV, 0.4s after the GW event was
detected, with a false alarm probability of 0.0022. This weak transient
lasting for 1s does not appear to be connected with other previously
known astrophysical, solar, terrestrial, or magnetospheric activities.
Its localization is ill-constrained but consistent with the direction of
GW150914. This is suggested to be a weak Short Gamma Ray Burst
(GRB)[158]. All the facts throw motivation for the modeling and pa-

rameter estimation of a GW event occurring from GRB that may help in studying the alternative theories of gravity. Also, a second detection of GWs from coalescence of two-stellar mass black holes is reported recently[159]. GRBs form one of the potential astrophysical sources that may provide us a strong field regime to study the existence of GWs in ETG[160, 161]. However it is to be noted that the production and detection of GWs on the basis of ETG for GRBs are not explored much. Another area of current interest is massive gravity which will result in a massive polarization component of GWs. $f(R)$ theory of gravity forms an easy-to-handle modification of GTR and hence is a wise choice for such studies. The LIGO response function for massive GWs produced from $f(R)$ gravity is derived in the following section of this chapter.

5.2 Response Function of Advanced LIGO Towards Massive Gravitational Waves

The production of GWs in $f(R)$ theory of gravity is detailed in chapter 4.2. The utilization of metric $f(R)$ gravity results in additional polarization sates compared to the usual polarization states, + and × in GTR. In f(R) theories, GWs can have a massive scalar mode besides the usual transverse-traceless modes in GTR. Six polarization modes are possible in f(R) theories [162]. In the work of Rizwana et al.[163], it is shown that in metric f(R) theory in addition to the + and ×, a breathing mode which goes along with the + and × modes

and a longitudinal scalar mode which moves propagating along the direction of propagation of the GWs with a velocity less than the velocity of light exists. But in Palatini formalism f(R) theories possess only the usual transverse-traceless modes as in GTR. GWs in most of the extended theories of gravity possess more than the two usual polarization modes. The detection of GWs is particularly a challenging issue and it may be capable of distinguishing the different modes and may help us to find the correct formulation of gravity. In this work, only the case of massive scalar polarization component[164] is considered. In an earlier work[165], the detection of scalar component of gravitational radiation in Brans-Dicke theory has been studied.

The effect of GWs is to produce a transverse shear strain and this fact makes the Michelson interferometer an obvious candidate for a detector. When GWs pass through the detector, one arm of the detector gets stretched in one direction whereas the other arm gets compressed. The dimensionless detector response function h of an interferometric detector is defined as the difference between the wave induced relative length change of the two interferometer arms and is computed from the formula given as[166],

$$(5.1) \qquad h(t) = \frac{1}{2}\mathbf{n}_1.[\tilde{H}(t)\mathbf{n}_1] - \frac{1}{2}\mathbf{n}_2.[\tilde{H}(t)\mathbf{n}_2],$$

where $\mathbf{n}_1$ and $\mathbf{n}_2$ are unit vectors parallel to the arms 1 and 2 respectively. Once a detector is built, it will be difficult to move it or even to change its orientation and hence the location and orientation of detector will decide how the detector is sensitive to GW sources and

likelihood of detection. Hence, the matrix $\tilde{H}(t)$ can be written as[167],

$$(5.2) \qquad \tilde{H}(t) = M(t)H(t)M^T(t),$$

where $H(t)$ is the spatial metric perturbation given by,

$$(5.3) \qquad \begin{pmatrix} h_+ & h_\times & 0 \\ h_\times & -h_+ & 0 \\ 0 & 0 & m^2 h_s \end{pmatrix}.$$

M is the three dimensional orthogonal matrix of transformation from the wave cartesian coordinates to the cartesian coordinates in the proper reference frame of the detector. m is the massive contribution of the GW. If we follow Kausar et al.[163], h_+ can be taken as $h_+ + h^b$, where h^b is the breathing polarization mode and $h_\times = h_\times + -h^b$. From (5.1), (5.2) and (5.3), we can write the response function as,

$$(5.4) \qquad h(t) = F_+(t)h_+(t) + F_\times(t)h_\times(t) + F_s(t)(m^2 h_s(t)),$$

$$(5.5) \qquad = F_+(t)h_+(t) + F_\times(t)h_\times(t) + F_s(t)h(t)'$$

where $h(t)' = m^2 h_s$ and we have ignored h^b; $F_+(t)$, $F_\times(t)$ and $F_s(t)$ are called beam pattern functions. The beam pattern function also called as response function determines the sensitivity of the detector towards an incoming GW from a source.

In order to express the beam pattern function in terms of right ascension (α) and declination (δ) of the GW source, we follow Jaranowski et al.[167]. Accordingly, the matrix M can be represented as,

$$(5.6) \qquad M = M_3 M_2 M_1^T,$$

where M_1 is the matrix of transformation from wave to detector frame coordinates, M_2 is the matrix of transformation from celestial to cardinal coordinates and M_3 is the matrix of transformation from cardinal to the detector proper reference frame coordinates.

$$(5.7) \qquad M_1 = \begin{pmatrix} A & B & C \\ D & E & F \\ G & H & I \end{pmatrix},$$

where,

$$A = \sin\alpha\cos\psi - \cos\alpha\sin\delta\sin\psi,$$
$$B = -\cos\alpha\cos\psi - \sin\alpha\sin\delta\sin\psi,$$
$$C = \cos\delta\sin\psi,$$
$$D = -\sin\alpha\sin\psi - \cos\alpha\sin\delta\cos\psi,$$
$$E = \cos\alpha\sin\psi - \sin\alpha\sin\delta\cos\psi,$$
$$F = \cos\delta\cos\psi,$$
$$G = -\cos\alpha\cos\delta,$$
$$H = -\sin\alpha\cos\delta,$$
$$I = -\sin\delta,$$

$$(5.8) \qquad M_2 = \begin{pmatrix} \sin\lambda\cos(\phi+\Omega t) & \sin\lambda\sin(\phi+\Omega t) & -\cos\lambda \\ -\sin(\phi+\Omega t) & \cos(\phi+\Omega t) & 0 \\ \cos\lambda\cos(\phi+\Omega t) & \cos\lambda\sin(\phi+\Omega t) & \sin\lambda \end{pmatrix},$$

and,

$$(5.9) \qquad M_3 = \begin{pmatrix} -\sin(\gamma+\zeta/2) & \cos(\gamma+\zeta/2) & 0 \\ -\cos(\gamma+\zeta/2) & -\sin(\gamma+\zeta/2) & 0 \\ 0 & 0 & 1 \end{pmatrix},$$

where λ is the latitude of the detector site, Ω is the rotational frequency of earth in the units $\frac{1}{\text{(sidereal hours)}}$ and ϕ is a deterministic phase which defines the position of the Earth in its diurnal motion at $t = 0$. γ determines the orientation of the arms of the detector with respect to local geographical directions, ζ is the angle between the arms of the interferometer and $\mathbf{n}_1$ and $\mathbf{n}_2$ have the coordinates,

$$(5.10) \qquad \mathbf{n}_1 = (1,0,0), \mathbf{n}_2 = (\cos\zeta, \sin\zeta, 0).$$

The beam pattern functions can be found from (5.1)-(5.9) and are given by,

$$(5.11) \qquad F_+ = \frac{1}{2}[(S^2 - T^2) - (S\cos\zeta + v\sin\zeta)^2 - (T\cos\zeta + w\sin\zeta)^2],$$

$$(5.12) \qquad F_\times = \frac{1}{2}\left[2ST\sin^2\zeta - \sin 2\zeta(Sw + Tv)^2 - 2vw\sin^2\zeta\right],$$

(5.13)

$$F_s = \frac{1}{4}\sin\zeta[2\cos(2(\gamma + \zeta))\sin\alpha[2\cos\delta^2\cos(2(\phi + \Omega t))\sin\alpha\sin\lambda +$$

$$\cos\lambda\sin 2\delta[-\cos(\phi + \Omega t) + \sin(\phi + \Omega t)]] +$$

$$\sin(2(\gamma + \zeta))[-2\cos\lambda^2\sin\delta^2 + \sin\alpha\sin 2\delta\sin 2\lambda[\cos(\phi + \Omega t) +$$

$$\sin(\phi + \Omega t)] + \cos\delta^2\sin\alpha^2[2\cos(\lambda)^2 + (-3 + \cos(2\lambda))\sin(2(\phi + \Omega t))]]],$$

where,

$$a = \sin\alpha\cos\psi - \cos\alpha\sin\delta\sin\psi,$$

$$b = -\sin\alpha\sin\psi - \cos\alpha\sin\delta\cos\psi,$$

$$c = -\cos\alpha\cos\delta,$$

$$d = -\cos\alpha\cos\psi - \sin\alpha\sin\delta\sin\psi,$$

$$e = \cos\alpha\sin\psi - \sin\alpha\sin\delta\cos\psi,$$

$$f = -\sin\alpha\cos\delta,$$

$$g = \cos\delta\sin\psi,$$

$$h = \cos\delta\cos\psi,$$

$$i = -\sin\delta,$$

$$j = \left[a\sin\lambda\cos(\phi+\Omega t)+d\sin\lambda\sin(\phi+\Omega t)-g\cos\lambda\right],$$

$$k = \left[b\sin\lambda\cos(\phi+\Omega t)+e\sin\lambda\sin(\phi+\Omega t)-h\cos\lambda\right],$$

$$l = \left[c\sin\lambda\cos(\phi+\Omega t)+f\sin\lambda\sin(\phi+\Omega t)-i\cos\lambda\right],$$

$$m = -a\sin(\phi+\Omega t)+d\cos(\phi+\Omega t),$$

$$n = -b\sin(\phi+\Omega t)+e\cos(\phi+\Omega t),$$

$$o = -c\sin(\phi+\Omega t)+f\cos(\phi+\Omega t),$$

$$S = -j\sin(\gamma+\zeta/2)+m\cos(\gamma+\zeta/2),$$

$$T = -k\sin(\gamma+\zeta/2)+n\cos(\gamma+\zeta/2),$$

$$u = -l\sin(\gamma+\zeta/2)+o\cos(\gamma+\zeta/2),$$

$$v = -j\cos(\gamma+\zeta/2)-m\sin(\gamma+\zeta/2),$$

$$w = -k\cos(\gamma+\zeta/2)-n\sin(\gamma+\zeta/2),$$

$$x = -l\cos(\gamma+\zeta/2)-o\sin(\gamma+\zeta/2).$$

Table 5.1 : GRB instances chosen for the analysis

Sl.No.	GRB Name	RA	DEC
1	100206A	$3^h 8^m 40^s$	$13^0 10'$
2	100213A	$23^h 17^m 30^s$	$42^0 22'$
3	100216A	$10^h 17^m 03^s$	$35^0 31'$
4	100225B	$23^h 31^m 24^s$	$15^0 02'$
5	091223B	$15^h 25^m 04^s$	$54^0 44'$
6	100410B	$21^h 16^m 59^s$	$37^0 26'$
7	070201	$0^h 44^m 21^s$	$42^0 18'$

In the present study, we are only concerned with the response function
of the massive polarization component. The behavior of the massive
response function with respect to the azimuth angle can be plotted
using (5.13). As examples we have chosen the GRB instances given in
Table 5.1. The sources given in the table corresponding to $Sl.No.1 - 3$
are short GRBs taken from Table I, $Sl.No.4 - 6$ are long GRBs taken
from Table II of Abadie et al.[168] and GRB 070201 from Table 5.1
of Abbott et al.[169]. Fig.5.2 shows the variation of beam pattern
function with ϕ for the above sources in the range $[-\pi, \pi]$ for the
detectors LIGO (Hanford) and LIGO (Livingston). From the figure
it can be seen that for different sources the pattern function vary
differently, which means that depending on the location of the detector,
the response function changes. Also, the response functions for the
same source are found to be different for the two LIGO detectors.

Fig.5.3 shows the beam pattern function behavior with the azimuth
angle ϕ and the polarization angle ψ. The antenna patterns are
in agreement with that proposed for massive scalar polarization
component[165]. It can be inferred from the figure that the beam
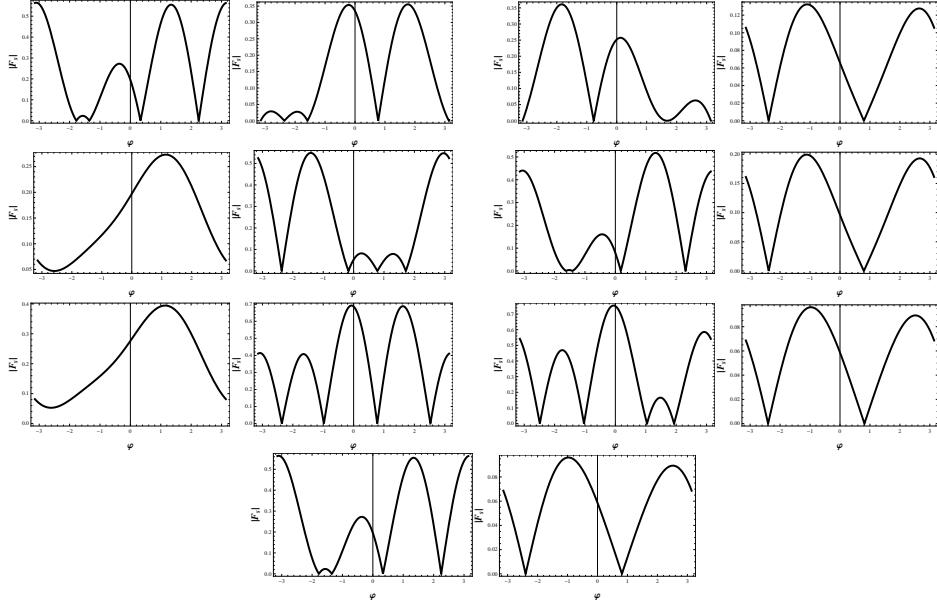
Figure 5.2: Variation of F_s with ϕ in the interval $[-\pi, \pi]$ for the sources described in Table 5.1 for the LIGO Hanford (left) and LIGO Livingston (right) respectively.

pattern function behaves in a highly directional manner towards an incoming wave of massive polarization. If a GW is present the detector should be able to identify it from other noises. To filter out the GW signal from the noise, a statistical analysis has to be done. If the waveform of the signal expected from a source is modeled using certain parameters, then based on the observation of a real signal it will be able to discard or accept the proposed model using Bayesian analysis and hence Bayesian analysis has gained much importance.

134
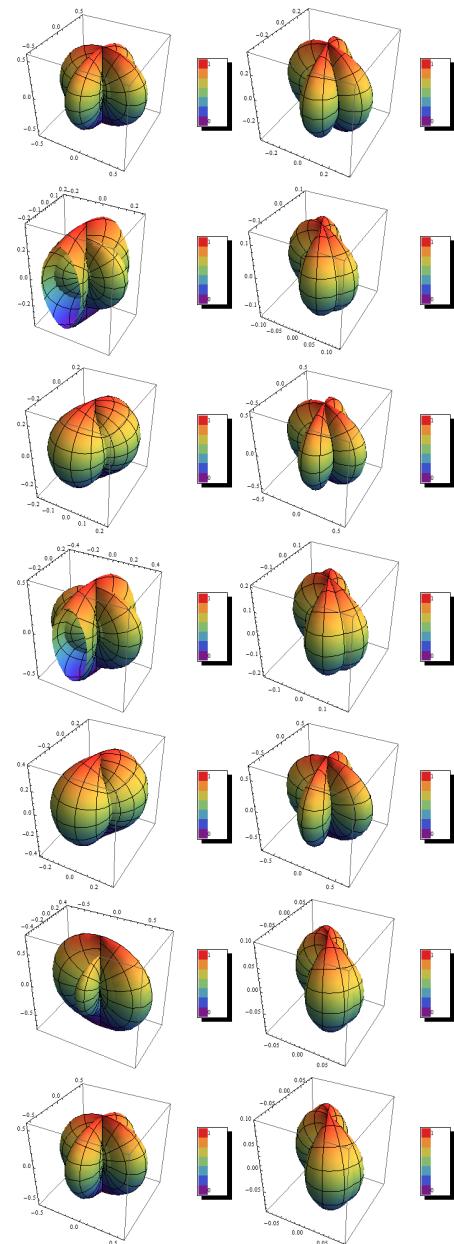
Figure 5.3: Beam pattern function for the massive wave as a function
of ϕ and ψ for the sources described above in their order for the LIGO
Hanford (left) and LIGO Livingston (right) respectively.

5.3   A Bayesian Approach to Signal Detection

In this section, the Bayesian method is invoked to analyze a massive GW signal. Bayesian data analysis has already been done for the case of Pulsar timing arrays for the + and × polarizations of GWs by Finn and Lommen[170]. The study of Bayes factor as a norm for model selection, as to which model describes the data best is also studied in this section.

5.3.1   Bayes theorem

The two fundamental rules of probability theory are[171]:

Sum Rule :

$$(5.14) \qquad p(x) = \sum_y p(x,y)$$

Product Rule :

$$(5.15) \qquad p(x,y) = p(y|x)p(x)$$

Here, $p(x,y)$ is the probability of x and y called as *Joint Probability*, $p(y|x)$ is the probability of y given x called as conditional probability, $p(x)$ is just the probability of x called as marginal probability. From the product rule, together with the symmetry property that $p(x,y) = p(y,x)$, one can arrive at a relationship between conditional probabilities as[156],

$$(5.16) \qquad p(y|x) = \frac{p(x|y)p(y)}{p(x)},$$

136

which is called '*Bayes Theorem*'. Using Sum rule the quantity in denominator can be expressed as,

$$(5.17) \qquad p(x) = \sum_y p(x|y)p(y),$$

which can be called as the normalization constant.

The Bayesian view is more general in which the probabilities provide a quantification of uncertainty ie., the result of Bayesian analysis is a quantitative measure stating how far the chosen proposition is true. The is especially useful for events that are nor repeated and one has to update the degree of uncertainty when the event is observed. Now, let $\vec{w}$ represent the choice of model parameters. The assumptions about $\vec{w}$ done before observing the data are captured as the prior probability distribution, $p(\vec{w})$. The effect of the observed data $\mathcal{D}$ is expressed through the conditional probability $p(\mathcal{D}|\vec{w})$. The Bayes theorem given by,

$$(5.18) \qquad p(\vec{w}|\mathcal{D}) = \frac{p(\mathcal{D}|\vec{w})p(\vec{w})}{p(\mathcal{D})}$$

then allows to evaluate the uncertainty in $\vec{w}$ after we have observed $\mathcal{D}$ in the form of the posterior probability $p(\vec{w}|\mathcal{D})$. $p(D)$ is the normalization constant that makes the posterior distribution a valid one and also ensure that it integrates to 1. $p(D)$ according to (5.17) can be written as,

$$(5.19) \qquad p(D) = \int p(D|w)p(w)dw.$$

$p(\mathcal{D}|\vec{w})$ is called the *likelihood function* that tells how probable the observed data set is for different settings of the parameter vector $\vec{w}$

and Bayes theorem in words looks like,

$$\text{posterior} \propto \text{likelihood} \times \text{prior}$$

One advantage of the Bayesian viewpoint is that the inclusion of prior
knowledge arises naturally. Bayesian analysis is completely controlled
by the Bayesian law of conditional probabilities that includes the sum
rule and the product rule.

5.3.2   GW signal analysis

Bayesian approach to the GW signal analysis is applied to analyze
the GWs from GRBs[170]. Suppose that the observed data is D and
let h be the proposed wave that describes the data D. The output
data that we receive from a detector will be a mixture of the original
waveform h and the noise, n of the detector, ie.,

$$(5.20) \qquad\qquad D = h(t) + n(t),$$

where $h(t)$ is given by (5.5). Here we deal only with the massive scalar
mode. Assuming that the wave exhibits only a single mode at a time,
the above equation can be written as,

$$(5.21) \qquad\qquad D = F_s(\theta, \phi) h_s + n(t).$$

In this equation, we have taken $m^2 = 1$ for convenience. The noise
is assumed to be a zero mean additive Gaussian noise. Then, the
Bayesian law given by (5.18) can be written in the form,

$$(5.22) \qquad\qquad p(h|D) = \frac{\Lambda(D|h)p(h)}{p(D)},$$

where $p(h|D)$ is the posterior probability density, Λ is the likelihood function, $p(h)$ is the prior probability density and $p(D)$, the normalization constant. The likelihood function Λ can be written as[171]

$$(5.23) \qquad \Lambda(h|D) = N(\mathbf{D} - \mathbf{F}_s\mathbf{h}_s|\mathbf{C}),$$

where N denotes data drawn independently from a multivariate Gaussian distribution. $\mathbf{C}$ is the noise covariance and $N(x|C)$. For a multivariate normal distribution with zero mean random deviate x given covariance C is given by,

$$(5.24) \qquad N(x|C) = \frac{exp(-\frac{1}{2}x^T C^{-1} x)}{\sqrt{(2\pi)^{\mathcal{N}} det||C||}}$$

where $\mathcal{N}$ is the number of elements in vector x. Assuming that the *a priori* probability distribution is of Gaussian form, we can write,

$$(5.25) \qquad \begin{aligned} p(h_s) &= N(h_s|\sigma_s I) \\ &= [(2\pi\sigma_s^2)]^{-1/2} exp(-\frac{1}{2}\frac{h_s^2}{\sigma_s^2}), \end{aligned}$$

As discussed already, the Bayesian non-parametric formulation depends on the dimension of the parameter space. Therefore, dimensionality should be included in the *a priori* distribution. The Gaussian distribution in higher dimensional space containing many input variables is then given by[170, 172, 173],

$$(5.26) \qquad p(h_s) = [(2\pi\sigma_s^2)^{\mathcal{N}}]^{-1/2} exp(-\frac{1}{2}\sum_{k=1}^{\mathcal{N}}\frac{h_k^2}{\sigma_s^2}),$$

where σ_s is an undetermined constant, $\mathcal{N}$ can be treated as the number of data taken and I denotes an appropriately dimensioned identity matrix. The normalization constant $p(D)$ is the integral of

the product of the likelihood function and the *a priori* probability
density over all possible values of h_s. Exploiting (5.19), (5.23), (5.24)
and (5.25), we can write,

$$
\begin{aligned}
p(D) &= \int \Lambda(h|D) p(h_s) d^{\mathcal{N}} h_s \\
&= \frac{exp(-\frac{1}{2}[\mathbf{h}(t)^T \mathbf{C}^{-1} \mathbf{h}(t)])}{\sqrt{(2\pi)^{\mathcal{N}} det||C||}} \\
&\quad \times \frac{exp(\frac{1}{2}(F_s^T C^{-1} h(t))^T A^{-1}(F_s^T C^{-1} h(t)))}{\sqrt{det||A|| \sigma_s^{2\mathcal{N}}}},
\end{aligned}
$$

(5.27)

where $\mathbf{A}$ is given by,

(5.28)
$$
A = \sigma_s^{-2} I_s + F_s^T C^{-1} F_s,
$$

and I_s is an appropriately dimensioned identity matrix. Finally, the
posterior probability density $p(h|D)$ can be written as[172],

(5.29)
$$
p(h|D) = \sqrt{\frac{det||A||}{(2\pi)^{\mathcal{N}}}} exp[\frac{1}{2}(h - h_0)^T A(h - h_0)],
$$

where h_0 satisfies,

(5.30)
$$
A h_0 = F_s^T C^{-1} h(t).
$$

It can be easily inferred from the above equation that h_0 is the wave-
form that maximizes the probability density $p(h_s|h(t))$. The amplitude
Signal-to-Noise Ratio, ρ associated with h_0 is given by[170],

(5.31)
$$
\rho^2 = (F_s h_0)^T C^{-1}(F_s h_0).
$$

Finally, the quantity *Bayes Factor* helps us to decide on whether a
signal is present or not. It chooses between different models. For

any observations D, the Bayes factor for M_1 against M_0 is defined by[174, 175],

$$(5.32) \qquad B_{10} \quad = \quad \frac{m_1(\theta)}{m_0(\theta)}$$

$$(5.33) \qquad \qquad = \quad \frac{p(D|M_1)}{p(D|M_0)},$$

θ is some unknown parameter. The probabilities given in (5.33) are nothing but the likelihood function. Therefore, one can express,

$$(5.34) \qquad p(D|M_1) = \Lambda(D|M_1, h_s, \sigma_s),$$

gives the probability density of observations D assuming the GW signal described by parameter σ_s is present,

$$(5.35) \qquad p(D|M_0) = \Lambda(D|M_0),$$

gives the probability density of D assuming no signal is present. The Bayes factor can then be written as[170],

$$(5.36) \qquad B_{(D)} = \int \frac{d^2\Omega_k}{4\pi} \frac{exp(-\frac{1}{2}[\mathbf{D}^T\mathbf{C}^{-1}\mathbf{D}])}{\sqrt{det|A|\sigma_s^{2dimh_s}}}.$$

Now, from Bayes theorem, the posterior probability of model M_1 can be expressed through Bayes factor as[174],

$$(5.37) \qquad p(M_1|D) \quad = \quad \frac{p(M_1)m_1(D)}{p(M_1)m_1(D) + p(M_0)m_0(D)}$$

$$(5.38) \qquad \qquad = \quad \frac{p(M_1)B_{10}}{p(M_0) + p(M_1)B_{10}},$$

where $p(M_i)$ is the prior probability of model M_i for $i = 0$. In the absence of any prior knowledge, $p(M_0) = p(M_1) = 1/2$. Therefore, the model M_1 is more likely to be chosen if $p(M_1|D) > \frac{1}{2}$ or equivalently

$B_{10} > 1.$

Thus, Bayes factor is always positive. On the average, Bayes factor will always favor the correct model. A Bayes factor that is large compared to unity will favor M_1 while a Bayes factor small compared to unity will favor the model M_0.

5.3.3 Methodology

Firstly, in order to check the possibility of detecting massive GW in the LIGO, the simulated data from (5.21) is used. For that a simplest adhoc waveform given by a Gaussian distribution is employed for h_s, and can be written as in Abbott et al.[176],

$$(5.39) \qquad h_s(t + t_0) = h_{s,0}(\omega_m)\cos(2\pi f_0 t)\exp(-\frac{(2\pi f_0 t)^2}{2Q^2}),$$

where t_0 is the central time, f_0 is the central frequency, which is taken in the range of 0 to 200Hz; $h_{s,0}$ is the amplitude parameter that is characterized by ω_m and is given as [177],

$$(5.40) \qquad \omega_m = \frac{m}{\sqrt{1 - v_g^2}},$$

m is the mass of the graviton, v_g is the velocity of propagation of GW and Q is a dimensionless constant which represents roughly the number of cycles with which the waveform oscillates more than half of the peak amplitude. A standard choice in LIGO burst searches for Q is 8.9. t will be very short and is taken in the range 0 to 1s. $h_{s,0}$ is given by[154],

$$(5.41) \qquad h_{s,0} = \frac{1}{r}\sqrt{\frac{5GE_{GW}}{c^3 Q f_0 4\pi^{3/2}}}$$

In order to simulate the detector output signal $h(t)$, (5.41) is substituted in (5.39). This in turn is substituted in (5.26). Simulated F_s are taken from (5.21). As an example to check whether massive scalar polarization resulting from metric $f(R)$ gravity will be detected, we take the random sample GRB070201. For this candidate $E_{GW} = 1.14 \times 10^{-4} M_\odot c^2$ and $r = 770 \text{Kpc}$[178]. Taking F_s from (5.14), the simulated waveform for different m are shown in Fig.5.4. The data
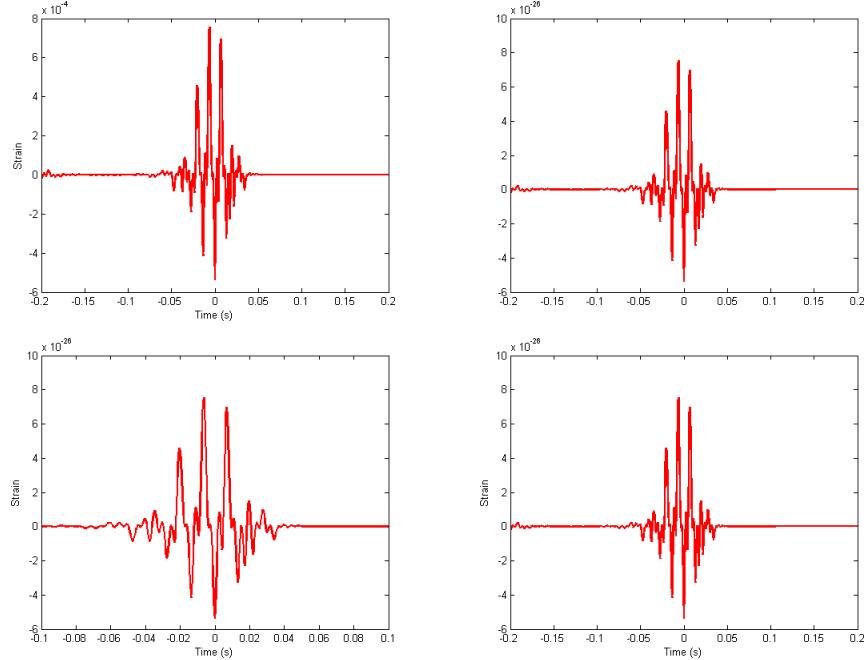

Figure 5.4: The simulated output signal for GRB070201 for $m = 1$, $m = 1 \times 10^{-21}$, $m = 1 \times 10^{-22}$ and $m = 1 \times 10^{-23} eV/c^2$ from top left

used in this section for Bayesian analysis is taken from this simulated output waveform. Also, the predicted waveform is taken from (5.39). Even though it is not the wisest choice, it will serve the purpose of the present work. After having the data D and the predicted waveform h_s,

the parameter σ_s is to be estimated in order to get the most probable waveform and also the Bayes factor. This is done by the optimization of (5.27) with respect to σ_s. While optimizing, maximization is used since it is more favored[179]. The equation as such is too complicated to optimize and therefore it is simplified taking logarithm of $p(D)$. This procedure is fully justified since logarithm is a monotonically increasing function of its argument. So, maximizing $\log p(D)$ with respect to σ_s is equivalent to maximizing $p(D)$. Then we can write,

$$
\begin{aligned}
\log p(D) = &\log[\frac{exp-\frac{1}{2}[\mathbf{h}(t)^T \mathbf{C}^{-1}\mathbf{h}(t)]}{\sqrt{(2\pi)^{dimx}det||C||}}] \\
&+ \log[\frac{exp\frac{1}{2}(F_s^T C^{-1}h(t))^T A^{-1}(F_s^T C^{-1}h(t))}{\sqrt{det||A||\sigma_s^{2dimh_s}}}].
\end{aligned}
$$
(5.42)

Since we are maximizing $\log p(D)$ with respect to σ_s, the first term on the right hand side can be suitably omitted as it is independent of σ_s. The second term is optimized. Using the values of matrix $\mathbf{A}$ that is obtained by optimizing, (5.30) is simultaneously solved for $\mathbf{h}_0$, the most probable waveform(inferred waveform) for the given data. After getting $\mathbf{h}_0$, the signal to noise ratio (ρ) can be calculated using (5.31). Then the Bayes factor can be evaluated using (5.36).

5.3.4 Results

The phenomenological limit on the graviton mass from recent discovery of GWs is given as[159] $1.2 \times 10^{-22} eV/c^2$ and hence using the method discussed in the previous subsection the optimization is done for $m = 10^{-21}, 10^{-22}$ and $10^{-23} eV/c^2$ and is shown in Table 5.2. Comparing the values given in Table 5.2 with those in Table 2 of the Ref.[170], it can be seen that the Bayes factor and SNR values are

Table 5.2 **:** Results showing the calculation of log of Bayes factor and SNR for different values of m.

$m(eV/c^2)$	σ_s	ρ	$\ln B_D$	signal
10^{-21}	1×10^{-11}	~ 0.1360	$\sim -1.7 \times 10^3$	weak/Absent
10^{-22}	1×10^{-11}	~ 0.1360	$\sim -1.7 \times 10^3$	weak/Absent
10^{-23}	1×10^{-11}	~ 0.1360	$\sim -1.7 \times 10^3$	weak/Absent

very low indicating the absence of the signal. Thus it can be concluded that with the given sensitivity and orientation of the LIGO detector, a massive scalar polarization from $f(R)$ theory with a value for the graviton mass in the range $m = 1 \times 10^{-21}$ to $1 \times 10^{-23} eV/c^2$ is unlikely to be detected. The comparison of most probable waveform with the actual one is shown in Fig.5.4. This null result can be compared with the results obtained in the works of Aasi et al.[180] and Xihao Deng[181] where they predicted null results for GRBs in the case of $+$ and $\times$ polarization with the existing observational set up.

5.4 Summary of the Chapter

In this chapter we have presented the studies on the production of massive GWs from a metric $f(R)$ gravity and the beam pattern it produces on an interferometer detector. We have calculated the antenna response function in the detector coordinates for massive GWs. These are then considered to find out the response function of LIGO Hanford and Livingston detectors using seven Gamma Ray Burst(GRB) sources. These sources are selected at random. It is found that the beam pattern functions are highly directional. They are sensitive to the direction in which the massive GW come. A Bayesian analysis has been done to check the possibility of detecting a massive GW compo-

nent from the source GRB 070201 using simulated data for LIGO for the values of graviton masses: $m = 10^{-21}, 10^{-22}$ and $10^{-23} eV/c^2$. The parameter of the predicted waveform, which is nothing but the rms amplitude of the wave, is determined by optimization method. The Bayes factor and the SNR values are also determined. For all the cases the analysis gave low values of SNR and Bayes factor. Thus with the model discussed in this work for a GRB event and the beam pattern function, the massive polarization is not likely to be detected. The results are prone to change with a different *a priori* waveform. Even though the results presented in this work are not conclusive enough, it gives insight in to the study of GWs from alternative theories or extended theories of gravity.
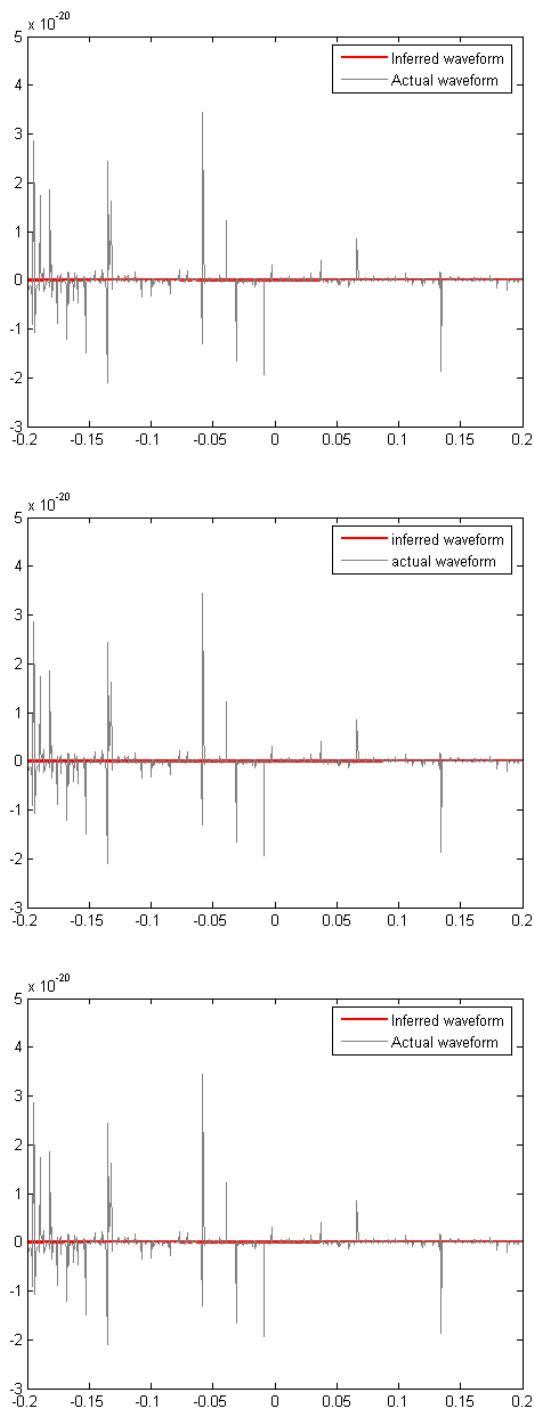
Figure 5.5: Comparison of the inferred and the actual waveforms for the LIGO detector for $m = 1 \times 10^{-21}$ (top) and for $m = 1 \times 10^{-22}$ (middle) and $1 \times 10^{-23} eV/c^2$ (bottom).

SUMMARY AND CONCLUSION

The existence of black holes and GWs are important predictions done by GTR and is now proved. Hence any massive theory of Gravity should also give similar solutions and should reproduce the same results when graviton mass becomes zero.

In this thesis, QNMs are calculated for the case of black holes in dRGT massive gravity in dS space-time and is found to be dependent on the graviton mass. Also the QNMs are found to be higher in magnitude compared to the Schwarzschild de Sitter (SdS) case. The thermodynamics and P-V criticality showed that the neutral black hole shows a near Van der Waals phase transition while a charged black hole shows exactly Van der Waals phase transition. The study of the entanglement entropy in the above cases too showed similar results which is interesting to note. The QNMs calculated for $(2+1)$

dimensional BTZ black hole in massive gravity shows phase transition and this phase transition behavior is found to be dependent on the mass of the graviton, charge and the cosmological constant. The thermodynamics of the above black hole also showed the existence of a phase transition. The phase transition behavior for dS and AdS space-time are compared and is found that phase transition is shown in the dS case for a wide range of charge values whereas for AdS space-time phase transition is shown only for a limited range of charge.

Thus, the QNMs which form the characteristic sound of a black hole are different for massive gravity when compared with the case of GTR and is also found that they take the same values as that predicted by GTR when the graviton mass is zero. And their thermodynamics shows interesting results like Van der Waals phase transition. Hence exploring these aspects help in paving way for a quantum gravity theory and at the same time the validity of the theory itself can be checked by searching for its QNMs via gravitational waves.

Another important aspect is to search for the GW itself coming out of such theories. The production of GWs from $f(R)$ theory of gravity is studied by varying the action and then linearizing. The resulting wave equation led to a massive polarization in addition to the $+$ and $\times$ polarizations familiar in GTR. The detection possibility of such a massive polarization using a spherical antenna is studied. A modified TIGA is proposed for its detection and the energy sensitivity of modified TIGA is calculated and it is found that the sensitivity shown

150

towards a massive polarization is higher compared to the massless modes. The detection possibility of the aforesaid massive polarization is then studied for the Advanced LIGO detector using Bayesian analysis employing Gamma Ray Burst (GRB) samples. The result showed that with the present configuration of LIGO it is difficult to detect the massive mode.

Future Plan of Work

The QNM study can be extended to more classes of massive gravity in both dS and AdS space-times and also the analogy of similar phase transition behavior from QNM study and thermodynamics can be utilized to study the entanglement entropy. The production of GWs from $f(R)$ theory is discussed in the work. This work can be extended to study the production and detection of GWs from different classes of Massive Gravity also. Since this work is time bound, the aforesaid works are planned for future studies.

BIBLIOGRAPHY

[1] Norton J., "How Einstein Found His Field Equations", Historical Studies in the Physical Sciences 14, 253-316 (1984).

[2] Stachel J., "History of Relativity", Twentieth Century Physics, Philadelphia: Institute of Physics, Vol. I, 249-356 (1995).

[3] Hobson M. P., Efstathiou G. P. and Lasenby A. N., "General Relativity: An introduction for Physicists", Cambridge University Press, UK (2006).

[4] Padmanabhan T., "Gravitation : Foundations and Frontiers", Cambridge University Press, New Delhi (2010).

[5] Narlikar J., "General Relativity And Cosmology", The Macmillan Company of India Ltd., New Delhi (1978).

[6] Einstein A., "The Meaning of Relativity", Oxford and IBH Publishing Co., Culcutta (1968).

[7] Einstein A., Annalen der Physik., 49 (7), 769-822 (1916).

[8] Dyson F. W., Eddington A. S., Davidson C., "A determination of the deflection of light by the Sun's gravitational field, from observa-

tions made at the total eclipse of 29 May 1919", Philosophical Transactions of the Royal Society. 220A, 291 (1920).

[9] Will C. M., Living Rev. Relativity., 9, 39 (2006). [arXiv:gr-qc/0510072]

[10] Schwarzschild Karl, "Über das Gravitationsfeld eines Massenpunktes nach der Einsteinschen Theorie", Königlich Preuflische Akademie der Wissenschaften (Berlin), Sitzungsberichte, 189-196; 191 (1916).

[11] Bolton C. T., Nature, 235 (5336), 271 (1972).

[12] Hulse R. A. and Taylor J. H., Astrophys. J., 191, L59 (1974).

[13] Weyl H., Ann. Phys., 59, 101 (1919).

[14] Eddington A. S., "Mathematical Theory of Relativity", Cambridge University Press, Cambridge (1923).

[15] Utiyama R. and De Witt B. S., J. Math. Phys., 3, 608 (1962).

[16] Stelle K. S., Phys. Rev. D, 16, 953 (1977).

[17] Birrell N. D. and Davies P. C. W., "Quantum Fields in Curved Spacetime", Cambridge University Press, Cambridge (1982).

[18] Vilkovisky G. A., Class. Quantum Grav., 9, 895 (1992).

[19] Sotiriou T. P, J. Phys.: Conf. Ser., 189, 012039 (2009).

[20] Weinberg S., Rev. Mod. Phys. 61, 1 (1989).

[21] Carroll S. M., Living Rev. Relativ., 4, 1 (2001).

[22] Capozziello S. and Francaviglia M., Gen. Relativ. Gravit., 40, 357 (2008).

[23] Nojiri S. and Odintsov S. D., Int. J. Geom. Methods Mod. Phys., 4, 115 (2007a).

[24] Capozziello S. and De Laurentis M., Physics Reports, 509, 167, (2011). [arXiv:1108.6266.]

[25] Sotiriou T. P., Faraoni V., Rev. Mod. Phys., 82, 451 (2010).

[26] Ostrogradksi M., Mem. Ac. St. Petersbourg VI, 385 (1850).

[27] Brans C. H., Dicke R. H., Phys. Rev., 124, 925 (1961).

[28] Yunes N. and Stein L. C., Phys. Rev. D, 83, 104002 (2011)

[29] Lightman A. P. and Lee, D. L., Phys. Rev. D, 8, 3293-3302 (1973).

[30] Deffayet C. and Menou K., Astrophys. J., 668, L143-L146 (2007).

[31] Connes A., "Noncommutative Geometry", Academic Press, New York (1995).

[32] Nelson W., Ochoa J. and Sakellariadou M., Phys. Rev. D, 82, 085021 (2010).

[33] Gupta S. N, Phys. Rev., 96, 1683 (1954).

[34] Weinberg S., Phys. Rev. B, 138, 988 (1965).

[35] Feynman R. P., Morinigo, F. B., Wagner, "W.G.: Feynman Lectures on Gravitation", Addison-Wesley, Reading, MA (1995).

[36] Mattingly D., Living Rev. Relativity, 8, lrr-2005-5 (2005).

[37] Hinterbichler K., Rev. Mod. Phys., 84, 671 (2012).

[38] de Rham C., Living Rev. Relativity, 17, 7 (2014).

[39] Fierz M., Pauli W., Proc. R. Soc. Lond. Ser. A., 173, 211232 (1939).

[40] Vainshtein A. I., Phys. Lett. B, 39, 393 (1972).

[41] Boulware D. G., Deser S., Phys. Rev. D, 6, 3368 (1972).

[42] de Rham C., Gabadadze G., Tolley A. J., Phys. Rev. Lett., 106, 231101 (2011).

[43] de Rham C., Gabadadze G., Phys. Rev. D, 82, 044020 (2010).

[44] de Rham C., Gabadadze G., Tolley A. J., Phys. Lett. B, 711, 190 (2012). [arXiv:1107.3820]

[45] Babichev E., Fabbri A., J. High Energy Phys., 07, 016 (2014).

[46] Bergshoeff E. A., Hohm O. and Townsend P. K., Phys. Rev. Lett., 102, 201301 (2009).[arXiv:0901.1766]

[47] Dubovsky S. L., J. High Energy Phys., 2004(10), 076 (2004).[arXiv:hep-th/0409124]

[48] Jaccard M., Maggiore M. and Mitsou E., Phys. Rev. D, 88, 044033 (2013).[arXiv:1305.3034]

[49] Michell J., "On the Means of Discovering the Distance, Magnitude, &c. of the Fixed Stars, in Consequence of the Diminution

of the Velocity of Their Light, in Case Such a Diminution Should be Found to Take Place in any of Them, and Such Other Data Should be Procured from Observations, as Would be Farther Necessary for That Purpose", Phil. Trans. Roy. Soc., London 74, 35 (1784).

[50] Schwarzschild Karl, "On the gravitational field of a mass point according to Einstein's theory", Sitzungsber Preuss., Akad. Wiss. Berlin (Math.Phys.), 189 (1916). [arXiv: physics/9905030]

[51] Chandrasekhar S., Astrophysical Journal, 74, 81 (1931).

[52] Chandrasekhar S., Philosophical Magazine(7th series), 11, 592 (1931).

[53] Reissner Hans, In: Annalen der Physik (Leipzig), 50, 106 (1916).

[54] Weyl Hermann, In: Ann. Phys. (Berlin), 54, 117 (1917).

[55] Nordstrom Gunnar, "On the energy of the gravitational field in Einstein's theory", Proceedings of the Koninklijke Nederlandse Akademie van Wetenschappen 20, 1238 (1918).

[56] Graves John C. and Brill Dieter R., Phys. Rev., 120, 1507 (1960).

[57] Kerr Roy P., Phys. Rev. Lett., 11, 237 (1963).

[58] Newman E. T. et al., J. Math. Phys., 6, 918 (1965).

[59] Berezhiani L., Chkareuli G., de Rham C., Gabadadze G., Tolley A. J., Phys. Rev. D, 85, 044024 (2012).

[60] Kodama H. and Arraut I., Prog. Theor. Exp. Phys., 023E02 (2014).

[61] Brian Whitt, Phys. Lett., 145B, 176-178 (1985).

[62] Cognola G. et al., JCAP, 0502:010 (2005).

[63] Dimitrios Psaltis et al., Phys. Rev. Lett., 902, 100:119 (2008).

[64] Regge T., Wheeler J. A., Phys. Rev., 108, 1063 (1957).

[65] Zerilli F. J., Phys. Rev. D, 9, 860 (1974).

[66] Vishveswara C. V., Nature, 227, 936 (1970).

[67] Kokkotas K. G., Schmidt, B. G., Living Rev. Relativity., 2, 2 (1999).

[68] Konoplya R. A., Zhidenko A., Rev. Mod. Phys., 83, 793 (2011).

[69] Andersson N., Jensen B., "Scattering by Black Holes", arXiv:gr-qc/0011025v2 (2001)

[70] Barakat T., Phys. Lett. A., 344 (2005).

[71] Joan C., John G. B., Bernard J.K., Rev. Mod. Phys., 82, 3069 (2010).

[72] Iyer S., Will C. M., Phys. Rev. D, 35, 3621 (1987).

[73] Iyer S., Phys. Rev. D, 35, 3632 (1987).

[74] Iyer S., Seidel M., Phys. Rev. D, 41, 374 (1990).

[75] Ferrari V., Mashhoon B., Phys. Rev. D, 30, 295 (1984).

[76] Leaver E. W., Proc. Royal Society. London A, 402, 285 (1985).

[77] Ciftci H., Hall R. L., Saad N., J. Phys. A: Math. Gen., 36, 11807 (2003).

[78] Cho H. T., Cornell A. S., Jason D., Wade N., Class. Quant.Grav., 27, 155004 (2010). [arXiv:0912.2740v3]

[79] Cho H. T., Cornell A. S., Jason D., Huang T.R ., Wade N., Adv. Math. Phys., 2012, 281705 (2012).

[80] Hawking S. W., Phys. Rev. Lett., 26, 1344 (1971).

[81] Bekenstein J. D., Phys. Rev. D, 9, 3292 (1974).

[82] Hawking S. W., Phys. Rev. D, 13, 191 (1976).

[83] Bekenstein J. D., Phys. Rev. D, 7, 2333 (1973).

[84] Hawking S. W., Comm. Math. Phys., 43, 199 (1975).

[85] Bardeen J. M., Carter B. and Hawking S. W., Comm. Math. Phys., 31, 161 (1973).

[86] Robert B. Mann, Black Holes and Thermodynamics, Springer, New York (2015). DOI 10.1007/978-3-319-14496-2

[87] Hawking S. W., Page D. N., Commun. Math. Phys., 87, 577 (1983).

[88] Bekenstein J. D., Lett. Nuovo Cim., 4, 737 (1972).

[89] Bekenstein J. D., "Do we understand black hole entropy?", (1994). [arXiv:gr-qc/9409015].

[90] 't Hooft G., Nucl. Phys. B, 256, 727 (1985).

[91] Cadoni M. and Melis M., Found. Phys. 40, 638 (2010). [arXiv:0907.1559]

[92] Nishioka T., Ryu S. and Takayanagi T., J. Phys. A: Math. Theor., 42 504008 (2009).

[93] Ryu S. and Takayanagi T., Phys. Rev. Lett., 96, 181602 (2006). [arXiv:hep-th/0603001v2]

[94] Clifford V. Johnson., J. High Energy Phys., 03 (2014). [arXiv:1306.4955v4]

[95] Santhosh Kumar S. and Shankaranarayanan S., Temperature from quantum entanglement (2015). [arXiv:1504.00501v1]

[96] Einstein A., "On gravitational waves", Sitzungsberichte Preuflische Akademie der Wissenschaften Berlin (Math. Phys.), 154 (1918).

[97] Misner C. W., Thorne K. S. and Wheeler J. A., "Gravitation", Freeman, San Francisco (1973).

[98] Schutz B. F., "A First Course in General Relativity", Cambridge University Press, UK (1990).

[99] Flanagan Eanna E., Hughes Scott A., New. J. Phys., 7, 204 (2005).

[100] Abbott B. P. et al., PRL 116, 061102 (2016).

[101] Abbott B. P. et al., Phys. Rev. Lett., 116, 221101 (2016).

[102] Accadia T. et al., Class. Quantum Grav., 28, 025005 (2011).

[103] Abadie J. et al., Phys. Rev. D, 85, 022001, (2012).

[104] Weber J., Phys.Rev. Lett., 22, 1320 (1969).

[105] Lobo J. A., Phys. Rev D, 52, 591 (1995).

[106] Gasparini M. A., Phys. Rev. D, 72, 104012 (2005).

[107] Bianchi M. et al., Class. Quant. Grav., 13, 2865-2874, (1996).

[108] Zhou C. Z., Michelson Peter F., Phys. Rev. D, 51, 6 (1995).

[109] Koyama K., Niz G., Tasinato G., Phys. Rev. D, 84, 064033 (2011). [arXiv:1104.2143].

[110] Rostami A., Progress in Electromagnetics Research B, 4, 171 (2008).

[111] Ciftci H., Hall R.L., Saad N., Phys. Lett. A, 340 (5), 388 (2005).

[112] Babichev E., Brito R., Class. Quantum Grav., 32, 154001 (2015)

[113] Ghosh Sushant G., Tannukij L. and Wongjun P., Eur. Phys. J. C, 76, 3, 119 (2016). [arXiv:1506.07119v1]

[114] Koyama K., Niz G., Tasinato G., Phys. Rev. Lett., 107, 131101 (2011). [arXiv:1103.4708].

[115] Sbisa F., Niz G., Koyama K., Tasinato G., Phys. Rev. D, 86, 024033 (2012). [arXiv:1204.1193].

[116] Vegh D., Holography without translational symmetry, Report No. CERN-PH-TH/2013-357 (2013). [arXiv:1301.0537v2]

[117] Zerilli F. J., Phys. Rev. Lett., 24, 737 (1970).

[118] Moss I. G., Norman J. P., Class. Quant. Grav. 19, 2323 (2002).

[119] Naylor W., Black Holes: AIM, *http://wade-naylor.com/aim/*

[120] Zhidenko A., Class. Quantum Grav., 21, 273ñ280 (2004).

[121] Zhidenko A., Quasi-normal modes of Schwarzschild-de Sitter black holes, arXiv:gr-qc/0307012v4 (2003).

[122] Zhidenko A., "Linear perturbations of black holes: stability, quasi-normal modes and tails", PhD Thesis [arXiv:0903.3555v2]

[123] Creighton J. D. E., Mann R. B., Phys. Rev. D, 52, 4569 (1995).

[124] Kstor D., Ray S., Traschen J., Class. Quant. Grav., 26, 195011 (2009).

[125] Dolan B. P., Class. Quant. Grav., 28, 235017 (2011).

[126] Xu J., Cao L., Hu Y., Phys. Rev. D, 91, 124033 (2015).

[127] Ryu S., Takayanagi T., J. High Energy Phys., 0608:045 (2006).

[128] Banados M., Teitelboim C., and Zanelli J., Phys. Rev. Lett., 69, 1849 (1992).

[129] Banados M., Henneaux M., Teitelboim C. and Zanelli J., Phys. Rev. D., 48, 1506 (1992).

[130] Horowitz G. T., and Hubeny V., Phys. Rev. D, 62, 024027 (2000).

[131] Cardoso V. and Lemos J. P. S., Phys. Rev. D, 63, 124015 (2001).

[132] Birmingham D., Phys. Rev. D, 64, 064024 (2001).

[133] Fernando S., Gen. Rel. Grav., 36, 71-82 (2004).

[134] Norman Cruz and Samuel Lepe, Phys. Lett. B, 593, 235 (2004).

[135] Chamblin A., Emparan R., Johnson C., and Myers R., Phys. Rev. D, 60, 064018 (1999).

[136] Cadoni M., Melis M. and Setare M. R., Class. Quantum Grav. 25, 195022 (2008)

[137] Setare M. R. and Adami H., Phys. Rev. D, 91, 104039 (2015).

[138] Debaprasad Maity et al., Nucl. Phys. B, 839:526 (2010). [arXiv:0909.4051v2]

[139] Hendi S. H., Eslam Panah B. and Panahiyan S., J. High Energy Phys., 05, 029 (2016).[arXiv:1604.00370v1]

[140] Fabio Capelaa and Peter G. Tinyakov., J. High Energy Phys., 1104:042 (2011). [arXiv:1102.0479]

[141] Forward R. L., Gen. Relativ. Gravit., 2, 149 (1971).

[142] Merkowitz S. M. , Johnson W. W., Phys. Rev. D, 51, 2546 (1995).

[143] Zhou C. Z. and Michelson P. F., Phys. Rev. D, 51, 2517 (1995).

[144] Christopher P. L. Berry, Jonathan R. Gair, Phys. Rev. D, 83, 104022 (2011).

[145] Forsyth A. R., "A Treatise on Differential Equations", sixth ed., Macmillan & Co Ltd., London (1961).

[146] Corda C., Astrophys. Space Sci., 317, 95–106 (2010).

[147] Lobo J. A., Phys. Rev D, 52, 591 (1995).

[148] Malik Rakhmanov, "Response of LIGO to gravitational waves at high freuencies and in the vicinity of the FSR(37.5kHz)", 060237-00 (2005).

[149] Capozziello S., Faraoni V., "Beyond Einstein Gravity", Springer, New York (2011).

[150] Coccia E., Dubath F., Maggiore M., Phys. Rev. D, 70, 084010 (2004).

[151] Abbott B. P. et al., Phys. Rev. D, 69, 082004 (2004).

[152] Lobo J. A., "Mathematics of gravitation part II", volume 41, Gravitational wave detection banach center publications (1997).

[153] Abbott B. P. et al., Rep. Prog. Phys., 72, 076901 (2009)

[154] Abbott B. P. et al., ApJ, 715, 1438 (2010).

[155] Abadie J. et al., ApJ, 760, 1 (2012)

[156] Maggiore M., "Gravitational Waves", Vol. 1, Oxford (2008).

[157] Orbanz Peter and M. Roy Daniel, IEEE Transactions Pattern Analysis and Machine Intelligence, 37, 437 (2015).

[158] V. Connaughton et al., ApJL, 826, L6 (2016). [arXiv:1602.03920v5]

[159] Abbott B. P. et al., Phys. Rev. Lett., 116, 241103 (2016).

[160] Emir Gumrukcuoglu A. et al., Class. Quantum Grav., 29, 235026 (2012).

[161] Emil Mottola, "Scalar Gravitational Waves in the Effective Theory of Gravity", Report number: LA-UR-16-23649(2016). [arXiv:1606.09220]

[162] Alves M. E. S., Miranda O. D. and de Araujo J. C. N., Phys. Lett. B, 679, 401 (2009).

[163] Rizwana Kausar H., Lionel Philippoz and Philippe Jetzer, Phys. Rev. D, 93, 124071 (2016).

[164] Alves M. E. S., Miranda O. D. and de Araujo J. C. N., Class. Quantum Grav., 27, 145010 (2010).

[165] Maggiore M. and Nicolis A., Phys. Rev. D, 62, 024004 (2000).

[166] Jaranowski P. and Krolak A., Phy. Rev. D, 49, 1723 (1994).

[167] Jaranowski P., Krolak A. and Schutz B. F., Phy. Rev. D, 58, 063001 (1998).

[168] Abadie J. et al., ApJ, 760, 12 (2012).

[169] Abbott B. P. et al., ApJ, 715, 1438ñ1452, (2010).

[170] Finn L. S. and Lommen A. N., ApJ, 718, 1400 (2010).

[171] Bishop C. M., Pattern Recognition and Machine Learning, Springer (2006).

[172] Finn L. S., Phys. Rev. D, 79, 022002 (2009).

[173] Wang Min and Sun Xiaoqian, J. Stat. Plan. Inference, 147, 95 (2014).

[174] Smith A. F. N. and Spiegelhalter D. J., J. R. Statist. Soc. B, 42, 2, 213 (1980).

[175] Wang Min and Sun Xiaoqian, Commun. Stat. Theory, 43, 5072 (2014).

[176] Abbott B. P. et al., Rep. Prog. Phys., 72, 076901 (2009).

[177] Capozziello S. et al., Eur. Phys. J. C, 70, 341 (2010).

[178] Abbott B. P. et al., Phys. Rev. D, 77, 062004 (2008).

[179] MacKay David J. C., Neural Computation, 4, 415 (1992).

[180] Aasai J. et al., Phys. Rev. Lett., 113, 011102 (2014).

[181] Deng Xihao, Phy. Rev. D, 90, 024020 (2014).